Fakultät für Physik und Astronomie

Ruprecht-Karls-Universität Heidelberg

Diplomarbeit

Im Studiengang Physik

vorgelegt von

Philipp Grothaus

geboren in Herford

2012

Das Zusammenspiel zwischen Natürlichkeit und direktem Nachweis von Neutralinos als Dunkle Materie

Die Diplomarbeit wurde von Philipp Grothaus

ausgeführt am

Max-Planck-Institut für Kernphysik

unter der Betreuung von

Herrn Prof. Manfred Lindner

Department of Physics and Astronomy

University of Heidelberg

Diploma thesis

in Physics

submitted by

Philipp Grothaus

born in Herford

2012

The Interplay between Naturalness and Direct Detection of Neutralino Dark Matter

This diploma thesis has been carried out by Philipp Grothaus

at the

Max-Planck-Insitut für Kernphysik

under the supervision of

Prof. Manfred Lindner

Das Zusammenspiel von Natürlichkeit und direktem Nachweis von Neutralinos als Dunkle Materie

In dieser Diplomarbeit untersuchen wir inwieweit Experimente zum direkten Nachweis von Dunkler Materie den natürlichen Parameterraum des minimalen supersymmetrischen Standard-Modells (MSSM) untersuchen können. Dazu berechnen wir das nötige Tuning, um einen bestimmten Punkt in der von der Neutralinomasse und dem Spin-unabhängigen direkten Detektionswirkungsquerschnitt σ^{SI} aufgespannten Ebene zu erreichen, indem wir einen elf-dimensionalen niedrig-Energie-Parameterraum scannen. Hierbei lassen wir insbesondere negative Werte des Higgs-Massenparameters μ zu. Die simulierten Modelle erfüllen alle aktuellen experimentellen Resultate, welche auch die Aktualisierungen der XENON100 Kollaboration und die Evidenz für ein Higgs-Boson vom LHC beinhalten. Für positive μ befinden sich nicht-getunete Lösungen hauptsächlich in Regionen, die resonante Neutralino-Annihilation per Z- oder leichtem Higgs-Boson-Austausch ermöglichen, da natürliche Szenarien in anderen Bereichen von XENON100 (2012) größtenteils ausgeschlossen wurden. In diesen anderen Bereichen findet man eine Tendenz zu größerem Tuning bei kleineren Werten von σ^{SI}. Ungetunete Modelle, welche die jetzigen Limits erfüllen, werden von XENON1t getestet werden. Wenn μ negativ ist, können nicht-getunete Szenarien durch Aufhebungen verschiedener Beiträge in σ^{SI} zu kleineren Werten verschoben werden, sodass ein negatives μ aus der Tuning-Perspektive bevorzugt wird. Viele Modelle vermeiden so sogar eine Überprüfung durch XENON1t. In diesem Zusammenhang zeigen wir, dass es sehr wohl möglich ist die Messung des anomalen magnetischen Moments des Muons mit negativem μ und positiven Gauginomassen einzuhalten und diskutieren auch die Wahrscheinlichkeitsverteilung unserer Modelle.

The Interplay between Naturalness and Direct Detection of Neutralino Dark Matter

In this thesis we investigate to which extent dark matter direct detection experiments can probe the natural parameter space of the minimal supersymmetric standard model (MSSM). We therefore calculate the amount of tuning necessary to reach a certain point in the plane spanned by the neutralino mass and the spin-independent direct detection cross-section σ^{SI} by scanning an eleven dimensional low-energy input parameter space of the phenomenological MSSM. We allow in particular for a negative supersymmetric Higgs mass parameter μ. The simulated models respect all current experimental results including the evidence for the Higgs boson from the LHC and the new update of the XENON100 collaboration. For positive μ untuned solutions are mainly situated at the Z- and Higgs resonance since the recent XENON100 (2012) update has excluded most of the natural solutions in other regions. In these other regions, one can find a clear increase of the tuning level for smaller σ^{SI}. Untuned models that survived the new limit will be tested by XENON1t. When μ is negative cancellations may shift the untuned scenarios to smaller values of σ^{SI}, such that a negative μ is favored from a fine-tuning perspective. Many models may in this way even avoid detection by XENON1t. In this context we show that it is possible to respect the muon anomalous magnetic moment condition for a negative μ-term and positive gaugino masses and also present the probability distribution of our models.

Contents

1. Introduction

The Standard Model (SM) of particle physics has been tested to a high accuracy and no significant deviation has been observed yet. Recently the ATLAS and CMS collaborations presented evidence for a new resonance that behaves in its production and decay channels very similar to the SM Higgs within the given statistics [1, 2]. Therefore, the SM might be complete in the next years, when this resonance is measured to a higher precision.

There are nevertheless still problems left over for particle physicists to think about. These include the explanation of the baryon asymmetry of the universe, the origin of neutrino masses and oscillations and also the nature of dark matter. In this thesis we will focus on the latter problem. A lot of evidence [3–5] has been collected over the past decades asking for a different kind of particle that interacts at most only weakly and gravitationally with ordinary matter. To test the large number of dark matter theories, searches for dark matter particles are one of the most important experiments of today's research in particle physics. Very recently the world leading dark matter direct detection experiment XENON100 has published new results [6, 7], but no positive signal has been reported, such that existing models are further constrained.

Other direct searches like DAMA/LIBRA [8], CRESST [9] and CoGeNT [10] have reported positive signals but there are doubts about the compatibility of these signals since the experiments all show a different preferred parameter region [11]. On top of that, all these signals are in contradiction to the XENON100 [6, 12, 13] and CDMS [14] experiments. This leads us to the assumption that so far there is no positive signal of dark matter direct detection experiments.

To explain the dark matter riddle one of the most promising and most extensively studied theories is the minimal supersymmetric extension of the standard model (MSSM), which contains a dark matter candidate that is stable due to R-parity conservation [15,16]. This lightest supersymmetric particle will in our analysis be the neutralino (for reviews see *e.g.* [17,18]). Since the MSSM can additionally solve the hierarchy problem of the SM and predicts a light Higgs mass [19–25], it has gained a lot of attention over the last years. Especially in light of the start of the LHC many researchers have waited for a positive

signal, but, as so many theories, also the MSSM has suffered from non-discovery in these early stages of the new particle collider.

Given the recent results from collider experiments and direct dark matter searches we perform a scan of the supersymmetric parameter space asking how natural the surviving region still is after all these negative searches. For this scan we use a measure of fine-tuning [26, 27] that indicates a large separation of the electroweak symmetry and supersymmetry breaking scales, and relate it to direct dark matter searches by investigating how high the level of tuning is to reach a certain region in the plane spanned by the neutralino mass and the spin-independent direct detection cross-section (direct detection plane). In this context the tuning measure allows us to restrict the vast supersymmetric parameter space and to state when signals become unnatural from a theoretical perspective.

To do so, we investigate the low-energy phenomenological MSSM, a simplified model of the complete MSSM, see for example [28–32]. Motivated by constraints on flavor changing neutral currents and CP-violation, the number of MSSM parameters is reduced to twenty-two allowing for a numerical analysis. Even though we further restrict the free parameters and take into account all experimental data, we are able to examine thoroughly the parameter space and point out the natural regions. This will be done for a neutralino mass range below 200 GeV since a detailed analysis is so far missing in the literature. Throughout the whole discussion we will distinguish between a positive and a negative sign of the supersymmetric Higgs mass parameter because there are big differences in the results.

This thesis is organized as follows: We start by motivating the existence of dark matter in chapter 2 where we also present the freeze-out mechanism as a standard way to calculate the relic abundance. The MSSM will be introduced in chapter 3 after giving a brief summary how supersymmetric Lagrangians can be constructed in the superspace formalism. In chapter 4 we present the exact model of the MSSM that we scan and discuss the applied constraints arising from cosmology, collider experiments and direct searches. Our results will be contained in chapter 5 that especially includes discussions about the neutralino annihilation mechanisms, the distribution of fine-tuning in the direct detection plane, the dependence of the direct detection cross-section on the sign of the supersymmetric Higgs mass parameter, the impact of the muon anomalous magnetic moment on our scenarios and the probability distribution of our models. Finally, we conclude in chapter 6.

2. Dark matter

2.1. Evidence for dark matter

The need for dark matter emerges from various observations on different length scales. The measurement of the angular velocity v_a with respect to the distance to the galactic center r, in other words a rotation curve, shows an unexpected behavior for large r. Far out from the galactic center simple application of Newtonian dynamics[1] gives a decrease of v_a with r:

$$v = \sqrt{\frac{MG}{r}}\,, \tag{2.1}$$

where G is Newton's constant and M the mass of the galaxy contained in the orbit of the test particle. Observations, however, tell us that this decrease is not present, but that v_a stays constant instead, see figure 2.1 [3].

This discrepancy between theory and observation could be solved in two ways. A modification of Newtonian dynamics (MOND) or a postulation of additional matter in the galaxy that cannot be seen, *i.e.* dark matter, may both give correct rotation curves. The tendency is for the latter one due to two reasons: The gravitational potential of galaxy clusters can be reproduced by lensing effects. This potential can then be compared to the distribution of the visible matter obtained through X-ray observations. If the distribution of the visible matter does not coincide with the gravitational potential, dark matter is favored over the MOND hypotheses. In the bullet cluster a clear mismatch between the center of gravity and the center of luminosity could be observed, see figure 2.2. Of course, the determination of the gravitational potential is dependent on the theory of gravity that is used, but according to reference [4]: "Any non-standard gravitational force that scales with baryonic mass will fail to reproduce these observations. The lensing peaks require unseen matter concentrations that are more massive than and offset from the plasma."

The second advantage of the dark matter hypothesis is its ability to explain the large scale structure of the universe. In the standard cosmological picture the grains for the

[1]Newtonian treatment is completely sufficient for these velocities and energy densities.

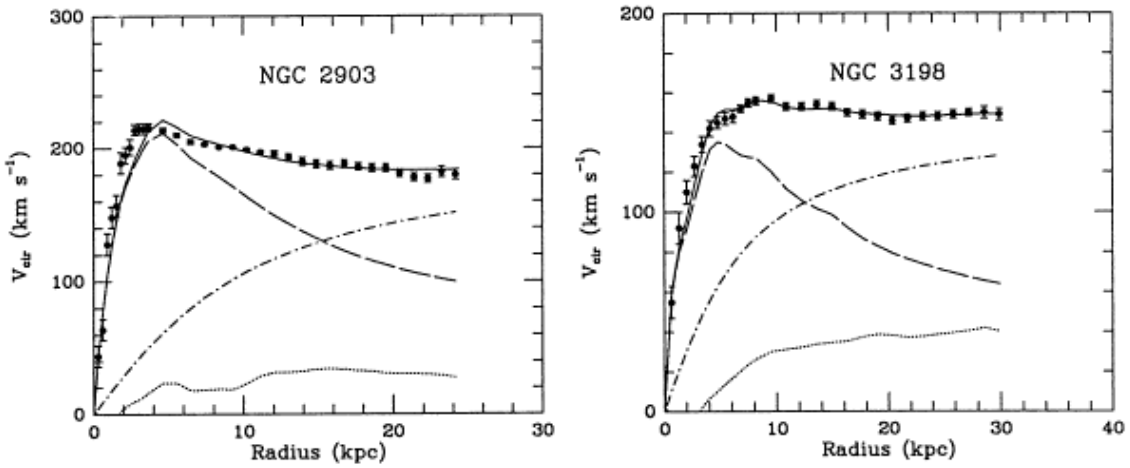

Figure 2.1.: Two examples of rotation curves of galaxies. A deviation of the thick black measured rotation curve from the expected Newtonian behavior (dashed line) is clearly visible. The dotted-dashed curve represents the contribution that is additionally needed to explain the behavior [3].

formation of galaxy clusters are seeded in the very early universe when density fluctuations emerge due to quantum fluctuations which are amplified by the inflationary expansion. For these regions to grow in density, more matter has to be accumulated. However, the hot plasma prevents matter, *i.e.* ionized gas, to fall into these denser regions because of interactions with radiation. In order to obtain a large enough density gradient, matter that does not interact with radiation has to be present. Then, the denser regions can start to grow early enough, meaning before recombination takes place, to form the seeds for galaxy clusters.

In fact, the MOND hypotheses are not able to explain structure formation and galaxy dynamics. Besides, constructing a covariant theory that has the MOND behavior in its non-relativistic limit has not been achieved yet. However, this could simply be ameliorated if more work was done.

2.2. The relic abundance

One of the standard ways to calculate the left over number density of a certain particle type from the early Universe is the so-called freeze-out mechanism (e.g. [17]). In this mechanism particles are assumed to initially be in thermal equilibrium with the plasma. To find the number density an integration over the distribution function, which for a

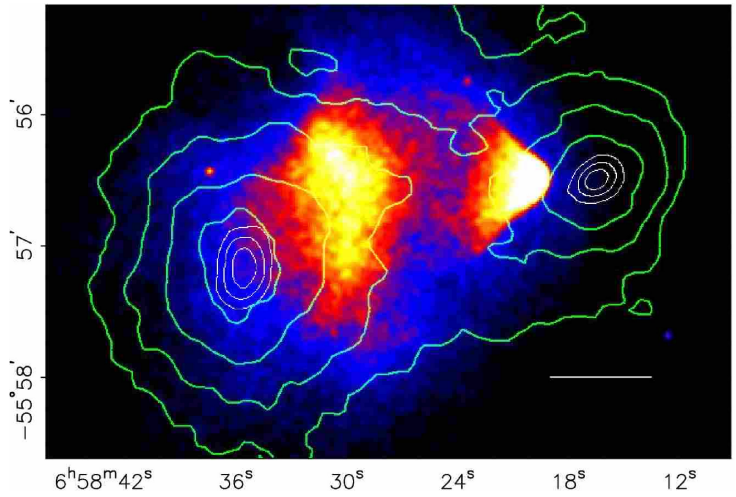

Figure 2.2.: The center of gravity (green lines) and the center of luminosity (white-yellow color map) show a clear mismatch that leads to the postulation of collision less dark matter [4].

fermion is given by the Fermi-Dirac statistic, has to be done:

$$n_{\tilde{\chi}} = \frac{g}{(2\pi)^3} \int_{-\infty}^{\infty} f(\vec{p})\, \mathrm{d}^3p = \frac{g}{(2\pi)^3} \int_{-\infty}^{\infty} \frac{1}{e^{\frac{\sqrt{p^2+m^2}}{T}} + 1}\, \mathrm{d}^3p \ . \tag{2.2}$$

Here, p is the momentum of the particle with mass m and T denotes the temperature. Shortly after the Big Bang the particles are relativistic($p \gg m$) so that by substituting $x = p/T$ one finds:

$$n_{\tilde{\chi}} = \frac{g}{(2\pi)^3} 2 \cdot 4\pi T^3 \int_0^{\infty} \frac{x^2 \mathrm{d}x}{e^x + 1} = \frac{g}{(2\pi)^3} 2 \cdot 4\pi T^3 \cdot 3\frac{\zeta(3)}{2} \propto T^3 \ , \tag{2.3}$$

where $\zeta(3) = 1.202$ is the Riemann zeta function. This shows that, when particles are treated massless the number density of fermions is (similar to the one of photons) given by a proportionality to the temperature cubed.
As the universe expands and the temperature of the plasma drops (for a detailed description of cosmology, see for example [33]), the distribution function reduces to the Boltzmann case and the number density is exponentially suppressed:

$$n_{\tilde{\chi}} \propto g(m_{\tilde{\chi}} T/2\pi)^{3/2} e^{-m_{\tilde{\chi}}/T} \ . \tag{2.4}$$

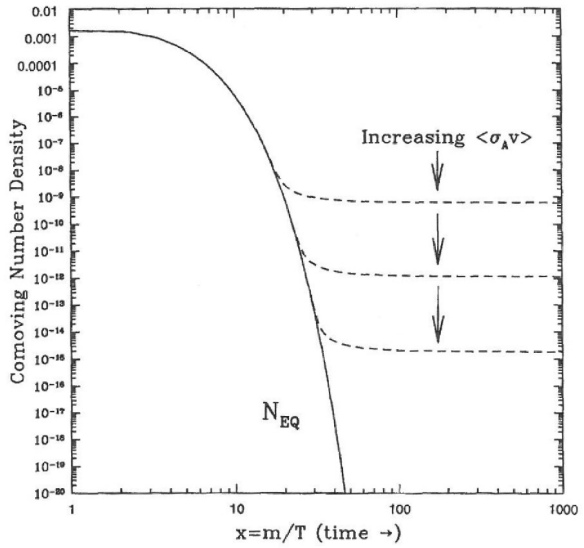

Figure 2.3.: Dependence of the relic abundance on the thermally averaged neutralino annihilation cross-section [17].

Roughly speaking, the creation of two dark matter particles by the plasma is heavily suppressed when the average energy drops below $2 \times m_{\tilde{\chi}}$. Hence, only annihilation of dark matter then occurs and the number density falls of sharply (exponentially). However, when the annihilation rate drops below the expansion rate of the universe, the dark matter falls out-of-equilibrium and their number density stays constant, see figure 2.3. This freeze-out condition

$$\langle \sigma_{ann} v \rangle n_{\tilde{\chi}} = \Gamma_{ann} \simeq H = \frac{\pi T_f^2}{M_{pl}} \sqrt{\frac{g_*}{90}} \ , \tag{2.5}$$

with $\langle \sigma_{ann} v \rangle$ as the thermally averaged annihilation cross-section, H the Hubble constant, Γ_{ann} the annihilation rate, M_{pl} the Planck mass, g_* the effective number of degrees of freedom (which is around 100) and T_f the freeze-out temperature, basically states that the universe expands too fast for two particles to collide and interact. This equation gives the freeze-out temperature T_f in dependence on the annihilation cross-section and $m_{\tilde{\chi}}$ if one substitutes equation (2.2) for $n_{\tilde{\chi}}$. One can then calculate the present dark matter relic abundance via:

$$\Omega h^2 = \frac{m_{\tilde{\chi}} n_{\tilde{\chi}0}}{\rho_c} = \frac{m_{\tilde{\chi}} n_{\tilde{\chi}_f} s_0}{\rho_c s_f} \ , \tag{2.6}$$

where s_f is the entropy density at the freeze-out temperature and ρ_c the critical energy density. To scale the dark matter number density from freeze-out to the present epoch, we used the conserved ratio of number to entropy density. Plugging in weak scale orders of magnitude for $\langle\sigma_{ann}v\rangle$ and $m_{\tilde{\chi}}$ the so-called WIMP-miracle arises: The correct order of magnitude for Ωh^2 is "miraculously" produced. This is the strong motivation for weakly interacting massive particles (WIMPs)

The sketched procedure above gives a first rough estimate for the relic abundance, but for a precise statement the Boltzmann equation has to be evaluated:

$$\frac{dn_{\tilde{\chi}}}{dt} + 3Hn_{\tilde{\chi}} = -\langle\sigma_{ann}v\rangle[(n_{\tilde{\chi}})^2 - (n_{\tilde{\chi}}^{eq})^2] \ . \tag{2.7}$$

The particle model gives $\langle\sigma_{ann}v\rangle$ and one can then solve for the time dependent number density $n_{\tilde{\chi}}(t)$ numerically. A different process discussed in the literature is the so called freeze-in mechanism, where the candidate's initial abundance is negligible and very weakly interactions provide for the necessary interactions to feed the number density. In that case annihilations of the dark matter particle are rare due to the small number density. However, this mechanisms is not applied to supersymmetric dark matter.

2.3. Candidates

There is a broad band of theories that try to explain the dark matter abundance. These cover dark matter particle masses from below the eV to above the TeV range. In this subsection we shortly name some candidates[2] in order to give a very brief overview. We simply want to stress that there are many more possibilities than the one we will consider in this thesis, *i.e.* supersymmetric dark matter [17]. See, for example reference [34] for a summary of dark matter.

Standard Model neutrinos exist in a large quantity in the universe, but since their are so light they fail to reproduce structure formation. Relativistic particles remove structure on small scales, which is called "free-streaming" [35], such that larger structures like galaxy clusters should be formed earlier than smaller objects like galaxies themselves. This, however, contradicts age determinations of our galaxy and the local group [36].

Sterile neutrinos that interact with Standard Model particles only via Yukawa interactions, on the other hand, are still a promising candidate [37]. Originally introduced to

[2]There is no chance of giving a complete collection.

explain neutrino masses via seesaw mechanisms, arising constraints from astrophysics can be avoided in the νMSM model [38]. Their mass usually lies in the keV range.

To solve the strong CP-problem, that basically asks why the CP violating parameter appearing in the QCD Lagrangian is as small as 10^{-11}, Peccei and Quinn introduced a new global $U(1)_{\mathrm{PQ}}$ symmetry [39, 40] that, when spontaneously broken, gives rise to a quasi-Nambu-Goldstone boson, the axion a. Constraints have ruled out a large fraction of the possible mass range but windows in the eV and 10^{-3} eV regions are still open [41].

Another possibility is to duplicate the SM and introduce a $\mathcal{Z}_2$ symmetry under which the "mirror" world is charged [42]. These new particles can then interact with the usual SM only through gravity and mixing of charge and color neutral particles and may explain the DM in the universe.

There are other, more minimal, approaches that only introduce a new scalar particle S which forms a singlet under the SM gauge group and may thus interact only via the Higgs sector: $\mathcal{L} \supset -\lambda S^2 H^\dagger H$. These models are, however, strongly tested by direct searches as a large coupling to the Higgs boson is present [43].

There are also very heavy candidates, so-called WIMPZILLAs that have masses of approximately 10^{13} GeV and only interact gravitationally [44]. Hence they do not offer any chance of detection.

We could go on with this list and talk about dark matter arising from extra dimensions [45], technicolor [46] or candidates like superWIMPs [47], gravitinos [48] and axinos [49]. It is clear that precise studies have to be performed for all of them and that in the end experiments will hopefully tell us which model is realized in nature.

In this thesis the neutralino of the minimal supersymmetric extension of the standard model is our considered dark matter candidate. As the lightest supersymmetric particle it is stable due to R-parity conservation. Details will follow in the next chapter.

3. Supersymmetry

Supersymmetry (SUSY) is a symmetry that transforms bosons into fermions and vice versa and offers enormous possibilities to construct new theories. For particle physicists especially the minimal supersymmetric standard model offers a great playground for phenomenology. The ability of the MSSM to solve the hierarchy problem and the dark matter riddle have made it one of the most extensive studied theory beyond the Standard Model. This introduction summarizes only the very basic ingredients of the MSSM and the complete chapter will notationally and structurally be close to the review by Stephen P. Martin.[1] [50]. We will start to give a brief classical example of a supersymmetric theory by considering a harmonic oscillator to get a feeling how a SUSY algebra emerges. Then, we will explain the superspace formalism, in which we will identify SUSY transformations with translations in superspace, and introduce chiral and vector superfields and the superpotential. These will enter the Lagrangian that we wish to construct as this is the object that ultimately defines a field theory[2]. After these technical details, we will describe the MSSM more specifically and discuss its field content, state the superpotential and the soft supersymmetry breaking mass terms. In the context of electroweak symmetry breaking, we will define our measure of fine-tuning. This tuning is seen as a problem of the MSSM and becomes worse the longer supersymmetric particles stay undetected.

3.1. Introduction

3.1.1. Motivation

If one tries to embed the Standard Model into another Field Theory, the so called "hierarchy problem" arises: The Higgs mass in the Standard Model suffers from loop corrections that give contributions to its mass which would theoretically make it unnaturally heavy. When calculating the self-energy of the Higgs boson especially top loops have to be in-

[1] We believe it is not possible for a student to give a better introduction.
[2] Of course, there are other possible formulations.

cluded. Regularizing the loop integral leads to contributions proportional to the cut-off scale Λ squared. Then the Higgs mass m_h^2 is to a first estimate given by:

$$m_h^2 \approx \frac{y_t^2}{8\pi}\Lambda^2 \ . \tag{3.1}$$

The value of the cut-off scale is set by the appearance of new physics beyond the Standard Model that contribute to the Higgs boson mass. These could be heavy right-handed neutrinos, grand unified theories or gravitational effects. Whichever scale is chosen, the prediction for the Higgs mass is very different to the natural mass set by electroweak symmetry breaking such that m_h is unstable against new physics appearing at high energies. This major problem, the hierarchy problem, is viewed as one of the main motivation for physics beyond the Standard Model. To give the Higgs a mass of order of the electroweak scale, new physics should appear already around a few TeV, in order to have a low cut-off scale. Low energy supersymmetry can free physics from this problem and stabilize the electroweak scale by introducing superpartners to all of the Standard Model (SM) particles. These new particles have opposite spin-statistics such that loop contributions from superpartners have a relative minus sign and can cancel if their masses are equal. Since supersymmetry must be broken, these cancellations cannot be exact. Fortunately, this does not spoil the stability as long as SUSY particles are not too heavy. This separation of the electroweak and supersymmetry breaking scales will lead us to the introduction of a fine-tuning measure in section 3.5.

Another motivation for the MSSM comes from the fact that the lightest supersymmetric particle (LSP) is stable against decays into SM particles due to R-parity conservation. This upgrades the LSP to a perfect dark matter candidate and we will investigate in our scan how natural the solutions of the MSSM explaining all dark matter in the Universe are by calculating the amount of tuning necessary to reach a certain point in the LSP mass-spin-independent direct detection plane (which we will call direct detection plane from now on for simplicity).

3.1.2. Supersymmetric harmonic oscillator

To get a feeling for supersymmetry and construct a SUSY algebra in a simple example, we will take a look at a system of a harmonic oscillator and supersymmetrize it [51]. In the classical bosonic oscillator an infinite number of states can be excited, whereas a fermionic oscillator is either excited or in its ground state due to the Pauli exclusion principle. Since

supersymmetry transforms a bosonic into a fermionic state, we need at least two quantum numbers n_B and n_F to describe the system. These come together with a set of creation and annihilation operators $l_B^+, l_B^-, l_F^+, l_F^-$. We briefly summarize the well-known relations for the ladder operators and the Hamiltonian:

$$\begin{aligned} l_B^+|n_B\rangle &= \sqrt{n_B+1}|n_B+1\rangle \ , & l_F^+|n_F\rangle &= \sqrt{n_F+1}|n_F+1\rangle \ , \\ l_B^-|n_B\rangle &= \sqrt{n_B}|n_B-1\rangle \ , & l_F^-|n_F\rangle &= \sqrt{n_F}|n_F-1\rangle \ , \\ N_B|n_B\rangle &= (l_B^+ + l_B^-)|n_B\rangle = n_B|n_B\rangle \ , & N_F|n_F\rangle &= (l_F^+ + l_F^-)|n_F\rangle = n_F|n_F\rangle \ , \\ H &= \hbar\omega(N_B+N_F) \ . \end{aligned}$$

For the fermions we need to impose the Pauli principle by demanding further:

$$(l_F^+)^2 = 0 \ . \tag{3.2}$$

One can then calculate the (anti)commutator relations and finds:

$$[l_B^-, l_B^+] = 1 = \{l_F^-, l_F^+\} \ , \tag{3.3}$$

$$[l_B^+, l_B^+] = [l_B^-, l_B^-] = 0 = \{l_F^-, l_F^-\} = \{l_F^+, l_F^+\} \ . \tag{3.4}$$

To construct a supersymmetric system we need to consider product states $|n_B n_F\rangle$ to deal with fermions and bosons at the same time. Then, a SUSY transformation takes us from a bosonic state ($n_F = 0$) to a fermionic state ($n_F = 1$) and vice versa. We therefore define the SUSY operators $Q_\pm$ to be:

$$\begin{aligned} Q_+|n_B n_F\rangle &\equiv l_B^- l_F^+|n_B n_F\rangle \propto |n_B - 1, n_F + 1\rangle \ , \\ Q_-|n_B n_F\rangle &\equiv l_B^+ l_F^-|n_B n_F\rangle \propto |n_B + 1, n_F - 1\rangle \ . \end{aligned} \tag{3.5}$$

With these definitions we have $Q_+^2 = Q_-^2 = 0$. Since we want a supersymmetric theory the energy of the system should not change when a SUSY transformation is performed, which means that the commutator of the Hamiltonian and the SUSY generators has to vanish $[H, Q_\pm] = 0$. This can easily be fulfilled, if we set the Hamiltonian to:

$$H = \{Q_+, Q_-\} \ . \tag{3.6}$$

Then, we have found a first formulation of a SUSY algebra. The (anti)commutators of each SUSY generator with itself vanishes ($Q_\pm^2 = 0$), the anticommutator of both SUSY

generators gives the Hamiltonian and the commutator of the hamiltonian with the SUSY generator is identically zero.

This is just an example and has no real physical background, but it shows in a very simple way how a SUSY algebra emerges. In the above, no spin has been considered even though we imposed the Pauli principle. Real particles, however, carry spin so that if the generators shall transform bosons into fermions, they themselves have to form spinors under Lorentz transformations. In the next section we will develop the superspace formalism to properly describe supersymmetry.

3.2. Superspace formalism

In everything that follows we make use of the Weyl representations of spinors. The essential ingredients and relations can be found in appendix A.
To formulate supersymmetry we extend the spacetime by four fermionic coordinates $\theta_\alpha, \theta^\dagger_{\dot\beta}$. These complex valued spinors are anticommuting objects; the fundamentals of Grassmann variables (*i.e.* anticommuting variables) can be found in appendix B.

$$x^\mu \longrightarrow (x^\mu, \theta^\alpha, \theta^\dagger_{\dot\alpha}) \ , \qquad \alpha = \{1,2\} \ , \qquad \dot\alpha = \{\dot1,\dot2\} \ . \tag{3.7}$$

In the superspace formalism we consider functions of these coordinates, the superfields. These can then be expanded in the fermionic variables. Note that for anticommuting objects expressions like $\theta_1\theta_1$ are identically zero. For that reason our expansion's highest term is $\theta\theta\theta^\dagger\theta^\dagger$, where a summation over α and $\dot\alpha$ is included[3]. The most general expansion of a superfield is:

$$S(x,\theta,\theta^\dagger) = a + \theta\xi + \theta^\dagger\chi^\dagger + \theta\theta b + \theta^\dagger\theta^\dagger c + \theta^\dagger\overline{\sigma}^\mu\theta v_\mu + \theta^\dagger\theta^\dagger\theta\eta + \theta\theta\theta^\dagger\zeta^\dagger + \theta\theta\theta^\dagger\theta^\dagger d \ . \tag{3.8}$$

Note that the Pauli matrices necessarily carry spinor indices. Our task is to relate the expansion coefficients $a, b, c, d, \xi, \chi, v_\mu, \eta, \zeta$ with meaningful physical fields in a way that the superfield contains fields of superpartners. For that we first have to talk about SUSY transformations and covariant derivatives to be able to construct chiral and vector superfields, which are the objects entering the Lagrangian.

[3] e.g.: $\theta\theta = \theta^\alpha\theta_\alpha = \theta^\alpha\epsilon_{\alpha\beta}\theta^\beta = \theta^1\theta^2 - \theta^2\theta^1 = 2\theta^1\theta^2$, but:$(\theta\theta)(\theta\eta) = 2\theta^1\theta^2(\theta^1\eta^2 - \theta^2\eta^1) = 0$.

3.2.1. The supersymmetry algebra

In this subsection we define the supersymmetry transformation in the superspace formalism and calculate the $\mathcal{N} = 1$ SUSY algebra. Then, we connect supersymmetry transformations with translations in superspace. The generators for supersymmetry transformations that act on functions in superspace are:

$$\hat{Q}_\alpha = i\frac{\partial}{\partial\theta^\alpha} - (\sigma^\mu\theta^\dagger)_\alpha\partial_\mu \ , \tag{3.9}$$

$$\hat{Q}^\alpha = -i\frac{\partial}{\partial\theta_\alpha} + (\theta^\dagger\overline{\sigma^\mu})^\alpha\partial_\mu \ , \tag{3.10}$$

$$\hat{Q}^{\dagger\dot{\alpha}} = i\frac{\partial}{\partial\theta^\dagger_{\dot{\alpha}}} - (\overline{\sigma}^\mu\theta^\dagger)^{\dot{\alpha}}\partial_\mu \ , \tag{3.11}$$

$$\hat{Q}^\dagger_{\dot{\alpha}} = -i\frac{\partial}{\partial\theta^{\dagger\dot{\alpha}}} + (\theta\sigma^\mu)_{\dot{\alpha}}\partial_\mu \ . \tag{3.12}$$

An infinitesimal supersymmetry transformation parameterized by $\epsilon, \epsilon^\dagger$ of a superfield S is then defined as:

$$\begin{aligned}\sqrt{2}\delta_\epsilon S = -i(\epsilon\hat{Q} + \epsilon^\dagger\hat{Q}^\dagger) = &\left(\epsilon^\alpha\frac{\partial}{\partial\theta^\alpha} + \epsilon^\dagger_{\dot{\alpha}}\frac{\partial}{\partial\theta^{\dagger\dot{\beta}}} + i[\epsilon\sigma^\mu\theta^\dagger + \epsilon^\dagger\bar{\sigma}^\mu\theta]\partial_\mu\right) S(x,\theta,\theta^\dagger) \\ = &\ S\left(x^\mu + i\epsilon\sigma^\mu\theta^\dagger + i\epsilon^\dagger\bar{\sigma}^\mu\theta, \theta + \epsilon, \theta^\dagger + \epsilon^\dagger\right) \ ,\end{aligned} \tag{3.13}$$

which follows by linear approximation. A supersymmetry transformation may therefore be seen as a translation in superspace. Now, we calculate the anticommutator of $\hat{Q}_\alpha$ and $\hat{Q}^\dagger_{\dot{\beta}}$. Here we make use of some relations that can be found in the appendix A.

$$\begin{aligned}\left\{\hat{Q}_\alpha, \hat{Q}^\dagger_{\dot{\beta}}\right\} &= \left\{i\frac{\partial}{\partial\theta^\alpha} - (\sigma^\mu\theta^\dagger)_\alpha\partial_\mu, -i\frac{\partial}{\partial\theta^{\dagger\dot{\beta}}} + (\theta\sigma^\mu)_{\dot{\beta}}\partial_\mu\right\} \\ &= \underbrace{\left\{\frac{\partial}{\partial\theta^\alpha}, \frac{\partial}{\partial\theta^{\dagger\dot{\beta}}}\right\}}_{A} + \underbrace{\left\{i\frac{\partial}{\partial\theta^\alpha}, (\theta\sigma^\mu)_{\dot{\beta}}\partial_\mu\right\}}_{B} \\ &\quad + \underbrace{\left\{(\sigma^\mu\theta^\dagger)_\alpha\partial_\mu, i\frac{\partial}{\partial\theta^{\dagger\dot{\beta}}}\right\}}_{C} - \underbrace{\left\{(\sigma^\mu\theta^\dagger)_\alpha\partial_\mu, (\theta\sigma^\mu)_{\dot{\beta}}\partial_\mu\right\}}_{D} \ .\end{aligned} \tag{3.14}$$

Term A is identically zero because the variables are anticommuting. For expression B some work needs to be done:

$$\left\{ i\frac{\partial}{\partial\theta^\alpha}, (\theta\sigma^\mu)_{\dot\beta}\partial_\mu \right\} = i\left[\frac{\partial}{\partial\theta^\alpha}(\theta\sigma^\mu)_{\dot\beta}\partial_\mu + (\theta\sigma^\mu)_{\dot\beta}\partial_\mu\frac{\partial}{\partial\theta^\alpha} \right] \tag{3.15}$$
$$= i\left[\sigma^\mu_{\alpha\dot\beta}\partial_\mu - (\theta\sigma^\mu)_{\dot\beta}\frac{\partial}{\partial\theta^\alpha}\partial_\mu + (\theta\sigma^\mu)_{\dot\beta}\partial_\mu\frac{\partial}{\partial\theta^\alpha} \right] .$$

The minus sign of the second term in the squared brackets appears because we have to interchange two anticommuting variables when moving the superspace derivative to the right side of $(\theta\sigma^\mu)_{\dot\beta}$. Since the partial derivative with respect to the "usual" spacetime is commuting with the partial derivative with respect to the superspace coordinate, the last two terms cancel out and we end up with:

$$\left\{ i\frac{\partial}{\partial\theta^\alpha}, (\theta\sigma^\mu)_{\dot\beta}\partial_\mu \right\} = i\sigma^\mu_{\alpha\dot\beta}\partial_\mu \ . \tag{3.16}$$

In a similar manner one can derive for the term C:

$$\left\{ (\sigma^\mu\theta^\dagger)_\alpha\partial_\mu, i\frac{\partial}{\partial\theta^{\dagger\dot\beta}} \right\} = i\sigma^\mu_{\alpha\dot\beta}\partial_\mu \ . \tag{3.17}$$

Term D vanishes again due to the anticommuting behavior of both terms and we get as a final result:

$$\left\{ \hat{Q}_\alpha, \hat{Q}^\dagger_{\dot\beta} \right\} = 2i\sigma^\mu_{\alpha\dot\beta}\partial_\mu \ , \tag{3.18}$$

which may be related to the 4-momentum operator that generates spacetime translations:

$$\{ \hat{Q}_\alpha, \hat{Q}^\dagger_{\dot\beta} \} = 2i\sigma^\mu_{\alpha\dot\beta}\partial_\mu = -2\sigma^\mu_{\alpha\dot\beta}\hat{P}_\mu \ . \tag{3.19}$$

All the other anti commutators vanish as may be computed analogously:

$$\{ \hat{Q}_\alpha, \hat{Q}_\beta \} = 0 \ , \ \ \{ \hat{Q}^\dagger_{\dot\alpha}, \hat{Q}^\dagger_{\dot\beta} \} = 0 \ . \tag{3.20}$$

We see that the SUSY algebra just found is similar to the one we derived for the classical system of a harmonic oscillator, see equation (3.6). Note that now spinor indices and therefore the spin structure are included correctly and that the Hamiltonian is replaced by the 4-momentum operator acting on functions in superspace. The next step is to define meaningful superfields.

3.2.2. Chiral and vector superfields

To construct supersymmetric invariant Lagrangians, we have to find supersymmetric covariant derivatives[4]:

$$\delta_\epsilon \left(D_\alpha S\right) = D_\alpha \left(\delta_\epsilon S\right), \qquad \delta_\epsilon \left(D^\dagger_{\dot\alpha} S\right) = D^\dagger_{\dot\alpha} \left(\delta_\epsilon S\right) \ . \tag{3.21}$$

These are given by:

$$D_\alpha = \frac{\partial}{\partial\theta^\alpha} - i(\sigma^\mu\theta^\dagger)_\alpha\partial_\mu, \qquad D^\alpha = -\frac{\partial}{\partial\theta_\alpha} + i(\theta^\dagger\overline{\sigma}^\mu)^\alpha\partial_\mu, \tag{3.22}$$

$$D^{\dagger\dot\alpha} = \frac{\partial}{\partial\theta^\dagger_{\dot\alpha}} - i(\overline{\sigma}^\mu\theta)^{\dot\alpha}\partial_\mu, \qquad D^\dagger_{\dot\alpha} = -\frac{\partial}{\partial\theta^{\dagger\dot\alpha}} + i(\theta\sigma^\mu)_{\dot\alpha}\partial_\mu \ . \tag{3.23}$$

One may then define a left-chiral superfield Φ by imposing that its covariant derivative with respect to the right-handed spinor index vanishes, and similar for a right-chiral superfield Φ^*:

$$D^\dagger_{\dot\alpha}\Phi = 0, \qquad D_\alpha\Phi^* = 0 \ . \tag{3.24}$$

This constraint forces several of the expansion coefficients from equation 3.8 to vanish. The most general expansion of a left-chiral and right-chiral superfield is:

$$\begin{aligned}\Phi &= \phi(x) - i\theta\sigma^\mu\theta^\dagger\partial_\mu\phi(x) - \frac{1}{4}\theta\theta\theta^\dagger\theta^\dagger\partial_\mu\partial^\mu\phi(x) + \sqrt{2}\theta\psi(x) \\ &\quad -\frac{i}{\sqrt{2}}\theta\theta\theta^\dagger\overline{\sigma}^\mu\partial_\mu\psi(x) + \theta\theta F(x), \end{aligned} \tag{3.25}$$

$$\begin{aligned}\Phi^* &= \phi^*(x) + i\theta\sigma^\mu\theta^\dagger\partial_\mu\phi^*(x) - \frac{1}{4}\theta\theta\theta^\dagger\theta^\dagger\partial_\mu\partial^\mu\phi^*(x) + \sqrt{2}\theta^\dagger\psi^\dagger(x) \\ &\quad -\frac{i}{\sqrt{2}}\theta^\dagger\theta^\dagger\theta\sigma^\mu\partial_\mu\psi^\dagger(x) + \theta^\dagger\theta^\dagger F^*(x) \ . \end{aligned} \tag{3.26}$$

Only three fields remain that we can interpret as a scalar ϕ, a spinor ψ and a field F, which will turn out to be non-dynamical when we solve for its equations of motion. Such a field is called "auxiliary" and will later be expressed by a combination of the other fields and is in this way removed of the physical theory. They are nevertheless important to also have off-shell supersymmetric invariance. For completeness we give the supersymmetry

[4]This is as in general gauge field theories where gauge-covariant derivatives are needed to construct gauge invariant Lagrangians.

transformations for the individual fields:

$$\begin{aligned}
\delta_\epsilon \phi &= \epsilon\psi, && (3.27)\\
\delta_\epsilon \psi_\alpha &= -i(\sigma^\mu \epsilon^\dagger)_\alpha \partial_\mu \phi + \epsilon_\alpha F, && (3.28)\\
\delta_\epsilon F &= -i\epsilon^\dagger \overline{\sigma}^\mu \partial_\mu \psi \ . && (3.29)
\end{aligned}$$

To formulate the MSSM, however, one main ingredient, gauge bosons, is still missing. These are contained in a vector superfield, which is defined to simply be a real superfield:

$$V = V^* \ . \tag{3.30}$$

The most general expansion of V in the fermionic variables is[5]:

$$\begin{aligned}
V(x,\theta,\theta^\dagger) &= a + \theta\xi + \theta^\dagger\xi^\dagger + \theta\theta b + \theta^\dagger\theta^\dagger b^* + \theta\sigma^\mu\theta^\dagger A_\mu + \theta^\dagger\theta^\dagger\theta(\lambda - \frac{i}{2}\sigma^\mu\partial_\mu\xi^\dagger)\\
&\quad + \theta\theta\theta^\dagger(\lambda^\dagger - \frac{i}{2}\overline{\sigma}^\mu\partial_\mu\xi) + \theta\theta\theta^\dagger\theta^\dagger(\frac{1}{2}D - \frac{1}{4}\partial_\mu\partial^\mu a) \ . \qquad (3.31)
\end{aligned}$$

Working out the SUSY transformations in components yields:

$$\begin{aligned}
\sqrt{2}\,\delta_\epsilon a &= \epsilon\xi + \epsilon^\dagger\xi^\dagger \ , && (3.32)\\
\sqrt{2}\,\delta_\epsilon \xi_\alpha &= 2\epsilon_\alpha b + (\sigma^\mu\epsilon^\dagger)_\alpha(A_\mu - i\partial_\mu a), && (3.33)\\
\sqrt{2}\,\delta_\epsilon b &= \epsilon^\dagger\lambda^\dagger - i\epsilon^\dagger\overline{\sigma}^\mu\partial_\mu\xi, && (3.34)\\
\sqrt{2}\,\delta_\epsilon A^\mu &= -i\epsilon\partial^\mu\xi + i\epsilon^\dagger\partial^\mu\xi^\dagger + \epsilon\sigma^\mu\lambda^\dagger - \epsilon^\dagger\overline{\sigma}^\mu\lambda, && (3.35)\\
\sqrt{2}\,\delta_\epsilon \lambda_\alpha &= \epsilon_\alpha D - \frac{i}{2}(\sigma^\mu\overline{\sigma}^\nu\epsilon)_\alpha(\partial_\mu A_\nu - \partial_\nu A_\mu), && (3.36)\\
\sqrt{2}\,\delta_\epsilon D &= -i\epsilon\sigma^\mu\partial_\mu\lambda^\dagger - i\epsilon^\dagger\overline{\sigma}^\mu\partial_\mu\lambda \ . && (3.37)
\end{aligned}$$

The vector superfield should contain the gauge bosons and their fermionic superpartners. However, in equation (3.31) we find additional fields, for example a real scalar field a or a complex scalar field b. To remove these from the theory a "supergauge" transformation can be done. We may always redefine the vector superfield V like:

$$V \ \rightarrow \ V + i(\Omega^* - \Omega) \ , \tag{3.38}$$

[5]Note for example the relation $(\theta\theta b)^* = (\theta^\dagger\theta^\dagger b^*)$.

where Ω is a chiral superfield. It is obvious, that after this transformation the superfield V stays real and still forms a vector superfield. For a specific choice of Ω this transformation can be used to eliminate the fields a, b and ξ completely. We may write V in the so-called Wess-Zumino gauge:

$$V_{\text{WZ gauge}} \;=\; \theta\sigma^{\mu}\theta^{\dagger}A_{\mu} + \theta^{\dagger}\theta^{\dagger}\theta\lambda + \theta\theta\theta^{\dagger}\lambda^{\dagger} + \frac{1}{2}\theta\theta\theta^{\dagger}\theta^{\dagger}D. \tag{3.39}$$

Now, we are left with a vector field A_{μ}, its superpartner, a fermionic field, λ plus an additional auxiliary field D. Let us point out that this supergauge transformation simplifies to the usual gauge transformation for the vector field A_{μ}: The term in Ω that has the same coefficient as A_{μ}, *i.e.* $\theta\sigma^{\mu}\theta^{\dagger}$, is as we can find in equation (3.25), $\partial_{\mu}\phi$. Thus, the corresponding change of A_{μ} induced by equation (3.38) is:

$$V + i(\Omega^{*} - \Omega) \supset \theta\sigma^{\mu}\theta^{\dagger}A_{\mu} + i(i\theta\sigma^{\mu}\theta^{\dagger}\partial_{\mu}\phi^{*} + i\theta\sigma^{\mu}\theta^{\dagger}\partial_{\mu}\phi) = \theta\sigma^{\mu}\theta^{\dagger}(A_{\mu} - \partial_{\mu}(\phi^{*} + \phi)), \tag{3.40}$$

which correctly reproduces the known $U(1)$ gauge transformation of a vector field, if we choose ϕ to be real:

$$A_{\mu} \;\;\rightarrow\;\; A_{\mu} - 2\partial_{\mu}\phi \;. \tag{3.41}$$

Now we collected all fields that should appear in a supersymmetric field theory. The only thing left to do is to construct the Lagrangian and properly introduce gauge transformations in the superspace formalism.

3.2.3. Constructing a Lagrangian

In this section we demonstrate how Lagrangians are formed within the superspace formalism. An interesting Lagrangian needs kinetic terms, field strength tensors, has to be supersymmetric and (super)gauge invariant[6] and all fields of superpartners have to be present. Fortunately, the last condition is automatically fulfilled as the chiral and vector superfields always contain the superpartner by construction. For the rest, some careful steps must be taken which we explain here. We start by showing which contributions from superfields automatically give a supersymmetric invariant action and then discuss how to construct terms including the interactions of fields, field strength tensors and how

[6] Total derivatives after a supersymmetry transformation may remain, since they do not contribute to the action.

everything can be made gauge invariant, such that the gauge interactions are included. An action in the superfield formalism is given by:

$$A = \int d^4x \int d^2\theta d^2\theta^\dagger \, S(x, \theta, \theta^\dagger) \ , \tag{3.42}$$

and has to fulfill $\delta_\epsilon A = 0$ for supersymmetric invariance. The Lagrangian density $\mathcal{L}$ is then simply $\int d^2\theta d^2\theta^\dagger \, S(x, \theta, \theta^\dagger)$. Note the fact that a total derivative of $\mathcal{L}$ vanishes upon integration. It then follows immediately that every term of $\mathcal{L}$ that under supersymmetry transformations transforms into a total derivative may constitute a part of $\mathcal{L}$, since such a contribution automatically leaves the action supersymmetric invariant. Looking at a general vector superfield, for example, we can directly read off from equation (3.31) the part that survives an integration over the superfield coordinates:

$$[V]_D \ \equiv \ \int d^2\theta d^2\theta^\dagger \, V(x, \theta, \theta^\dagger) \ = \ V(x, \theta, \theta^\dagger)\Big|_{\theta\theta\theta^\dagger\theta^\dagger} = \ \frac{1}{2}D - \frac{1}{4}\partial_\mu\partial^\mu a \ . \tag{3.43}$$

By the transformation laws of the auxiliary field D, equation (3.37) we realize that this part indeed transforms into a total derivative and therefore forms an adequate candidate for the Lagrangian. We hence conclude that any vector superfield may contribute to $\mathcal{L}$ via this real "D-term" contribution. Note that a vector superfield does not have to be of the form given in equation (3.31). We can also form a real superfield using chiral superfields. The expression $\Phi^*\Phi$ for instance will be of great use later.

We may also find contributions to the action from chiral superfields. See equation (3.29) to note that also the auxiliary field F transforms into a total derivative under SUSY transformations. To single out this part of the chiral superfield when integrating over the complete superspace, we need to add a delta function for the $\theta^\dagger_{\dot\alpha}$ such that the integration does not give zero. This is called an F-term contribution:

$$[\Phi]_F \ \equiv \ \Phi\Big|_{\theta\theta} = \ \int d^2\theta \, \Phi\Big|_{\theta^\dagger=0} = \ \int d^2\theta d^2\theta^\dagger \, \delta^{(2)}(\theta^\dagger) \, \Phi \ = \ F, \tag{3.44}$$

and to have a real action we need to add the complex conjugate to A:

$$[\Phi]_F + \text{c.c.} \ = \ \int d^2\theta d^2\theta^\dagger \ \left[\delta^{(2)}(\theta^\dagger) \, \Phi + \delta^{(2)}(\theta) \, \Phi^*\right] \ . \tag{3.45}$$

We have now found two possibilities to construct supersymmetric invariant actions. Using only D- and F-term contributions from vector or chiral fields respectively, we ensure

that we end up with total derivatives after a SUSY transformation and have an invariant action. The task is now to use this recipe and build a meaningful theory by specifying the superfields. As a first step we construct the kinetic terms for chiral fields and their superpartners. For this we consider the shortly mentioned combination of chiral superfields $\Phi^*\Phi$ to form a vector superfield:

$$\begin{aligned}
\Phi^{*i}\Phi_j \;=\; & \phi^{*i}\phi_j + \sqrt{2}\theta\psi_j\phi^{*i} + \sqrt{2}\theta^\dagger\psi^{\dagger i}\phi_j + \theta\theta\phi^{*i}F_j + \theta^\dagger\theta^\dagger\phi_j F^{*i} \\
& + \theta\sigma^\mu\theta^\dagger\left[-i\phi^{*i}\partial_\mu\phi_j + i\phi_j\partial_\mu\phi^{*i} - \psi^{\dagger i}\overline{\sigma}_\mu\psi_j\right] \\
& + \frac{i}{\sqrt{2}}\theta\theta\theta^\dagger\overline{\sigma}^\mu(\psi_j\partial_\mu\phi^{*i} - \partial_\mu\psi_j\phi^{*i}) + \sqrt{2}\theta\theta\theta^\dagger\psi^{\dagger i}F_j \\
& + \frac{i}{\sqrt{2}}\theta^\dagger\theta^\dagger\theta\sigma^\mu(\psi^{\dagger i}\partial_\mu\phi_j - \partial_\mu\psi^{\dagger i}\phi_j) + \sqrt{2}\theta^\dagger\theta^\dagger\theta\psi_j F^{*i} \\
& + \theta\theta\theta^\dagger\theta^\dagger\Big[F^{*i}F_j + \frac{1}{2}\partial^\mu\phi^{*i}\partial_\mu\phi_j - \frac{1}{4}\phi^{*i}\partial^\mu\partial_\mu\phi_j - \frac{1}{4}\phi_j\partial^\mu\partial_\mu\phi^{*i} \\
& \quad + \frac{i}{2}\psi^{\dagger i}\overline{\sigma}^\mu\partial_\mu\psi_j + \frac{i}{2}\psi_j\sigma^\mu\partial_\mu\psi^{\dagger i}\Big]\,,
\end{aligned} \tag{3.46}$$

which is real for $i = j$. This expression is obtained by going back to equations (3.25) and (3.26) keeping in mind that $\theta\theta\theta^\dagger\theta^\dagger$ is the highest possible expansion term. To see that it is real, note for example relations like $(\theta\psi\phi^*)^* = (\theta^\dagger\psi^\dagger\phi)$. Equation (3.46) looks quite complicated at first sight, but remember that only D-term contributions will be important for the Lagrangian density from a vector superfield. We can simply read off the coefficients that survive an integration over the superspace coordinates:

$$[\Phi^*\Phi]_D = \int d^2\theta d^2\theta^\dagger\,\Phi^*\Phi \;=\; \partial^\mu\phi^*\partial_\mu\phi + i\psi^\dagger\overline{\sigma}^\mu\partial_\mu\psi + F^*F + \dots. \tag{3.47}$$

All other terms that are indicated by $\dots$ are total derivatives, such that they do not contribute to the action. The above expressions transforms into a total derivative under a SUSY transformation since it is a D-term contribution. Equation (3.47) contains chiral fermions $\psi, \psi^\dagger$ with their scalar superpartners ϕ, ϕ^* and the auxiliary field F.

To construct a meaningful F-term contribution, we point out, that products from chiral superfields are also chiral superfields. Thus, we may form combinations of chiral superfields, where we already drop the terms that will not appear in any F-term contribution to $\mathcal{L}$:

$$\Phi_i\Phi_j = \phi_i\phi_j + \sqrt{2}\theta(\psi_i\phi_j + \psi_j\phi_i) + \theta\theta(\phi_i F_j + \phi_j F_i - \psi_i\psi_j), \tag{3.48}$$

$$\begin{aligned}\Phi_i\Phi_j\Phi_k &= \phi_i\phi_j\phi_k + \sqrt{2}\theta(\psi_i\phi_j\phi_k + \psi_j\phi_i\phi_k + \psi_k\phi_i\phi_j) \\ &\quad + \theta\theta(\phi_i\phi_j F_k + \phi_i\phi_k F_j + \phi_j\phi_k F_i - \psi_i\psi_j\phi_k - \psi_i\psi_k\phi_j - \psi_j\psi_k\phi_i)\ .\end{aligned} \tag{3.49}$$

To bring this into a function for the Lagrangian density we need to include a summation over the free indices i, j, k. We therefore introduce two new objects M^{ij} and y^{ijk} which correspond to mass terms and Yukawa interactions of the interacting fields respectively. We define the scalar function, called the superpotential as[7]:

$$W = \frac{1}{2}M^{ij}\Phi_i\Phi_j + \frac{1}{6}y^{ijk}\Phi_i\Phi_j\Phi_k\ . \tag{3.50}$$

Now, we just add both terms and take their D- and F-contributions respectively. We end up with a Lagrangian for free fields with Yukawa interactions and mass terms:

$$\mathcal{L}(x) = [\Phi^{*i}\Phi_i]_D + ([W(\Phi_i)]_F + c.c.)\ . \tag{3.51}$$

We still have to eliminate the auxiliary, non-dynamical field F from the Lagrangians. This is done by solving for the equations of motion of F, obtained by a variation of A. These equations do not include any kinetic part, and we can simply express F by a combination of the other fields. The final result for $\mathcal{L}$ is then:

$$\begin{aligned}\mathcal{L} &= \partial^\mu\phi^{*i}\partial_\mu\phi_i - V(\phi,\phi^*) + i\psi^{\dagger i}\overline{\sigma}^\mu\partial_\mu\psi_i - \frac{1}{2}M^{ij}\psi_i\psi_j - \frac{1}{2}M^*_{ij}\psi^{\dagger i}\psi^{\dagger j} \\ &\quad -\frac{1}{2}y^{ijk}\phi_i\psi_j\psi_k - \frac{1}{2}y^*_{ijk}\phi^{*i}\psi^{\dagger j}\psi^{\dagger k}\ ,\end{aligned} \tag{3.52}$$

where $V(\phi,\phi^*)$ is:

$$\begin{aligned}&V(\phi,\phi^*) = \\ &M^*_{ik}M^{kj}\phi^{*i}\phi_j + \frac{1}{2}M^{in}y^*_{jkn}\phi_i\phi^{*j}\phi^{*k} + \frac{1}{2}M^*_{in}y^{jkn}\phi^{*i}\phi_j\phi_k + \frac{1}{4}y^{ijn}y^*_{kln}\phi_i\phi_j\phi^{*k}\phi^{*l}\ .\end{aligned} \tag{3.53}$$

Note that at this stage no gauge interactions are included and the theory is therefore still incomplete. Hence, our next task is to construct field strengths for the gauge fields

[7] The superpotential can in general be any holomorphic funtion of chiral superfields but the expression given here corresponds to reasonable phenomenology.

and afterwards enforce gauge invariance. To construct a field strength we introduce the following two objects:

$$\mathcal{W}_\alpha = -\frac{1}{4}D^\dagger D^\dagger D_\alpha V \ , \qquad \mathcal{W}^\dagger_{\dot\alpha} = -\frac{1}{4}DDD^\dagger_{\dot\alpha}V \ . \tag{3.54}$$

This definition seems arbitrary but a lengthy calculation of the F-term contribution shows the connection to usual field theories:

$$[\mathcal{W}^\alpha\mathcal{W}_\alpha]_F = D^2 + 2i\lambda\sigma^\mu\partial_\mu\lambda^\dagger - \frac{1}{2}F^{\mu\nu}F_{\mu\nu} + \frac{i}{4}\epsilon^{\mu\nu\rho\sigma}F_{\mu\nu}F_{\rho\sigma} \ . \tag{3.55}$$

We see the occurrence of the field strength tensor $F_{\mu\nu} = \partial_\mu A_\nu - \partial_\nu A_\mu$ and also find the kinetic terms of the superpartner λ to the vector field A_μ. The last term in equation (3.55) may be rewritten into a total derivative, such that we add to $\mathcal{L}$:

$$\frac{1}{4}([\mathcal{W}^\alpha\mathcal{W}_\alpha]_F + c.c) = \frac{1}{2}D^2 + i\lambda^\dagger\overline{\sigma}^\mu\partial_\mu\lambda - \frac{1}{4}F^{\mu\nu}F_{\mu\nu} \ . \tag{3.56}$$

Again, compared to the standard field theory case we get two additional fields: The auxiliary field D and the fermionic superpartner of the gauge fields, λ. We know already that this term possesses supersymmetric invariance, but is it also gauge invariant?

We first show, that the chiral fields $\mathcal{W}^\alpha$ are invariant under the gauge transformation for the vector superfield that we introduced already earlier:

$$\begin{aligned}
\mathcal{W}_\alpha \ \to \ -\frac{1}{4}D^\dagger D^\dagger D_\alpha\big[V + i(\Omega^* - \Omega)\big] &= \mathcal{W}_\alpha + \frac{i}{4}D^\dagger D^\dagger D_\alpha\Omega && (3.57)\\
&= \mathcal{W}_\alpha + \frac{i}{4}D^{\dagger\dot\beta}\big\{D^\dagger_{\dot\beta}, D_\alpha\big\}\Omega && (3.58)\\
&= \mathcal{W}_\alpha - \frac{1}{2}\sigma^\mu_{\alpha\dot\beta}\partial_\mu D^{\dagger\dot\beta}\Omega && (3.59)\\
&= \mathcal{W}_\alpha \ . && (3.60)
\end{aligned}$$

In the first step we ust that Ω^* is right-chiral. The second step is correct since Ω is left-chiral; then we used the anti-commutators of the covariant derivatives (see appendix) and again that Ω is left-chiral. Keeping equation (3.40), the supergauge transformation of a vector field A_μ, in mind we can reproduce the well-known $U(1)$ gauge transformations for our system of chiral, scalar and vector fields appearing in the superfields, when we define the (super)gauge transformations for chiral superfields to be:

$$\Phi_i \ \to \ e^{2igq_i\Omega}\Phi_i, \qquad \Phi^{*i} \ \to \ e^{-2igq_i\Omega^*}\Phi^{*i} \ . \tag{3.61}$$

This would simply be a phase rotation for $\Omega = \phi$ Let us now see, if the other parts of the Lagrangian are gauge invariant. The F-term contribution from the superpotential is only gauge-invariant if we enforce the conditions that either $q_i + q_j = 0$ or $M^{ij} = 0$, and likewise, $q_i + q_j + q_k = 0$ or otherwise $y^{ijk} = 0$. This basically corresponds to charge conservation at each vertex; in any other case the interaction is simply forbidden[8]. The only part left that is not gauge-invariant is the D-term contribution:

$$\Phi^{*i}\Phi_i \quad \rightarrow \quad e^{2igq_i(\Omega-\Omega^*)}\Phi^{*i}\Phi_i \ . \tag{3.62}$$

This can be cured when we redefine the D-term:

$$\left[\Phi^{*i}e^{2gq_iV}\Phi_i\right]_D \ , \tag{3.63}$$

and remember the transformation of the vector superfield V, equation (3.38), which exactly cancels the part left over in equation (3.62). An expansion of the exponential stops after the second polynomial when we go to the Wess-Zumino gauge, see equation (3.39):

$$V^2 = \frac{1}{2}\theta\theta\theta^\dagger\theta^\dagger A_\mu A^\mu, \tag{3.64}$$

$$V^n = 0 \qquad (n \geq 3) \ . \tag{3.65}$$

We therefore find:

$$e^{2gq_iV} = 1 + 2gq_i(\theta\sigma^\mu\theta^\dagger A_\mu + \theta^\dagger\theta^\dagger\theta\lambda + \theta\theta\theta^\dagger\lambda^\dagger + \frac{1}{2}\theta\theta\theta^\dagger\theta^\dagger D) + g^2q_i^2\theta\theta\theta^\dagger\theta^\dagger A_\mu A^\mu \ , \tag{3.66}$$

such that the D-term contribution finally reads as:

$$\begin{aligned}\left[\Phi^{*i}e^{2gq_iV}\Phi_i\right]_D &= F^{*i}F_i + \nabla_\mu\phi^{*i}\nabla^\mu\phi_i + i\psi^{\dagger i}\overline{\sigma}^\mu\nabla_\mu\psi_i - \sqrt{2}gq_i(\phi^{*i}\psi_i\lambda + \lambda^\dagger\psi^{\dagger i}\phi_i) \\ &\quad + gq_i\phi^{*i}\phi_i D \ ,\end{aligned} \tag{3.67}$$

where we introduced the gauge covariant derivatives:

$$\nabla_\mu\phi_i = \partial_\mu\phi_i + igq_iA_\mu\phi_i, \qquad \nabla_\mu\phi^{*i} = \partial_\mu\phi^{*i} - igq_iA_\mu\phi^{*i}, \tag{3.68}$$

$$\nabla_\mu\psi_i = \partial_\mu\psi_i + igq_iA_\mu\psi_i \ . \tag{3.69}$$

[8]Equivalently: Interacting Φ_i and Φ_j have to transform under the gauge group in conjugate representations.

A complete, supersymmetric and gauge invariant Lagrangian that contains gauge and Yukawa interaction plus mass terms is then finally given by[9]:

$$\mathcal{L} \;=\; \left[\Phi^{*i} e^{2g q_i V} \Phi_i\right]_D + \left([W(\Phi_i)]_F + \text{c.c.}\right) + \frac{1}{4}\left([\mathcal{W}^\alpha \mathcal{W}_\alpha]_F + \text{c.c.}\right) \;. \tag{3.70}$$

To generalize to the non-abelian case, we need to alter the transformation rules slightly. Assuming that the matrix generators of the gauge transformation are T_i^{aj} when the chiral superfield is in a representation R, it is instructive to define the gauge transformation for a chiral superfield Φ as:

$$\Phi_i \to \left(e^{2ig_a \Omega^a T^a}\right)_i{}^j \Phi_j, \qquad\qquad \Phi^{*i} \to \Phi^{*j}\left(e^{-2ig_a \Omega^a T^a}\right)_j{}^i \;, \tag{3.71}$$

and redefine the D-term accordingly to:

$$\mathcal{L} \;=\; \left[\Phi^{*i}(e^{2g_a T^a V^a})_i{}^j \Phi_j\right]_D \;. \tag{3.72}$$

The gauge fields appear as before in the vector superfields V^a. Now, however, there is one gauge boson with its superpartner, the gaugino, for each generator T^a of the gauge group. When we define $V_i{}^j = 2g_a T_i^{aj} V^a$ and $\Omega_i{}^j \;=\; 2g_a T_i^{aj}\Omega^a$ as matrix-valued superfields we find that for gauge invariance the gauge transformation of V^a has to be:

$$e^V \;\to\; e^{i\Omega^\dagger} e^V e^{-i\Omega} \;, \tag{3.73}$$

which, when expanded, translates into the transformation of V^a:

$$V^a \;\to\; V^a + i(\Omega^{a*} - \Omega^a) + g_a f^{abc} V^b (\Omega^{c*} + \Omega^c) - \frac{i}{3} g_a^2 f^{abc} f^{cde} V^b V^d (\Omega^{e*} - \Omega^e) + \tag{3.74}$$

where the structure constants $[T^a, T^b] = i f^{abc} T^c$ have been inserted. The complete D-term contribution is therefore gauge invariant in the non-abelian case. For an invariant F-term we need to generalize the definition of the field-strength chiral superfields $\mathcal{W}_\alpha$:

$$\mathcal{W}_\alpha \;=\; -\frac{1}{4} D^\dagger D^\dagger \left(e^{-V} D_\alpha e^V\right) \;, \tag{3.75}$$

[9]Since we are not talking about supersymmetry breaking mechanisms in this thesis, we neglected a possible Fayet-Iliopoulos term in our discussion.

which transforms under supergauge transformations like:

$$\mathcal{W}_\alpha \;\rightarrow\; e^{i\Omega}\mathcal{W}_\alpha e^{-i\Omega}\ , \tag{3.76}$$

when expression (3.73) is used. In the Wess-Zumino gauge, we find $\mathcal{W}_\alpha$ to be:

$$(\mathcal{W}^a_\alpha)_{\text{WZ gauge}} \;=\; \lambda^a_\alpha + \theta_\alpha D^a + \frac{i}{2}(\sigma^\mu\overline{\sigma}^\nu\theta)_\alpha F^a_{\mu\nu} + i\theta\theta(\sigma^\mu\nabla_\mu\lambda^{\dagger a})_\alpha\ , \tag{3.77}$$

and the complete gauge-invariant F-term contribution:

$$[\mathcal{W}^{a\alpha}\mathcal{W}^a_\alpha]_F \;=\; D^aD^a + 2i\lambda^a\sigma^\mu\nabla_\mu\lambda^{\dagger a} - \frac{1}{2}F^{a\mu\nu}F^a_{\mu\nu} + \frac{i}{4}\epsilon^{\mu\nu\rho\sigma}F^a_{\mu\nu}F^a_{\rho\sigma}\ . \tag{3.78}$$

Then, we have the complete non-abelian gauge invariant Lagrangian density:

$$\mathcal{L} \;=\; \frac{1}{4}\left[\mathcal{W}^{a\alpha}\mathcal{W}^a_\alpha\right]_F + \text{c.c.} + \left[\Phi^{*i}(e^{2g_aT^aV^a})_i{}^j\Phi_j\right]_D + \left([W(\Phi_i)]_F + \text{c.c.}\right)\ , \tag{3.79}$$

where we only allow for those terms in the superpotential that are gauge invariant[10].

3.3. The minimal supersymmetric standard model

In this section we present the minimal supersymmetric standard model (MSSM). In the last section we described how supersymmetric Lagrangians can be constructed and identified occurring fields with usual fermions or bosons and their superpartners. Now we explicitly build the minimal supersymmetric extension of the standard model. The gauge group stays unchanged: $SU(3)_C \times SU(2)_L \times U(1)_Y$. The task is to specify all necessary fields and the superpotential to obtain phenomenologically valid interactions. Since SUSY must be broken, we also have to add explicit mass terms for the superfields. After defining the theory, we will see how electroweak symmetry is spontaneously broken and introduce a measure of tuning to quantify how well the correct electroweak scale is reproduced. Performing a numerical analysis asks for a reduction of the large number of new parameters, which will lead us to the phenomenological MSSM (pMSSM).

[10]Since we are not considering CP violating effects we neglected a possible CP-violating parameter here.

Names		spin 0	spin 1/2	$SU(3)_C$, $SU(2)_L$, $U(1)_Y$
squarks, quarks	Q	$(\widetilde{u}_L \;\; \widetilde{d}_L)$	$(u_L \;\; d_L)$	$(\mathbf{3}, \mathbf{2}, \frac{1}{6})$
($\times$3 families)	$\overline{u}$	$\widetilde{u}_R^*$	$u_R^\dagger$	$(\overline{\mathbf{3}}, \mathbf{1}, -\frac{2}{3})$
	$\overline{d}$	$\widetilde{d}_R^*$	$d_R^\dagger$	$(\overline{\mathbf{3}}, \mathbf{1}, \frac{1}{3})$
sleptons, leptons	L	$(\widetilde{\nu} \;\; \widetilde{e}_L)$	$(\nu \;\; e_L)$	$(\mathbf{1}, \mathbf{2}, -\frac{1}{2})$
($\times$3 families)	$\overline{e}$	$\widetilde{e}_R^*$	$e_R^\dagger$	$(\mathbf{1}, \mathbf{1}, 1)$
Higgs, higgsinos	H_u	$(H_u^+ \;\; H_u^0)$	$(\widetilde{H}_u^+ \;\; \widetilde{H}_u^0)$	$(\mathbf{1}, \mathbf{2}, +\frac{1}{2})$
	H_d	$(H_d^0 \;\; H_d^-)$	$(\widetilde{H}_d^0 \;\; \widetilde{H}_d^-)$	$(\mathbf{1}, \mathbf{2}, -\frac{1}{2})$

Table 3.1.: Chiral supermultiplets in the MSSM [50].

3.3.1. Field content

In table 3.1 and 3.2 we list the field content of the MSSM. The fields are written in so-called supermultiplets that are basically extensions of the SM multiplets including additionally the corresponding superpartners. There are chiral supermultiplets containing a two-component Weyl fermion and a complex scalar field and gauge supermultiplets that contain a vector boson and its fermionic partner. Scalar superpartners for every fermion (sfermions) and fermionic superpartners (gauginos) for every gauge boson of the Standard Model are now present. Hence, we have squarks like the stop or sleptons like the stau as superpartners of the top-quark and the tau-lepton, respectively. For a consistent theory, the Higgs sector has to be extended by adding another Higgs-doublet. This has two reasons: Anomaly cancellation asks for an even number of fermions in the theory. If there was only one Higgs-doublet, we would introduce only one additional fermion (the higgsino) which would then spoil the anomaly cancellations. This is cured by adding a second Higgs-doublet with a second fermionic superpartner and opposite third component of the weak hypercharge T^3. Besides, we need two Higgs doublets to give masses to all the fermions since the superpotential is constrained in its form[11].

Note that the neutralino, our dark matter candidate, is a mixed state of the neutral gauginos (bino $\widetilde{B}$ and neutral wino $\widetilde{W}^0$) and the two neutral higgsinos $\widetilde{H}_d^0$ and $\widetilde{H}_u^0$:

$$\widetilde{\chi} = N_{11}\widetilde{B}^0 + N_{12}\widetilde{W}^0 + N_{13}\widetilde{H}_d^0 + N_{14}\widetilde{H}_u^0 \;\; . \tag{3.80}$$

[11]Remember: It may only be a function of chiral superfields.

Names	spin 1/2	spin 1	$SU(3)_C$, $SU(2)_L$, $U(1)_Y$
gluino, gluon	$\widetilde{g}$	g	(**8**, **1** , 0)
winos, W bosons	$\widetilde{W}^{\pm}$ $\widetilde{W}^{0}$	$W^{\pm}$ W^{0}	(**1**, **3** , 0)
bino, B boson	$\widetilde{B}^{0}$	B^{0}	(**1**, **1** , 0)

Table 3.2.: Gauge supermultiplets in the MSSM [50].

3.3.2. The superpotential and R-parity

In this subsection we briefly discuss the superpotential of the MSSM. As we mentioned in subsection 3.2.3 there is freedom involved in constructing this part of the Lagrangian. All terms built from chiral superfields that are gauge invariant are in principal allowed. To give a reasonable phenomenology the superpotential of the MSSM is defined as:

$$W_{\text{MSSM}} = \overline{u}\mathbf{y_u}QH_u - \overline{d}\mathbf{y_d}QH_d - \overline{e}\mathbf{y_e}LH_d + \mu H_u H_d \,. \tag{3.81}$$

Here, $\mathbf{y_u}, \mathbf{y_d}$ and $\mathbf{y_e}$ are 3×3 matrices that contain the Yukawa couplings and H_u, H_d, Q, L, $\overline{u}$, $\overline{d}$, $\overline{e}$ are chiral superfields corresponding to the supermultiplets in table 3.1. The last term in (3.81) is called the μ-term and gives masses to the gauginos. Let us see which kind of interactions are included in this superpotential by considering the arising interactions of the term $\overline{u}\mathbf{y_u}QH_u = \overline{u}^{ia}\,(\mathbf{y_u})_i{}^j\,Q_{j\alpha a}\,(H_u)_\beta \epsilon^{\alpha\beta}$ when assuming that the Yukawa matrix has only one vanishing entry at the (3,3)-component. We will now neglect the color index a and with the assumption just made, we can set the family indices i, j to 3. Then, only a summation over the $SU(2)_L$ indices $\alpha, \beta = 1, 2$ remains[12] and the emerging interactions, when following the recipe introduced in subsection 3.2.3, are:

$$\begin{aligned} &\widetilde{t}^{*}_R y_t \widetilde{t}_L H^0_u \,, \qquad &&\widetilde{t}^{*}_R y_t t_L \widetilde{H}^0_u \,, \\ &t^{\dagger}_R y_t \widetilde{t}_L \widetilde{H}^0_u \,, \qquad &&t^{\dagger}_R y_t t_L H^0_u \,. \end{aligned}$$

We find Higgs-quark-quark couplings as in the Standard Model but additional squark-Higgs-squark and squark-Higgsino-quark couplings that are all equal in strength. There are four additional vertices when we make the replacements $H^0_u \to H^+_u$ and $t_L \to -b_L$ (with possible tildes). Note also, that masses arising from these couplings, when the up-type Higgs boson acquires a vacuum expectation value (VEV), are identical for quarks

[12] $SU(2)_L$ indices are also contracted by $\epsilon_{\alpha\beta}$.

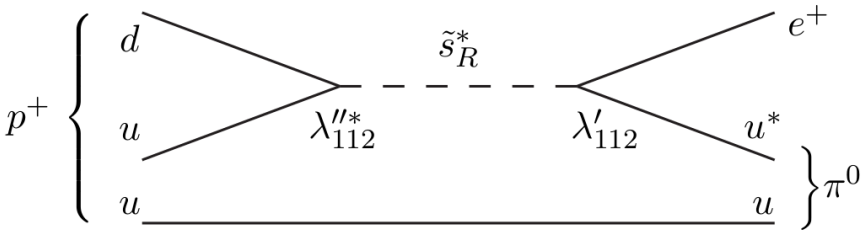

Figure 3.1.: Proton decay arising from possible L- and B-violating terms in the superpotential. This motivates the introduction of R-parity [50].

and squarks. To explain the splitting of the masses we hence need to introduce explicit mass terms for the superparticles, see section 3.3.3

The form of the superpotential is our free choice as long as it respects the phenomenology. There are further terms possible that would also respect gauge invariance, like:

$$W_{\Delta \mathrm{L}=1} = \frac{1}{2}\lambda^{ijk} L_i L_j \overline{e}_k + \lambda'^{ijk} L_i Q_j \overline{d}_k + \mu'^i L_i H_u \tag{3.82}$$

$$W_{\Delta \mathrm{B}=1} = \frac{1}{2}\lambda''^{ijk} \overline{u}_i \overline{d}_j \overline{d}_k \ . \tag{3.83}$$

However, these would lead to proton decay, as they violate baryon number B and lepton number L (see figure 3.1). Instead of simply neglecting and not including these terms in the superpotential, a forbidding symmetry is introduced. This "R-parity" is a multiplicative conserved quantum number defined as:

$$P_R = (-1)^{3(\mathrm{B}-\mathrm{L})+2s} \ . \tag{3.84}$$

With this definition, Standard Model particles have $P_R = +1$ and all superpartners $P_R = -1$. There are three immediate consequences: The lightest supersymmetric particle (LSP) is stable as a decay into SM particles is forbidden. The LSP is therefore a good dark matter candidate. SUSY particles may also only be produced in pairs at colliders and will always decay into an odd number of LSP's in the final state.

3.3.3. Soft supersymmetry breaking terms

As we just noticed, superpartners have by construction the same mass. If this was the case, however, SUSY particles should have been observed already at colliders, which is not the case. To separate the SUSY and the SM particle masses we need to introduce explicit mass terms in the Lagrangian. This is done by introducing so-called soft terms, which do not spoil the removal of quadratic loop divergences when calculating the self-energy of the Higgs boson. The most general soft SUSY breaking part of the Lagrangian is given by:

$$\begin{aligned}\mathcal{L}_{\text{soft}}^{\text{MSSM}} &= -\frac{1}{2}\left(M_3\widetilde{g}\widetilde{g} + M_2\widetilde{W}\widetilde{W} + M_1\widetilde{B}\widetilde{B} + \text{c.c.}\right) \\ &\quad -\left(\widetilde{\overline{u}}\,\mathbf{a_u}\,\widetilde{Q}H_u - \widetilde{\overline{d}}\,\mathbf{a_d}\,\widetilde{Q}H_d - \widetilde{\overline{e}}\,\mathbf{a_e}\,\widetilde{L}H_d + \text{c.c.}\right) \\ &\quad -\widetilde{Q}^\dagger\,\mathbf{m_Q^2}\,\widetilde{Q} - \widetilde{L}^\dagger\,\mathbf{m_L^2}\,\widetilde{L} - \widetilde{\overline{u}}\,\mathbf{m_{\overline{u}}^2}\,\widetilde{\overline{u}}^\dagger - \widetilde{\overline{d}}\,\mathbf{m_{\overline{d}}^2}\,\widetilde{\overline{d}}^\dagger - \widetilde{\overline{e}}\,\mathbf{m_{\overline{e}}^2}\,\widetilde{\overline{e}}^\dagger \\ &\quad - m_{H_u}^2 H_u^* H_u - m_{H_d}^2 H_d^* H_d - (bH_uH_d + \text{c.c.})\,. \end{aligned} \tag{3.85}$$

Here, $\widetilde{g}$ is the gluino, $\widetilde{W}$ the wino and $\widetilde{B}$ the bino field with corresponding mass parameters M_3, M_2, M_1. The matrices $\boldsymbol{a_i}$ are generalizations of the Yukawa interactions and are called A-terms. The fields $\widetilde{Q}, \widetilde{L}, \widetilde{Q}, H_d, H_u, \widetilde{\overline{u}}, \widetilde{\overline{d}}, \widetilde{\overline{e}}$ denote the scalar and gaugino fields only and not their superpartners. Matrices $\boldsymbol{m_i}$ are mass matrices for the corresponding fields, b is the bilinear coupling of the Higgs sector, and m_{H_u} and m_{H_d} mass terms for the Higgs fields.

3.4. Electroweak symmetry breaking

In this section we summarize how electroweak symmetry breaking takes place in the MSSM. The key features are to understand which parameters determine the Z- and h-boson masses. During the symmetry breaking both scalar Higgses acquire a VEV when the potential develops a minimum, which then gives masses to the aforementioned bosons. We hence need to start with the scalar potential:

$$\begin{aligned} V &= (|\mu|^2 + m_{H_u}^2)(|H_u^0|^2 + |H_u^+|^2) + (|\mu|^2 + m_{H_d}^2)(|H_d^0|^2 + |H_d^-|^2) \\ &\quad + [b\,(H_u^+ H_d^- - H_u^0 H_d^0) + \text{c.c.}] \\ &\quad + \frac{1}{8}(g^2 + g'^2)(|H_u^0|^2 + |H_u^+|^2 - |H_d^0|^2 - |H_d^-|^2)^2 + \frac{1}{2}g^2|H_u^+ H_d^{0*} + H_u^0 H_d^{-*}|^2. \end{aligned} \tag{3.86}$$

Due to the $SU(2)_L$ symmetry we may rotate the fields in such a way that on Higgs field has a vanishing VEV. In order to avoid charge breaking minima this is taken to be $\langle H_u^- \rangle$. Calculating the minimization condition $\partial V/\partial H_u^- = 0$ we then find that $\langle H_d^+ \rangle$ must also vanish[13]. Thus, only the neutral charge Higgs boson fields will take a non-zero VEV. The scalar potential simplifies to:

$$\begin{aligned} V &= (|\mu|^2 + m_{H_u}^2)|H_u^0|^2 + (|\mu|^2 + m_{H_d}^2)|H_d^0|^2 - (b\, H_u^0 H_d^0 + \text{c.c.}) \\ &\quad + \frac{1}{8}(g^2 + g'^2)(|H_u^0|^2 - |H_d^0|^2)^2. \end{aligned} \tag{3.87}$$

Note here, that the potential depends on four input parameters $(\mu, m_{H_u}, m_{H_d}, b)$ and that b can be chosen to be real as a phase can be absorbed by a redefinition of the Higgs fields. This potential is bounded from below in most of the cases. The quartic couplings will dominate and assure that the potential is greater than zero for large values of the fields. A special case, called D-flat directions, may occur when $|H_u^0| = |H_d^0|$, *i.e.* vanishing quartic couplings. In that case we need to fulfill $2|\mu|^2 + m_{H_u}^2 + m_{H_d}^2 - 2b > 0$ for stability.

For EWSB to occur we need a saddle point in the potential at $H_u = H_d = 0$ and get another condition on the mass parameters from:

$$\det \left| \frac{\partial^2 V_H}{\partial H_i^0 \partial H_j^0} \right| < 0 \;\; \Rightarrow \;\; (|\mu|^2 + m_{H_u}^2)(|\mu|^2 + m_{H_d}^2) < b^2 \tag{3.88}$$

Now a close connection between EWSB and SUSY breaking can be seen. If we assume both soft SUSY masses m_{H_u}, m_{H_d} to be zero we immediately run into problems since both conditions cannot be fulfilled at the same time. If we want to break the electroweak symmetry, we hence also have to break supersymmetry. Finally we can start to find the minima of the simplified scalar potential, equation (3.87). Calculating both minimization conditions $\partial V/\partial H_u^0 = \partial V/\partial H_d^0 = 0$, giving VEV's to both scalar fields and using the relation from the Standard Model:

$$v_u^2 + v_d^2 = v^2 = \frac{2M_Z^2}{g^2 + g'^2} \;\; , \tag{3.89}$$

[13]Note that we only talk about tree-level relations in this chapter and that charge breaking minima are not generally excluded in the MSSM.

and introducing $\tan\beta = \frac{v_u}{v_d}$, we can express the two arising conditions as follows:

$$m_{H_u}^2 + |\mu|^2 - b\cot\beta - (m_Z^2/2)\cos(2\beta) \;=\; 0, \tag{3.90}$$

$$m_{H_d}^2 + |\mu|^2 - b\tan\beta + (m_Z^2/2)\cos(2\beta) \;=\; 0\ , \tag{3.91}$$

and use these to write for m_Z:

$$\sin(2\beta) \;=\; \frac{2b}{m_{H_u}^2 + m_{H_d}^2 + 2|\mu|^2}, \tag{3.92}$$

$$m_Z^2 \;=\; \frac{|m_{H_d}^2 - m_{H_u}^2|}{\sqrt{1-\sin^2(2\beta)}} - m_{H_u}^2 - m_{H_d}^2 - 2|\mu|^2\ . \tag{3.93}$$

This important equation (3.93) will be the starting point for our fine-tuning definition.

It is also interesting to solve for the Higgs boson masses. The two complex Higgs doublets have eight degrees of freedom. Three of them will become massless Goldstone bosons by Goldstone's theorem, such that five physical Higgs fields will remain. If we develop the Higgs fields around the vacuum into real and imaginary parts and perform a rotation into the mass eigenstates, we find for the tree-level masses of the five Higgs bosons:

$$m_{A^0}^2 \;=\; 2b/\sin(2\beta) \;=\; 2|\mu|^2 + m_{H_u}^2 + m_{H_d}^2 \tag{3.94}$$

$$m_{h^0,H^0}^2 \;=\; \frac{1}{2}\Big(m_{A^0}^2 + m_Z^2 \mp \sqrt{(m_{A^0}^2 - m_Z^2)^2 + 4m_Z^2 m_{A^0}^2\sin^2(2\beta)}\Big), \tag{3.95}$$

$$m_{H^\pm}^2 \;=\; m_{A^0}^2 + m_W^2. \tag{3.96}$$

Note that the light Higgs boson mass is bounded from above to be smaller than $m_Z|\cos 2\beta|$ and sizable loop corrections need to be present to rise its value into the region where current experimental limits are respected. The largest contribution comes from stop loops and is given by:

$$m_h^2 \approx m_Z^2\cos^2 2\beta + \frac{3m_t^4}{(4\pi)^2\,v^2}\left[\ln\frac{m_{\tilde{t}}^2}{m_t^2} + \frac{X_t^2}{m_{\tilde{t}}^2}\left(1 - \frac{X_t^2}{12m_{\tilde{t}}^2}\right)\right] \quad , \tag{3.97}$$

with $X_t = A_t - \mu\cot\beta$ and $m_{\tilde{t}} = \sqrt{m_{\tilde{t}_1}\,m_{\tilde{t}_2}}$, the SUSY scale [52]. One can see that heavy stops and a large mixing parameter X_t are necessary to increase the Higgs mass.

3.5. Fine-tuning

Equation (3.93) demands for mass parameters at the order of the weak scale to naturally create the correct Z-mass. Otherwise two large quantities would be subtracted from each other and the Z-mass would in this sense be tuned. This has been quantified by introducing a fine-tuning measure defined as the sensitivity of the Z-mass [26, 27]:

$$\Delta p_i \equiv \left| \frac{p_i}{M_Z^2} \frac{\partial M_Z^2(p_i)}{\partial p_i} \right| = \left| \frac{\partial \ln M_Z^2(p_i)}{\partial \ln p_i} \right| \ . \tag{3.98}$$

This quantity serves as a qualitative indicator how well a specific SUSY scenario can solve the hierarchy problem of the Standard Model or, equivalently, how large the SUSY and electroweak symmetry breaking scales are separated. The parameters p_i that determine the Z-mass on tree-level are μ, the two soft Higgs mass parameters m_{H_u} and m_{H_d} and the bilinear coupling b. We define the total measure of fine-tuning:

$$\Delta_{\text{tot}} \equiv \sqrt{\sum_{p_i=\mu^2,b,m_{H_u}^2,m_{H_d}^2} \{\Delta p_i\}^2} \ , \tag{3.99}$$

with the individual Δp_i's obtained as in reference [53]:

$$\Delta\mu^2 = \frac{4\mu^2}{m_Z^2}\Big(1 + \frac{m_A^2 + m_Z^2}{m_A^2} \tan^2 2\beta\Big) \ , \tag{3.100}$$

$$\Delta b = \Big(1 + \frac{m_A^2}{m_Z^2}\Big) \tan^2 2\beta \ , \tag{3.101}$$

$$\Delta m_{H_u}^2 = \Big|\frac{1}{2}\cos 2\beta + \frac{m_A^2}{m_Z^2}\cos^2\beta - \frac{\mu^2}{m_Z^2}\Big|\Big(1 - \frac{1}{\cos 2\beta} + \frac{m_A^2+m_Z^2}{m_A^2}\tan^2 2\beta\Big) \ , \tag{3.102}$$

$$\Delta m_{H_d}^2 = \Big| -\frac{1}{2}\cos 2\beta + \frac{m_A^2}{m_Z^2}\sin^2\beta - \frac{\mu^2}{m_Z^2}\Big|\Big(1 + \frac{1}{\cos 2\beta} + \frac{m_A^2+m_Z^2}{m_A^2}\tan^2 2\beta\Big) . \tag{3.103}$$

These are only tree-level computations,have often been extended in the literature. In reference [53], for example, the fine-tuning of the Z-mass is quantified by the ratio between stop loop contributions to m_Z and m_Z itself:

$$\Delta_t = \left| \frac{\delta_t M_Z^2}{M_Z^2} \right| \ , \tag{3.104}$$

with $\delta_t M_Z^2 \approx -\delta_{m_{H_u}^2}(1 - 1/\cos 2\beta)$, where $\delta_{m_{H_u}^2}$ is the loop correction to the up-type Higgs from stop loops, given by:

$$\delta_{m_{H_u}^2} \approx \frac{3y_t^2}{16\pi^2}\left(m_{\widetilde{Q}_3}^2 + m_{\widetilde{t}}^2 + A_t^2\right)\log\left(\frac{2\Lambda^2}{m_{\widetilde{Q}_3}} + m_{\widetilde{t}}^2\right) \quad , \tag{3.105}$$

where Λ is the cut-off scale of the logarithmic divergence. Here, a cut-off scale must be chosen and a scale-dependence of the fine-tuning value cannot be avoided. This shows, that the exact value of fine-tunings has no physical meaning, but depends strongly on the definition. A similar scale-dependence can be found in reference [32], where leading log contributions to the Z-mass have been included to calculate the fine-tuning analogously to equation (3.99). These contributions are always proportional to the logarithm of the cut-off scale Λ, $X \equiv \log(\Lambda/\Lambda_{\mathrm{SUSY}})$, which is usually set to 3. Then, their minimal tuning level is always larger than $\Delta_{\mathrm{tot}} \approx 50$. In our work we only concentrate on the low-energy phenomenology of supersymmetry and the cut-off scale is the SUSY scale per definition. Therefore leading log terms of fine-tuning vanish and the fine-tuning will generally be smaller.

Apart from the sensibility of the Z-mass, a Higgs mass tuning may also be considered and defined equivalently to equation (3.98). This has been discussed in reference [52] and found to be of order 100 already. However, we want to point out again that a scale dependence cannot be avoided. Another discussions of fine-tuning in the Higgs sector may be found in reference [54].

Next to this parameter-tuning we will discuss an equation-tuning in order to quantify possible cancellations that may lead to "unnaturally" small predictions for an observable. Since these relations may only be exact on a specific hypersurface of the parameter space, we take the viewpoint that being close to this surface is an instance of tuning. We will apply this to the direct detection cross section of neutralino dark matter and define its tuning measure analogously to the Z-mass tuning to cope with both tunings on equal footing. The implications are discussed in section 5.6. For completeness:

$$\Delta \mathrm{f_i} \equiv \left|\frac{\partial \ln \sigma^{\mathrm{SI}}(p_i)}{\partial \ln p_i}\right| \quad , \tag{3.106}$$

with $p_i = \{\mu, \tan\beta, M_1, M_2, m_A\}$, see also [55].

3.6. The phenomenological MSSM

To study the MSSM parameter space one needs to make some assumptions and/or simplifications on the parameters, as it is not yet possible to conduct a complete analysis taking all 105 free additional parameters into account. Many simplified models of the MSSM exist. For example, in the constrained MSSM (CMSSM) parameters are assumed to fulfill some GUT relations, such that only five input parameters at the GUT scale remain and are evolved down to the electroweak scale by renormalization group evolution. Extensive studies have been done and can be found here: [56–58]. However, these models clearly put very strong constraints on the SUSY parameter space and do not represent the full possibilities of the MSSM.

We will therefore take a closer look at the so-called phenomenological MSSM (pMSSM) that has 22 input parameters at the SUSY scale. It is motivated by the existent strong constraints on flavor changing neutral currents (FCNC) and CP-violation effects for theories beyond the Standard Model. Measurements in these sectors already show a very good agreement with theoretical predictions from the Standard Model, such that new contributions must be significantly suppressed in new theories. To respect these bounds in the MSSM, the phenomenological MSSM (pMSSM) was constructed in a way that there are no new phases of CP violation, which means that the parameters are real, and no possible FCNC at tree level emerge, by demanding the sfermion mass matrices of the first two generations to be diagonal. Also, degeneracy of the first two sfermion generations is assumed, such that after a careful count a total number of 22 variables is left over: three gaugino masses M_1, M_2, M_3; six masses of the squarks $m_{\tilde{q}_L}, m_{\tilde{Q}_L}, m_{\tilde{u}_R}, m_{\tilde{d}_R}, m_{\tilde{t}_R}, m_{\tilde{b}_R}$, four slepton masses $m_{\tilde{l}_L}, m_{\tilde{L}_L}, m_{\tilde{e}_R}, m_{\tilde{\tau}_R}$, two Higgs mass parameters[14] $m^2_{H_u}, m^2_{H_d}$, the ratio of their VEV's $\tan\beta = \frac{v_1}{v_2}$, and six trilinear couplings $A_u, A_d, A_t, A_b, A_e, A_\tau$.

For existing studies of the pMSSM, we point toward a number of papers [28–32] and want to stress that, in general, a careful examination of the neutralino mass range under 200 GeV is missing in the literature and a negative μ-term has always been neglected. Also there has been no work that investigated how direct detection experiments test the natural SUSY parameter space.

[14] Note that these may be exchange for μ and the pseudo-Higgs boson mass m_A

4. The Scan

This chapter contains details about our scanning method. We explain shortly the working procedures of the used programs and discuss our parameters and their ranges. Also the applied constraints arising from cosmology, colliders and direct dark matter searches are presented and examples are given how they can cut into the (natural) supersymmetric parameter space.

4.1. Utilities and scanning method

Observables of interest include especially the cosmological abundance Ωh^2 and the spin-independent neutralino-proton cross-section σ^{SI}. Both are calculated by the C-program `micrOMEGAs 2.4.5` [59] which will also give us the individual annihilation channels of each scenario. We will only pay attention to the dominant mechanism in our analysis. It is clear that for a correct calculation of these quantities we need the supersymmetric mass spectrum and mixing angles which are obtained by the FORTRAN code `SuSpect 2.41` [60]. The leptonic observables that we apply as constraints are evaluated by the C-program `SuperIso 3.0` [61] at two loop precision and explained in section 4.3.

In section 3.6 we presented the low energy model of the MSSM that we will examine, the pMSSM. As already explained, this model is defined at the SUSY scale. No assumptions are made on SUSY breaking mechanisms or on possible relations arising from a grand unified theory (GUT). We choose eleven free low-energy input parameters defined at the SUSY scale with the ranges that we will give in section 4.2. The SUSY scale is hereby defined as $\Lambda_{\mathrm{SUSY}} = \sqrt{m_{\tilde{t}_1} m_{\tilde{t}_2}}$. The first step, the calculation of the spectrum, involves an iteration algorithm. This is necessary, because, for example, the SUSY scale is not known from the start: Since we use soft SUSY breaking terms as input parameters the physical stop masses are not known at the beginning. This iteration includes renormalization group evolution from the SUSY scale down to the electroweak symmetry breaking (EWSB) scale and back, as long as stability to a satisfying precision is reached. The full two-loop RGE's are applied here for the evolution between Λ_{SUSY} and Λ_{EWSB}. During this procedure

`SuSpect` performs consistency checks with electroweak symmetry breaking. This includes a test if the scalar potential is bounded from below, if its minimum is not a charge or color breaking minimum and whether or not tachyonic particles are present. We gave a short discussion on these matters in section 3.4. If consistent, `SuSpect` gives the SUSY spectrum back to the micrOMEGAs code, which deletes scenarios whose Higgs, gluino or squark masses lie below the current experimental limits, that we will give in section 4.3. After this, `SuperIso` will evaluate all the leptonic variables and, if every experimental constraint is respected, micrOMEGAs finally calculates the relic density and the spin-independent neutralino proton cross-section σ^{SI} and stores the final output if $\Omega h^2 < 0.2$.

This line of actions has to be done extremely often due to the vastness of our chosen parameter space and the strong bounds from experiments.

4.2. Parameter ranges

For this work we made further assumptions on the pMSSM parameters. We took the masses of the superpartners of the left- and right-handed quarks to be degenerated but different in generations: $m_{\tilde{q}_{1,2}} \neq m_{\tilde{q}_3}$. In the slepton sector we chose different masses for the superpartners of the left- and right-handed leptons $m_{\tilde{\ell}_R} \neq m_{\tilde{\ell}_L}$, but did not distinguish between generations. The trilinear couplings (also called A-terms), that can be interpreted as the supersymmetric analog to the SM Yukawa couplings, are parametrized proportional to the third generation of the squark and the geometric mean of the slepton masses respectively with a universal proportionality factor a_0. We may neglect the A-terms of the first and second generations, because the corresponding Yukawa couplings are already known to be small. To summarize:

$$A_t = a_0 Y_t m_{\tilde{q}_3}\,,\ A_b = a_0 Y_b m_{\tilde{q}_3}\,,\ A_\tau = a_0 Y_\tau \sqrt{m_{\tilde{\ell}_L} m_{\tilde{\ell}_R}}\,. \tag{4.1}$$

We are then left with eleven input parameters [62] that we randomly scan in the following ranges:

$$\begin{array}{ccc}
M_1 \in [10, 200]\ \mathrm{GeV}, & M_2 \in [100, 2000]\ \mathrm{GeV}, & M_3 \in [100, 4000]\ \mathrm{GeV}, \\
m_A \in [90, 4000]\ \mathrm{GeV}, & |\mu| \in [90, 2000]\ \mathrm{GeV}, & a_0 \in [-4.0, 4.0], \\
m_{\tilde{q}_{1,2}} \in [400, 4000]\ \mathrm{GeV}, & m_{\tilde{q}_3} \in [200, 4000]\ \mathrm{GeV}, & \tan\beta \in [2, 65], \\
m_{\tilde{\ell}_L} \in [100, 4000]\ \mathrm{GeV}, & m_{\tilde{\ell}_R} \in [60, 4000]\ \mathrm{GeV}. &
\end{array}$$

The choice of these scanning ranges will be motivated throughout chapter 5, but we will make some anticipatory comments here. The bino mass parameter, M_1 will basically determine the emerging light neutralino mass range. A decent discussion of the pMSSM parameter space with the neutralino mass $m_{\widetilde{\chi}}$ between 60 and roughly 200 GeV has been missing in the literature so far, asking for a thorough examination. In general negative gaugino mass parameters are not forbidden, because gauginos are majorana particles[1]. A specific aim of our work is, however, to show that it is possible to fulfill the muon anomalous magnetic moment condition, a_μ, for a negative μ-term and positive gaugino masses. Choosing different parameterizations for $m_{\widetilde{\ell}_R}$ and $m_{\widetilde{\ell}_L}$ will help us respecting a_μ and offers a possibility to obtain light staus which will be important to fulfill the relic density condition in certain areas of the parameter space.

4.3. Constraints

The supersymmetric parameter space can be constrained by many observables. These include measurements from cosmology, hadron and lepton collider experiments and direct dark matter searches.

The cosmological dark matter abundance has been determined by analysis of the WMAP data [5]. We set the neutralino relic density, Ωh^2, within the 2 σ range [63] $\Omega h^2 \in [0.089, 0.136]$, where experimental and theoretical uncertainties are included and, hence, claim that all dark matter is made out of neutralinos. This does not have to be the case. It is thinkable that the dark matter sector is formed by a number of different kinds of particles. Many works on the MSSM therefore only take the upper bound on Ωh^2 as a strict constraint and relax the lower limit. However, if we claim supersymmetry to be true we have such a nice dark matter candidate, the neutralino, that the possibility to explain all the relic abundance in the Universe by one single particle should be seized. We hence put the strongest possible bounds from the cosmological side on our models. In the following we will discuss constraints from collider physics more detailed.

4.3.1. Supersymmetric particle masses

General searches for supersymmetric particles performed by the LHC have an important impact on our study [64]. The particles easiest to discover are the gluinos and squarks

[1]Note that one of the three gaugino masses can always be chosen to be positive by a redefinition of the fields

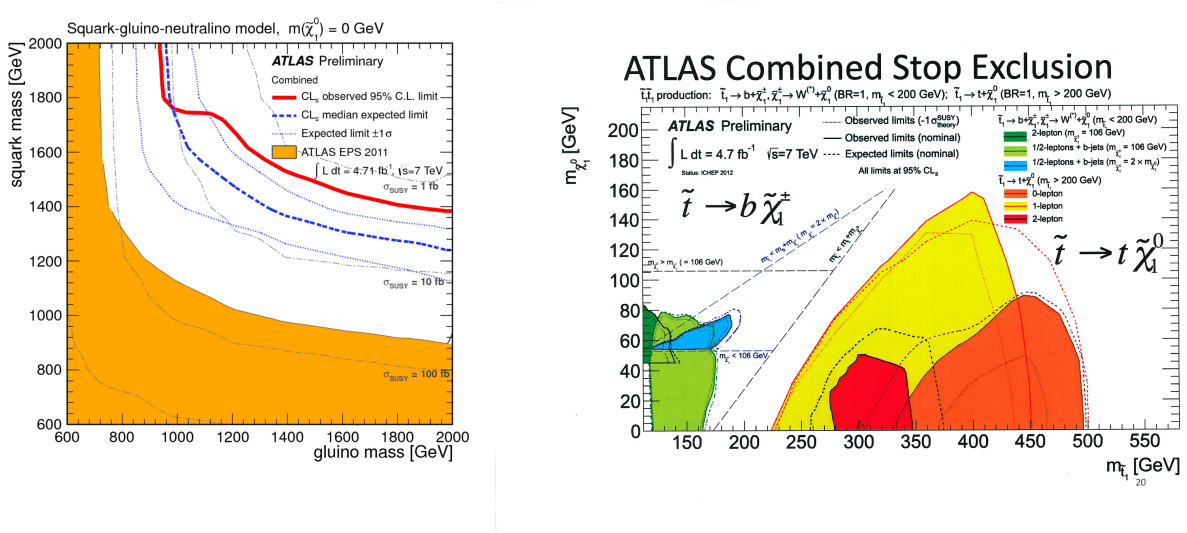

Figure 4.1.: Presenting mass limits on gluinos and light squarks (left panel) [67] and excluded regions in the light stau-neutralino plane (right panel) [68]. The space above the thick red line and the colored regions are, within the specific assumptions, excluded.

of the first two generations. By analyzing signatures of missing transverse energy [65, 66] bounds on their minimal masses can be found. The presentation of these results is not yet done in a model independent way, such that some caution must be taken to not choose too conservative or too strong limits. Recently published results [67, 68] can be found in the left panel of figure 4.1. Note that the neutralino was assumed to be massless to present these results. We choose a lower cut on the gluino mass of 800 GeV and on the first two generation of squarks of 1 TeV. Additionally, we used exclusion limits for light stops originating from LHC analysis, see the right panel in figure 4.1.

Our mass limits on charginos comes from the LEP collider. Charginos lighter than 94 GeV are excluded [69]. Further constraints come from pseudo-Higgs boson, A, searches [70, 71] that have excluded a large region of the $m_A - \tan\beta$ plane at small m_A and large values of $\tan\beta$. The limits applied in our analysis may be seen in the left panel of figure 4.2.

4.3.2. Leptonic observables

The LEP collider still gives the strongest bounds on high-precision leptonic observables like the invisible Z-decay width to neutralinos $\Gamma(Z \to \widetilde{\chi}_1\widetilde{\chi}_1) < 3$ MeV [69], the neutralino pair production cross-section $\sigma(ee \to \widetilde{\chi}_1\widetilde{\chi}_{2,3}) < 100$ MeV [72] and $\Delta\rho < 0.002$ [64], that

roughly speaking measures deviations from the Standard Model relation between the Z- and W-boson masses.

For other quantities, like branching ratios of heavy meson decays, the LHC is beginning to become more important than LEP and increases the limits on supersymmetric parameters. We will discuss some quantities in detail and demonstrate how the parameter space can be constrained by collider physics. One example is the decay of the B-meson into a tau lepton τ and its neutrino ν. Charged Higgses play an important role for the SUSY contributions, that always decreases the Standard Model value. Experimental limits are given in the quantity $R_{B\tau\nu}$, the ratio of the SUSY and the SM predicted branching ratios, with the currently allowed range $0.52 < R_{B\tau\nu} < 2.61$. The expression including threshold corrections to the Yukawas[2] ϵ is:

$$R_{B\tau\nu} \equiv \frac{Br(B \to \tau\nu)_{\text{SUSY}}}{Br(B \to \tau\nu)_{\text{SM}}} \simeq \left[1 - \frac{m_B^2}{m_{H^\pm}^2} \frac{\tan^2\beta}{1 + \epsilon \tan\beta}\right]^2 , \tag{4.2}$$

where $m_B \approx 5.3$ GeV is the mass of the B-meson. A heavy charged Higgs suppresses the SUSY contribution and the constraint is easily fulfilled. On the other hand, for light charged Higgs bosons a significant contribution may arise. As argued in reference [73], two allowed regions for $\tan\beta$ emerge. For small $\tan\beta$ the SUSY contribution is, even for light charged Higgs bosons, small and the experimental bound is respected. Increasing $\tan\beta$ will at the end, however, decrease the value of $R_{B\tau\nu}$ out of the allowed range. Nevertheless, for even larger $\tan\beta$, the deviation itself may become greater than one, such that a reentry into the allowed region is possible. In this way two bands of allowed $\tan\beta$ emerge.

A similar behavior is found for the kaon decay quantity $R_{\ell 23}$ that characterizes the decay $K \to \ell\nu$. It is defined as follows:

$$R_{\ell 23} \equiv \left| \frac{V_{us}(K \to \ell\nu)}{V_{us}(K \to \pi\ell\nu)} \times \frac{V_{ud}(\beta \text{ decay})}{V_{ud}(\pi \to \ell\nu)} \right| , \tag{4.3}$$

with elements of the CKM mixing matrix V_{ij} determined by the processes in the brackets. The SUSY deviation is given by:

$$R_{\ell 23} = \left| 1 - \frac{m_K^2}{m_{H^\pm}^2} \left[1 - \frac{m_d}{m_s}\right] \frac{\tan^2\beta}{1 + \epsilon \tan\beta} \right| , \tag{4.4}$$

[2]Since threshold corrections are loop effects they are suppressed by a loop factor and ϵ can be as a first estimate be approximated with $1/(16\pi^2)$.

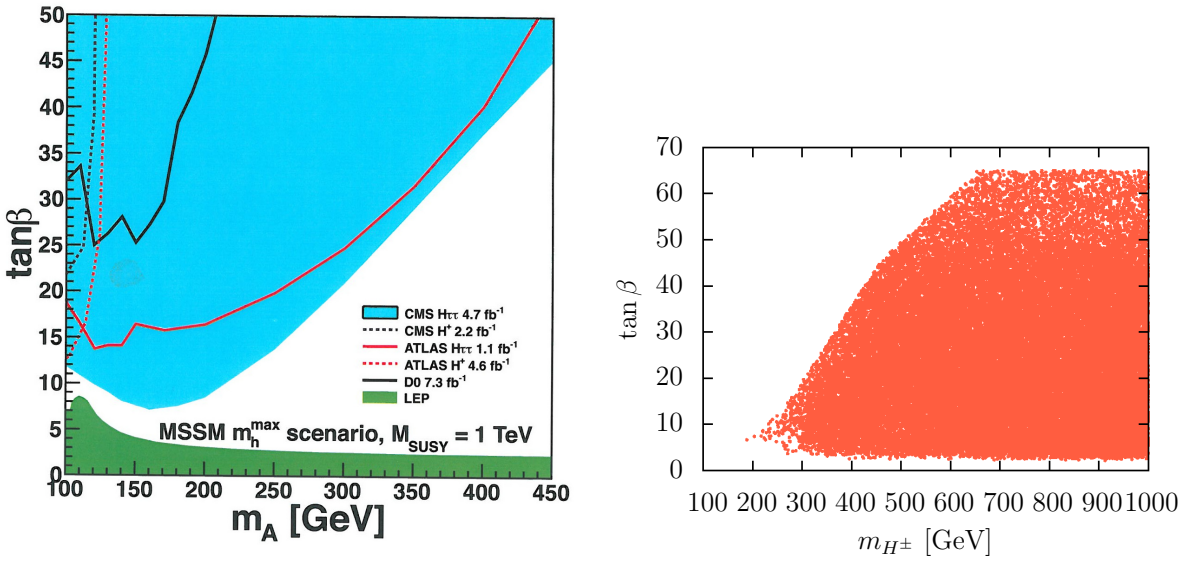

Figure 4.2.: Showing the effect of the LHC exclusion limits for the pseudo-Higgs mass (left panel) [71] and of the leptonic quantities $R_{B\tau\nu}$ and $R_{\ell 23}$ on our parameter space in the charged Higgs mass-tan β plane (right panel). Both constraints probe similar parameter regions.

where $m_K \approx 0.5$ GeV is the mass of the kaon and m_d and m_s masses of the d- and s-quark, respectively. This quantity again probes medium to high ranges of tan β when light charged Higgs bosons are present and is complementary to $R_{B\tau\nu}$ excluding most of the high tan β regions. Since the kaon is lighter than the B-meson by a factor of approximately ten, a reentry into the experimental allowed region is impossible by increasing tan β. Large values of tan β are therefore tested and, as shown in the right panel of figure 4.2, excluded. Note, that the previously discussed pseudo-Higgs boson searches also probe this region of the parameter space, since at tree level the charged Higgs mass is basically given by m_A:

$$m_{H^\pm}^2 = m_A^2 + m_W^2. \tag{4.5}$$

Another quantity that shows a strong dependence on the Higgs sector is the branching ratio of the B-meson decay into two muons: BR($B_s \to \mu^+\mu^-$). It is proportional to the sixth power of tan β and constrained by LHC to be smaller than 4.5×10^{-9} at 95% confidence level [74]. By the end of the year the LHC is supposedly sensitive to the SM value (which is approximately 1.5×10^{-9}) and a deviation might be excluded completely.

A first measurement that deviates from Standard Model predictions is the anomalous

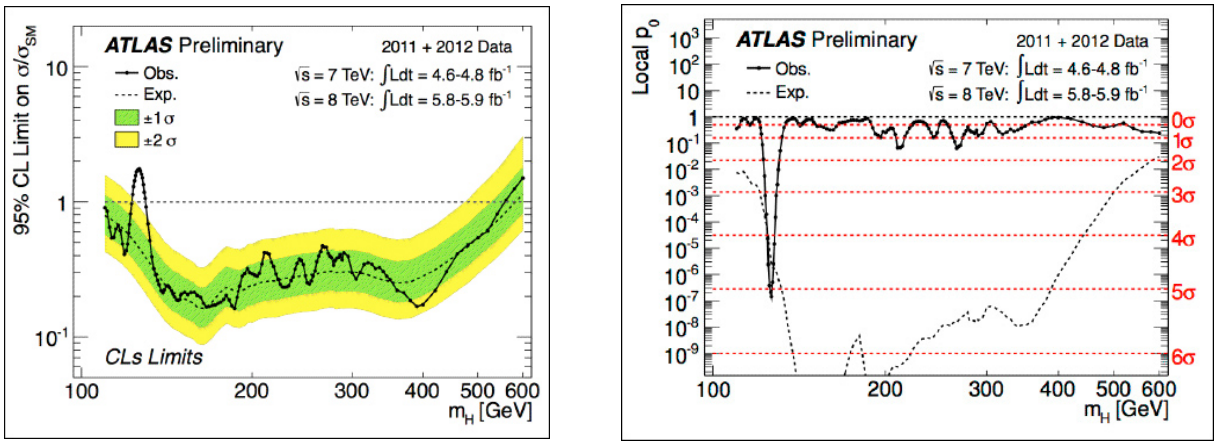

Figure 4.3.: The exclusion limit at 95% confidence level (left) and the local p_0 value (right) summarizing the evidence for a new Higgs-like resonance (the plots are shown from the ATLAS collaboration [1, 2]).

magnetic moment of the muon a_μ. In $e^+e^- \to$ hadrons collisions a 3σ deviation has been found: $\delta a_\mu \equiv a_\mu^{exp} - a_\mu^{\mathrm{SM}} = 29.5 \pm 8.8 \times 10^{-10}$ [75].

4.3.3. Evidence for a Higgs boson

Recent measurements of ATLAS and CMS [76–81] have found a bump in the $\gamma\gamma$ invariant mass at approximately 125 GeV with close to 5σ-level local significance and strongly points to the existence of the Higgs boson.

We show the exclusion plot of the Higgs mass in the left panel of figure 4.3. The ratio of the total measured production cross-section σ to the one expected from the Standard Model σ_{SM} for a given Higgs mass at 95% confidence level is plotted on the y-axis. Measured cross-sections smaller than σ_{SM} obviously exclude a Higgs at that specific mass. Therefore, a Higgs may not be found in those regions, where the thick black measured exclusion curve is below unity. The dotted line represents the expected exclusion curve from simulations with indicated confidence levels by the green and yellow bands. If the y-value is above one, only cross sections larger than the one expected from the SM may be excluded, such that the detectors are not yet sensitive in these regions.

An eventual discovery may better be seen in the right panel of figure 4.3, where the so-called local p_0-value is plotted. This symbolizes to which probability exclusively a background fluctuation may create the observed signal-like excess. Hence, the smaller it is the better. The strong decrease of the p_0-value near 125 GeV indicates the strong

Quantity		Reference(s)
Ωh^2	$[0.089, 0.136]$	[5]
m_h	$(121.0, 129.0)$ GeV	[1, 2, 76–81]
$\mathrm{Br}(B \to s\gamma)$	$[2.89, 4.21] \times 10^{-4}$	[82]
$\mathrm{Br}(B_s \to \mu^+\mu^-)$	$< 4.5 \times 10^{-9}$	[74]
$\mathrm{Br}(B_u \to \tau\bar{\nu})$	$0.52 < R_{B\tau\nu} < 2.61$	[83]
$\mathrm{Br}(K \to \mu\nu)$	$0.985 < R_{l23} < 1.013$	[84]
a_μ	$[0.34, 4.81] \times 10^{-9}$	[75]
$\Gamma(Z \to \widetilde{\chi}_1\widetilde{\chi}_1)$	< 3 MeV	[69]
$\sigma(ee \to \widetilde{\chi}_1\widetilde{\chi}_{2,3})$	< 100 MeV	[69]
$\Delta\rho$	< 0.002	[69]

Table 4.1.: The experimental constraints.

evidence for a new resonance. Note that both plots above are taken from the ATLAS collaboration but that the CMS collaboration has measured comparable results that have been presented simultaneously.
Due to the decay into two photons it is clear, that the new particle must be a boson. Whether this really is the Standard Model Higgs will have to be examined at a lepton collider, where the decay and production channels and the total width can be measured with higher accuracy. Nevertheless, as the signal excess of occurs in the di-photon channel, the "silver channel" of the SM Higgs boson, we will interpret this data as the light Higgs boson of the MSSM. Since the recent results of both collaborations are still preliminary, we take the range not too restrictive and choose as the mass range $m_h \in [121.0, 129.0]$ GeV. A smaller mass range would not affect our results except that the numerical simulations would be more time-consuming[3].

All experimental constraints including flavor and collider physics applied in our analyses are listed in table 4.1.

4.3.4. The Higgs invisible decay width

A way to exclude models with a small μ-term is to investigate the invisible Higgs decay width [85]. Since neutralinos have a non-zero coupling to the Higgs boson, a decay of h into two neutralinos is possible and would alter its decay width. This is defined as the inverse lifetime of a particle ($\Gamma = 1/\tau$) and is equivalent to the full width at half maximum of the resonance curve. In general, if the decay of h into new particles was possible these new final states would increase the decay width compared to the SM prediction and serve as

[3]Note again, that our fine-tuning definition is independent of the stop mass.

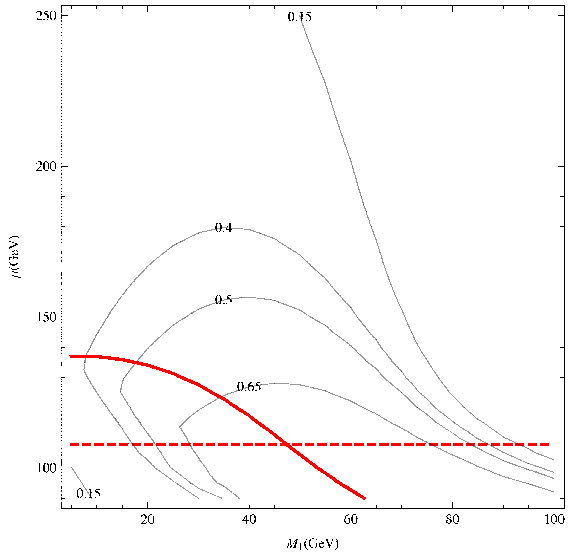

Figure 4.4.: The invisible decay width may cut into the SUSY parameter space [85].

a signal to new physics. Since the neutralinos remain undetected in the detector (except missing energy), their contribution is dubbed "invisible" and counted to the invisible decay width. Then, the invisible branching ratio is defined as follows:

$$\mathrm{BR}_{\mathrm{inv}} = \frac{\Gamma_{\mathrm{inv}}}{\Gamma_{\mathrm{tot}}} \ . \tag{4.6}$$

Assuming that the excess in the di-photon channel is completely due to a SM like Higgs boson, an upper limit on the invisible decay width may be given through:

$$\mathrm{Rate}_{\gamma\gamma} = \sigma(pp \to h + \mathrm{X}) \times \mathrm{Br}_{\gamma\gamma} \times \mathrm{L} \ , \tag{4.7}$$

where L denotes the luminosity. Now, the observable, the $\gamma\gamma$ rate, is indirectly dependent on the total, and therefore also to the invisible, decay width. In this way one can derive upper limits on the invisible branching ratio. This was done by two groups independently and found to be smaller than 0.13 [86] or 0.39 [87]. The analysis of reference [85] then shows how the SUSY parameter space is tested.

The dashed red line in figure 4.4 shows the current LEP chargino mass limit, the thick red line signalizes bounds from the Z-decay width and the black curves show lines of constant Higgs to two neutralinos branching ratio. If we take the more conservative limit of [87] all the parameter space below the corresponding black line representing 0.4

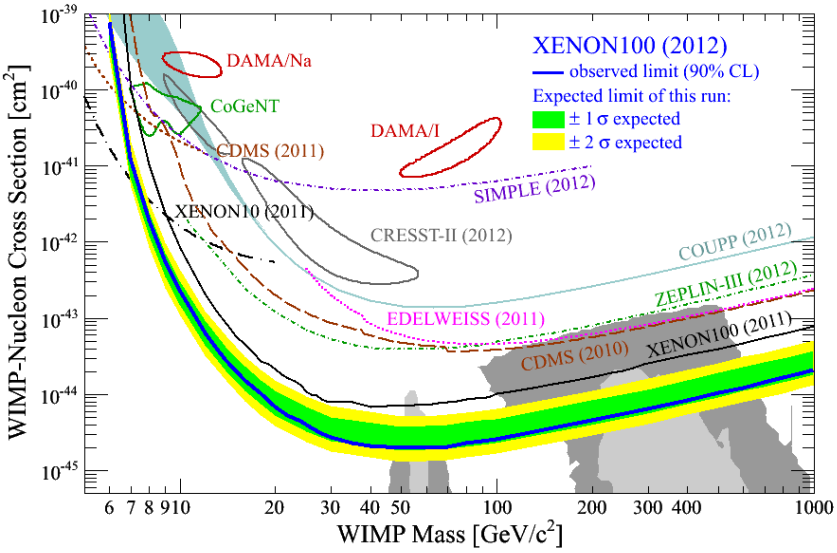

Figure 4.5.: Presenting direct detection experiments and their exclusion limits or detection regions (taken from [7]).

is excluded. As the measurements become more precise, this offers an opportunity to excluded low values of μ for light neutralino masses and the natural SUSY parameter space can be probed. One must note, however, that these bounds are not competitive with the chargino mass limit and the Z-decay width for negative μ. This is due to a decrease of the Higgs-neutralino-neutralino coupling. (compare the approximations to the neutralino components in section 5.3 and equation (5.13)).

4.3.5. Direct detection experiments

There are many diverse experiments that are looking for a direct dark matter signal. It is beyond the scope of this thesis to discuss all of them in great detail. We will briefly describe the XENON100 detector and discuss whether claimed signals from DAMA and CoGeNT can be interpreted by the MSSM. A summary of all claimed signals and exclusion curves is given in figure 4.5 from reference [7].

DAMA measures an annual modulation signal due to the rotation of the earth around the sun. Assuming the DM halo is static in the galactic plane, the relative velocity between the earth and the DM halo changes between summer and winter, when the angular velocity of the earth either adds up to the motion of the sun around the galactic halo or subtracts. A signal of 8.9 σ confidence level has been reported [8].

CoGeNT tests the interaction cross-section of WIMPs by measuring the ionization

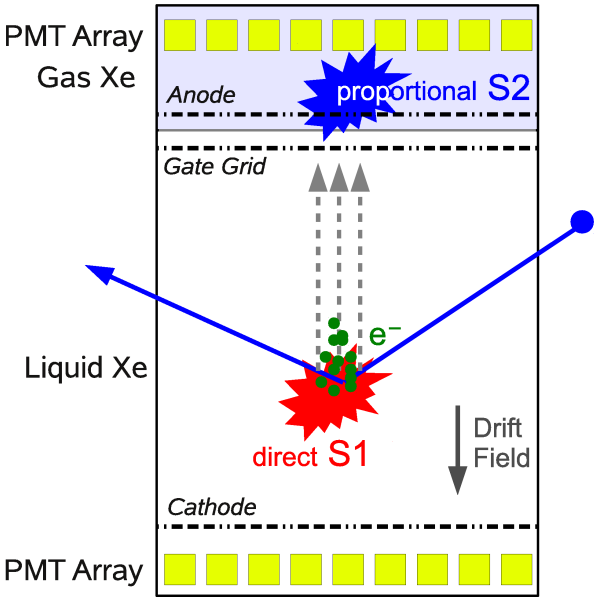

Figure 4.6.: A description of the XENON100 detector [88].

charge from nuclear recoils and, due to the very low energy threshold, they can probe especially very light WIMP particles. They also claim a signal with a corresponding dark matter mass of 7-11 GeV [10].

Besides, there has been an event excess reported by the CRESST [9] (Cryogenic Rare Event Search with Superconducting Thermometers) experiment which detects WIMPs through a temperature change due to the energy deposit of dark matter collisions on nuclei in a cryogenic detector.

Apart from the fact that DAMA/LIBRA, CRESST and CoGENT are contradicting each other by themselves, they are all excluded by XENON100 (2012) [6]. There have been dark matter models trying to move the individual regions together, but no consent could be achieved yet. In the framework of low-energy supersymmetry these signals cannot be explained after taking into account all experimental data [73]. This is confirmed by our study. We will therefore take the viewpoint that the limits of XENON100 (2012) are correct and exclude any of the above possible dark matter signals.

The XENON100 detector [88] has two planes of photo multipliers, see figure 4.6, that will measure two different light signals from a possible WIMP-Xenon collision. There is a first light signal $S1$ when the collision occurs that is observed by both detectors simultaneously. The energy of the collision ionizes Xenon and the set free electrons are pulled toward the second array of photomultipliers by an electric field. When the charges

enter the gas phase of Xenon, scintillation light is produced that is then detected as the $S2$ signal at the top of the detector. To tell apart electronic WIMP collisions from nuclear recoil through neutrons, the ratio of $S2/S1$ is crucial and shows a characteristic behavior for both cases. The background can be significantly reduced and controlled by the opportunity to specify the location of the collision with high precision and distinguish it in this way from radioactive contributions from the boundaries of the detector. The behavior of the XENON exclusion limit in figure 4.5 is determined by two effects: At small neutralino masses the recoil energy is low, such that the signal strength is low and exclusion becomes more difficult. Going to larger masses a strong decrease of the expected neutralino flux due to cosmological bounds pushes down the expected event rate and makes it harder to put limits on σ^{SI}. Therefore, a minimum at approximately 50 GeV occurs.

We will in the next chapter present the results of our scan and always show the recently new measured XENON100 (2012) exclusion limit. This then directly shows which parts of the natural SUSY parameter space have already been excluded. We will additionally show a prediction for the exclusion limit of the future XENON1t experiment [89] in order to see how far direct searches can test the parameter space.

5. Results

In this chapter we will present the results of our scan. This discussion includes a presentation of the neutralino annihilation mechanisms and their arrangement in plane spanned by the neutralino mass and the spin-independent direct detection-cross section σ^{SI} (direct detection plane). The necessary amount of tuning for each accesible point in this plane will be presented in order to see where there are natural regions that have avoided direct detection so far. We will analyze each annihilation mechanism separately, such that the emerging picture is fully understood. This will also include a description of the behavior of the direct detection cross-section on the sign of the supersymmetric Higgs mass parameter μ and the wino component N_{12} of the neutralino. In this context we will introduce a new tuning measure to account for accidental cancellations σ^{SI}. Finally, we show the probability to reach a certain point in the direct detection plane by performing a homogeneous scan of the input parameter space. The results presented here have been publicized on the 12th of July [90].

5.1. Obtaining the correct relic abundance

In this section we will discuss which mechanisms may bring the relic density into the cosmological interesting region. As explained in section 5.1, the relic density is basically set by the thermally averaged annihilation cross-section, $\langle\sigma_{ann}v\rangle$, using a freeze-out mechanism. We indicate the most important annihilation channel by a color coding in figure 5.1 where the relic density is plotted on a log scale versus the neutralino mass. For simplicity we only show $\Omega h^2 < 0.2$ since other models would always over produce dark matter. Efficient mechanism, *e.g.* resonant annihilation, are needed to get a high enough $\langle\sigma_{ann}v\rangle$, which can produce the correct relic abundance.

The most dominant annihilation channel has lepton final states (dark-blue points in figure 5.1) and is present in our complete neutralino mass range. The two resonant Z- and light Higgs-boson, h, allow annihilations into a pair of light quarks (red points) and are situated at masses around 40 and 60 GeV, respectively. As the mass of the

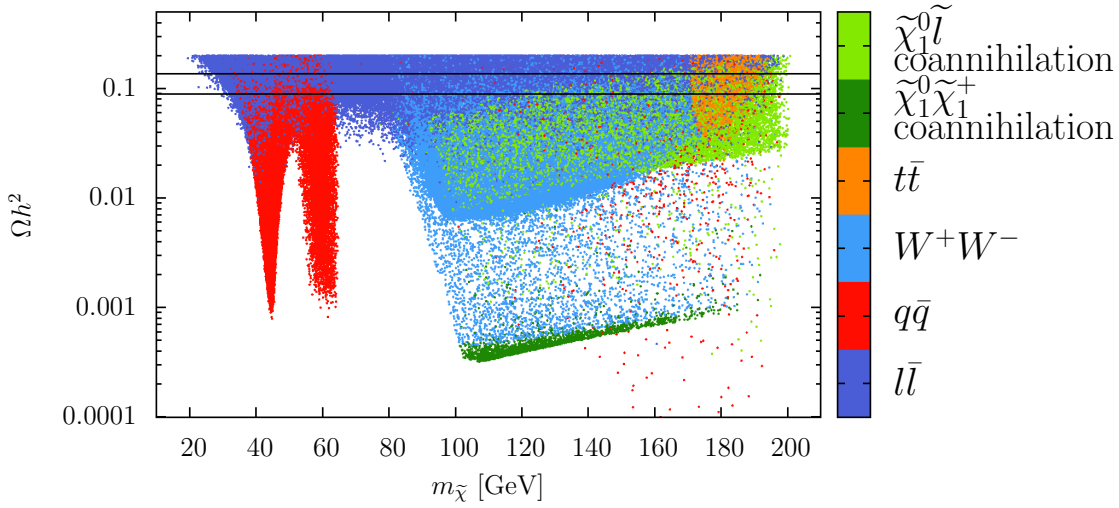

Figure 5.1.: The different (co)annihilation mechanisms presented by the color code and the corresponding relic abundance. All collider and flavor constraints have been applied. The black lines indicate the bounds that will be applied as the relic density cuts; $\Omega h^2 \in [0.089, 0.136]$. Here $q\bar{q}$ stands for a light quark and $\ell\bar{\ell}$ for a lepton pair. The plot contains only scenarios with a negative μ-term, but is similar for the positive sign case.

h-boson is not yet precisely known, its resonance is not as sharp as the Z-resonance. For neutralinos heavier than roughly 80 GeV the neutralino may annihilate into two W-bosons (light-blue). There are further scenarios with dominant annihilations into light quarks for $m_{\tilde{\chi}} \gtrsim 80$ GeV hidden behind the lepton final states. The lower branch (dark-green) corresponds to neutralino-chargino coannihilations, which for our chosen range of the lightest neutralino mass always produce under abundant dark matter. Therefore, these coannihilations are unimportant for our further discussion, as we are also taking into account the lower bound from the WMAP measurement. Slepton coannihilations, on the other hand, will play an important role at neutralino masses above 90 GeV (light-green). They are accompanied by a region of top final states at approximately 180 GeV (orange).

Mapping the different models with their mechanisms into the $m_{\tilde{\chi}} - \sigma^{\mathrm{SI}}$ plane a well ordered picture emerges. We show an example for scenarios with a negative μ-term in figure 5.2, where all constraints except the anomalous magnetic moment of the muon have been applied and where we split the results into two figures for better visibility.

The most prominent mechanism, the annihilation into a pair of leptons, is homoge-

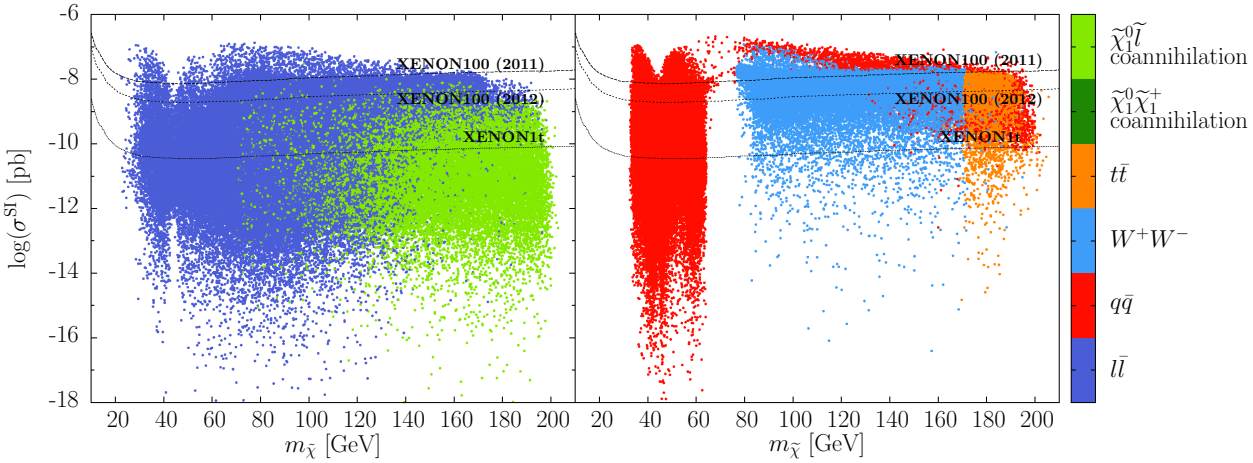

Figure 5.2.: The dominant neutralino annihilation mechanism in the direct detection plane. All constraints except the anomalous magnetic moment of the muon have been applied.

neously distributed over the complete plane and mainly mediated through t-channel light stau or s-channel Z, h, A, H exchange and their interference terms. Quark final states at neutralino masses between 40 and 60 GeV are due to s-channel Z- and light Higgs boson, h, resonances. Chargino mediated t-channel and neutral Higgs mediated s-channel annihilations into W-bosons fill a band at $\sigma^{\rm SI} \simeq 10^{-9}$ pb (light-blue). There also quark final states H and A exchanges are present. Slepton coannihilations are situated at higher neutralino masses mainly below the predicted XENON1t exclusion limit. We note here, that some scenarios of chargino coannihilations have been present even after cutting the relic density, however, these were extremely rare (they only made up 0.02% of the total scenarios) and we decided to remove them for the rest of our analyses. For positive μ the situation is similar except for the different scaling behavior of $\sigma^{\rm SI}$, which will be discussed in section 5.3.

A remark must be made here for some scenarios that we completely excluded from our analyses. Via coupled Boltzmann equations we obtained scenarios in the simulations for which the dominant freeze-out mechanism is none of the ones stated above. There have been dominant annihilation channels, such as gluino fusion into gluons, $\tilde{g}\tilde{g} \to GG$, that allowed the neutralino to produce the correct relic abundance. However, since the neutralino does not directly take part in those processes, we neglect them in our study.

We also calculated the annihilation cross-sections of two DM into two photons, $\langle\sigma_{\chi\chi\to\gamma\gamma}v\rangle$, in order to decide whether the claimed γ-ray line in the Fermi-LAT data [91] is consistent

	initial state	final states
chargino coannihilation	$\widetilde{\chi}_1^0\ \widetilde{\chi}_1^+$	sc, ud, tb, $e\nu_e$, $\mu\nu_\mu$, ZW
slepton coannihilation	$\widetilde{\chi}_1^0\ \widetilde{\tau}_1$	$\gamma\tau$, τh,$W\nu_\tau$, $Z\tau$
	$\widetilde{\chi}_1^0\ \widetilde{e}_R$	γe
	$\widetilde{\chi}_1^0\ \widetilde{\nu}_\tau$	$W\tau$, $Z\nu_\tau$, $\nu_\tau h$
	$\widetilde{\chi}_1^0\ \widetilde{\nu}_e$	We, $Z\nu_e$

Table 5.1.: List of the dominant annihilation channels as obtained by our simulation.

with our models. However, we found that $\langle\sigma_{\chi\chi\to\gamma\gamma}v\rangle$ is too small to serve as an explanation. Nevertheless, it is not clear that this excess is due to DM annihilations and does not exclude our models.

5.2. The level of fine-tuning in the direct detection plane

In this section we discuss the level of fine-tuning, equation (3.99), and its relation to dark matter direct detection experiments. By mapping the simulated scenarios into the direct detection plane and indicating the amount of fine-tuning by a color scheme, we are able to draw conclusions where the natural pMSSM parameter space is situated, where a dark matter signal should be expected and whether direct searches can exclude completely the untuned, well-motivated parameter combinations. We show our results applying all experimental constraints discussed above except the muon anomalous magnetic moment. To stress its impact we consider this quantity separately in section 5.5. Let us discuss the two possible sign cases of μ in turn and start with positive μ.

In figure 5.3 we plot the distribution of the level of fine-tuning in the direct detection plane. Untuned scenarios can be found in three regions: First, a long, horizontal branch of t-channel light chargino mediated neutralino annihilation into two W-bosons plus s-channel heavy Higgs and CP-odd Higgs mediated annihilations into a pair of quarks appears at $\sigma^{\rm SI} > 10^{-8}$ pb and at neutralino masses above 80 GeV. Second, two vertical stripes belonging to the Z- and h-resonances emerge at the corresponding masses. Note also the third untuned region at $m_{\widetilde{\chi}} \in [65, 80]$ GeV and $\sigma^{\rm SI} \approx 10^{-8}$ pb due to light stau annihilations. Away from the Z- and h- resonances higher tuning will become necessary if future direct searches do not report a positive signal: A tendency for more tuning for smaller $\sigma^{\rm SI}$ is clearly visible (see also [55]). This effect is not noted at the Z- and h-resonance regions. Instead we find an increase of $\Delta_{\rm tot}$ when the neutralino mass ap-

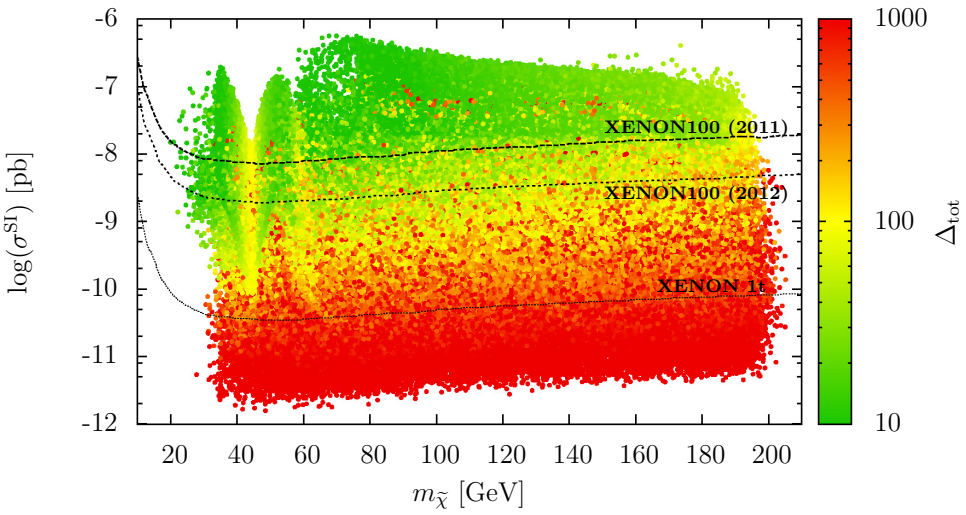

Figure 5.3.: The level of fine-tuning for our models with positive μ in the direct detection plane. The color coding indicates the amount of tuning Δ_{tot} necessary to reach a certain point. Scenarios with $\Delta_{\text{tot}} < 10$ are given the value 10 and $\Delta_{\text{tot}} > 1000$ the value 1000. The lines represent the XENON100 (2011), XENON100 (2012) and the prediction for XENON1t, respectively.

proaches $m_Z/2$. This will be explained when the quark final states are discussed in greater detail in section 5.4.1. Taking the XENON100 (2012) limit into account the horizontal untuned branch is already excluded, such that low fine-tuned dark matter for positive μ preferably sits at masses between 20 and 60 GeV. As the XENON experiment will further investigate the parameter space, these regions will be probed as well and, if no signal is detected, a neutralino with a mass less than 200 GeV for positive μ is excluded completely, if the fine-tuning measure is considered to be meaningful. Let us now switch to a negative μ:

We again show the level of tuning in the direct detection plane in figure 5.4 and see that, compared to positive μ, a different picture arises: Direct dark matter searches have just begun to probe the parameter space. Scenarios that explain the dark matter riddle with low electroweak fine-tuning and that have avoided direct detection so far can be found in the complete neutralino mass regions. This could be interpreted as the reason why no positive signal has been reported yet: A great part of the untuned parameter space has not been tested. Note that σ^{SI} is shifted to smaller values that may be as

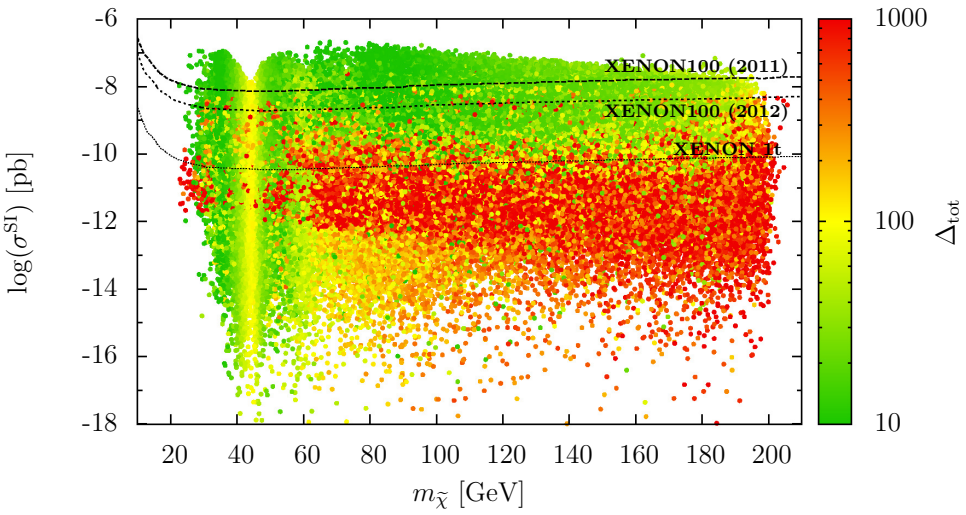

Figure 5.4.: Again the level of fine-tuning analogously to figure 5.3, but for scenarios with negative μ.

small as 10^{-18} pb. For a neutralino mass smaller than 65 GeV very low direct detection cross-sections and, at the same time, low fine-tuning is possible. Thus, direct searches alone will not be capable to test the complete MSSM parameter space, but complement searches, for example production at the LHC or indirect detection are necessary.

Another feature that can be observed in figure 5.4 is a thick red band that crosses the allowed region at a direct detection cross-section of about 10^{-12} pb. This band contains the most tuned scenarios of the simulations. However, different to positive μ, highest tuning does not correspond to the smallest possible direct detection cross-sections, as models with even smaller σ^{SI} exists that show less tuning. How this arises will be discussed when we turn to the detailed discussion of lepton final states in section 5.4.2. First, however, we must understand the dependence of the direct detection cross-section on the sign of μ.

5.3. The direct detection cross-section

In this section we will explain why a negative μ-term shifts the spin-independent neutralino-proton cross-section σ^{SI} to smaller values and why the lower border of σ^{SI}, which could be noted for positive μ vanishes. To understand this behavior we first need to clarify which

parameters determine the mixture of the neutralino and how these influence σ^{SI}. The neutralino mass matrix in the basis given in section 3.3.1 is:

$$M_{\widetilde{N}} = \begin{pmatrix} M_1 & 0 & -M_Z \sin\theta_W \cos\beta & M_Z \sin\theta_W \sin\beta \\ 0 & M_2 & M_Z \cos\theta_W \cos\beta & -M_Z \cos\theta_W \sin\beta \\ -M_Z \sin\theta_W \cos\beta & M_Z \cos\theta_W \cos\beta & 0 & -\mu \\ M_Z \sin\theta_W \sin\beta & -M_Z \cos\theta_W \sin\beta & -\mu & 0 \end{pmatrix} .$$

There exist exact solutions for the mixing angles in the literature, but since these are too complicated for our discussions, we used the large SUSY scale approximation $(M_i \pm |\mu|)^2 \gg M_Z^2$ $(i = 1, 2)$ from reference [92] to find first estimates for each of the components. Note their dependence on the sign of the μ-term:

$$N_{12} \simeq -M_Z^2 \cos\theta_W \sin\theta_W \frac{M_1 + \mu \sin 2\beta}{(M_1 - M_2)(M_1^2 - \mu^2)} , \tag{5.1}$$

$$N_{13} \simeq -M_Z \sin\theta_W \frac{M_1 \cos\beta + \mu \sin\beta}{M_1^2 - \mu^2} , \tag{5.2}$$

$$N_{14} \simeq M_Z \sin\theta_W \frac{M_1 \sin\beta + \mu \cos\beta}{M_1^2 - \mu^2} . \tag{5.3}$$

The unitary condition on the mixing angles then yields the bino component N_{11}:

$$N_{11} = \sqrt{1 - N_{12}^2 - N_{13}^2 - N_{14}^2} . \tag{5.4}$$

These approximations are in good agreement with the mixing angles found in our simulations. One strong deviation occurs for scenarios with a dominant annihilation into W-bosons near a neutralino mass of around 80 GeV. For all other mechanisms these formulas give sufficient precision for a reliable qualitative discussion. Note that especially the higgsino components N_{13} and N_{14} strongly depend on the μ-term. Since $|\mu|$ is usually much greater than M_1 these components will always decrease when μ is increased. The same is valid for the wino component N_{12}. This means that whenever a large μ (or equivalently a high level of tuning) is present, the neutralino almost forms a pure singlet, namely a bino. Since a smaller higgsino component leads to a smaller neutralino-neutralino-Higgs coupling (for both light and heavy Higgses) it is true as a general statement that a bino-like neutralino has a smaller σ^{SI}, but also that the corresponding tuning level is worse. A neutralino with a larger higgsino component should, on the other hand, be easier to detect and is from a fine-tuning perspective also more natural. However, we will see that

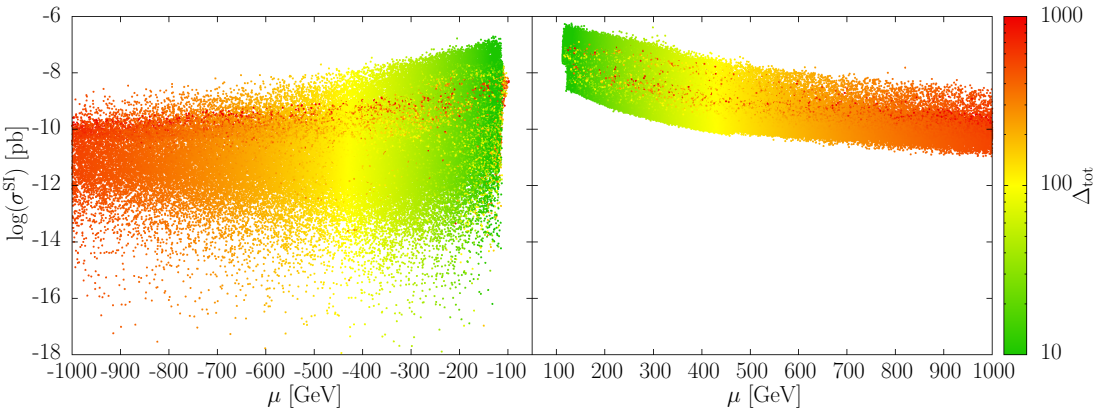

Figure 5.5.: The level of fine-tuning and the direct detection cross-section for negative (left) and positive (right) values of μ. The possibility to obtain smaller cross-sections for scenarios with a negative μ-term is visible.

there are exceptions to this statement when cancellations between different contributions to the direct detection cross-section allow $\sigma^{\rm SI}$ to be decreased so far that even neutralinos with a large higgsino component will be very difficult to trace with direct dark matter searches. This will be the explanation for the appearance of the vertical green region at the Z- and h-resonances from figure 5.4.

In figure 5.5 we notice again the clear difference in the scales of $\sigma^{\rm SI}$ when the sign of μ is flipped. Now it is already clear that also higgsino-like neutralinos, *i.e.* those with a small μ-term, may have avoided direct detection experiments if μ is negative. Note that the red points showing up at small absolute values of μ possess a large m_A and a small $\tan\beta$, such that equation (3.101) becomes large and dominates the fine-tuning.

Let us now explain the origin of the different scaling behavior of $\sigma^{\rm SI}$ for the two sign cases: The dominating terms in σ^{SI} are t-channel light and heavy Higgs boson exchanges. In references [17, 93, 94] we find:

$$\sigma^{\rm SI} \simeq \frac{8G_F^2}{\pi} M_Z^2 m_{\rm red}^2 \left[\frac{F_h I_h}{m_h^2} + \frac{F_H I_H}{m_H^2}\right]^2 \quad , \tag{5.5}$$

where G_F is the Fermi constant and $m_{\rm red}$ is the neutralino-nucleon reduced mass:

$$m_{\rm red} \equiv \frac{m_{\tilde\chi} m_N}{m_{\tilde\chi + m_N}} \quad . \tag{5.6}$$

The functions $F_{h,H}$ and $I_{h,H}$ are defined as follows:

$$F_h \equiv ([-N_{11}\sin\theta_W + N_{12}\cos\theta_W)\,(N_{13}\sin\alpha + N_{14}\cos\alpha) \quad , \tag{5.7}$$

$$F_H \equiv (-N_{11}\sin\theta_W + N_{12}\cos\theta_W)\,(N_{13}\cos\alpha - N_{14}\sin\alpha) \quad , \tag{5.8}$$

$$I_{h,H} \equiv \sum_q k_q^{h,H} m_q \langle N|\bar{q}q|N\rangle \ . \tag{5.9}$$

The angle α is the mixing of the mass eigenstates ($h$and H), and the coefficients $k_q^{h,H}$ are given by:

$$k^h_{u\text{-type}} = \cos\alpha/\sin\beta \quad , \qquad k^h_{d\text{-type}} = -\sin\alpha/\cos\beta \ ,$$
$$k^H_{u\text{-type}} = -\sin\alpha/\sin\beta \quad , \quad k^H_{d\text{-type}} = -\cos\alpha/\cos\beta \quad ,$$

for the up-type and down-type quarks, respectively. Threshold corrections will be neglected for simplicity in our discussion. Evaluating the complete expression with our approximations for the neutralino components in the decoupling limit[1] yields the following formula:

$$\sigma^{\rm SI} \simeq \frac{8G_F^2}{\pi} m_{\rm red}^2 \frac{M_Z^4 \sin^2\theta_W}{(M_1^2-\mu^2)^2} \cdot \left[\frac{I_H}{m_H^2}\mu\cos 2\beta + \frac{I_h}{m_h^2}(M_1 + \mu\sin 2\beta)\right]^2 (N_{11}\sin\theta_W - N_{12}\cos\theta_W)^2 \ . \tag{5.10}$$

Note, that $\cos 2\beta$ is smaller than zero, *i.e.* $\cos 2\beta \approx -1$ ($\tan\beta > 2$), such that both contributions in the square brackets seem to have a different sign. However, the k-coefficients tell us that I_h and I_H preferably have an opposite sign in the decoupling regime and actually add up for positive μ. On the other hand, cancellations between both terms are possible and $\sigma^{\rm SI}$ may be suppressed when μ is negative. This is only correct when $M_1 + \mu\sin 2\beta$ is positive. In this case we see from equation (5.1) that the wino component is negative since $M_2 > M_1$ and $|\mu| > M_1$ for most of our models. These statements are nicely summarized in figure 5.6. The boundary at $M_1 + \mu\sin 2\beta \approx 200$ GeV occurs for the maximal values of M_1 and $\tan\beta$ when, at the same time, $|\mu|$ is small.

In the next sections we will use this knowledge to correctly explain in detail the behavior of the level of tuning with respect to the spin-independent cross-section when we discuss every annihilation mechanism separately. In these discussions we will mainly concentrate on the quark and lepton final states, since they form the most common annihilation channels of our scenarios.

[1] $\sin^2(\alpha-\beta) \simeq 1$, *i.e.* $\sin\alpha \simeq \cos\beta$, $\cos\alpha \simeq -\sin\beta$.

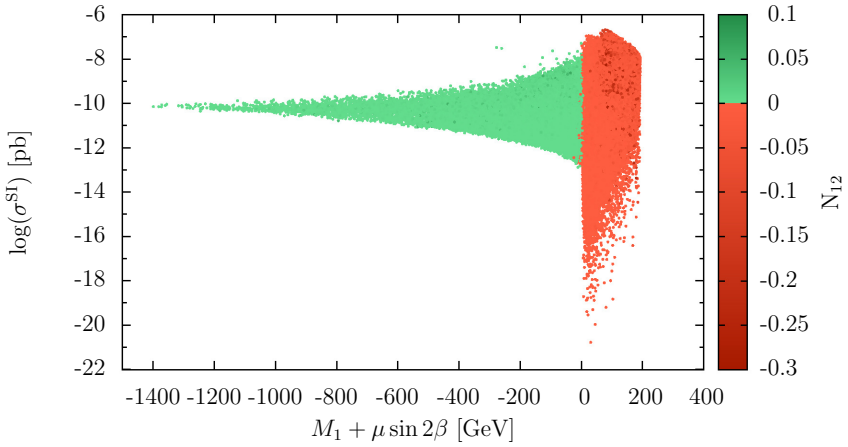

Figure 5.6.: The dependence of σ^{SI} on the quantity $M_1 + \mu \sin 2\beta$ and the wino component N_{12} as obtained by our simulations. Only negative N_{12} allow for cancellations of the light and heavy Higgs contributions to σ^{SI}.

5.4. The annihilation mechanisms

5.4.1. Quark final states

In this section we will take a closer look at the scenarios with neutralino annihilation into light quarks and a negative μ-term. The situation is similar for positive μ except for the different scale of the direct detection cross section. We choose to discuss the negative μ case in order to explain the more complicated behavior of σ^{SI}.

Regions of quark final states are, as we mentioned in section 5.1, situated at the Z- and h-resonances and in a band at $\sigma^{\mathrm{SI}} \gtrsim 10^{-10}$ pb above neutralino masses of 80 GeV. The behavior of the fine-tuning at the Z-resonance is an interplay between the values of μ and the relic density condition. The neutralino-neutralino-Z coupling $C^{\tilde{\chi}\tilde{\chi}Z}$ is determined by the higgsino components of the neutralino [95]:

$$C_A^{\chi_1^0\chi_1^0 Z} = \frac{g}{2\cos\theta_W}(N_{14}^2 - N_{13}^2), \tag{5.11}$$

which in turn are mainly given by the μ-term, see equations (5.2) and (5.3). If we fixed the μ-term, *i.e.* kept the $C^{\tilde{\chi}\tilde{\chi}Z}$ almost constant, and moved closer to the exact resonance at $m_{\tilde{\chi}} = m_Z/2$, the neutralino would be under abundant due to the resonant enhancement

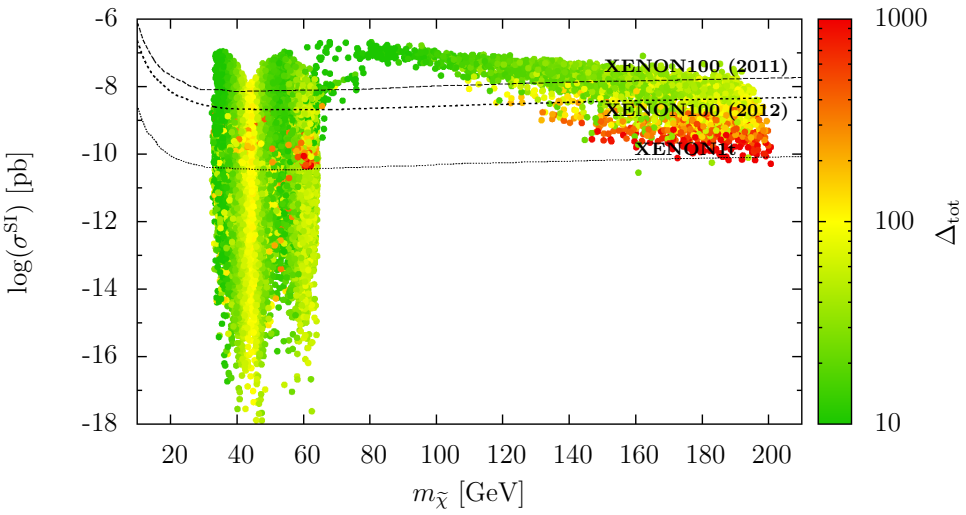

Figure 5.7.: The level of fine-tuning in the direct detection plane for models with dominant neutralino annihilations into light quarks only. Z, light Higgs h, heavy Higgs H and CP-odd Higgs A mediated annihilations appear and are to a great part untuned. The latter two mechanisms may be tested completely by the predicted XENON1t exclusion limit.

that occurs for $\langle \sigma_{ann} v \rangle$. To obtain the correct relic abundance we therefore need to decrease the $C^{\tilde{\chi}\tilde{\chi}Z}$ through a decrease of the higgsino components by an increase of μ. This then directly translates into a higher amount of tuning close to the exact resonance. Note that the μ-term is fixed at the Z-resonance through this connection between the relic density condition and $C^{\tilde{\chi}\tilde{\chi}Z}$.

Near the h-resonance ($m_{\tilde{\chi}} \approx 60$ GeV) the explanation of the fine tuning behavior is more difficult. First, one notes that Δ_{tot} can be two orders of magnitude larger than before. These tuned scenarios gather at a spin-independent cross-section of about 10^{-10} pb. Let us discuss in detail the origin of this difference: The MSSM contains an additional Higgs-doublet, as we explained in chapter 3. The propagating light Higgs mass eigenstate h is a superposition of both gauge eigenstates H_u, H_d. In the calculation of a Higgs-quark-quark interaction the Higgs mixing angle and the ratio of the two VEVs, *i.e.* $\tan\beta$, appear. The coupling to the light quark pair $b\bar{b}$ is then given by:

$$C^{hb\bar{b}} = \frac{g m_b \cos\alpha}{2 m_W \sin\beta} = \frac{g \cos\alpha Y_b v \cos\beta}{2 m_W \sin\beta \sqrt{2}} = \frac{g Y_b v \cos\beta}{2\sqrt{2} m_W} \propto Y_b \cos\beta \ , \tag{5.12}$$

where we used the fact that we are in the decoupling regime and expressed the b-quark mass with the Yukawa coupling and the VEV. We see that the parameter β, so to say $\tan\beta$, plays an important role for $C^{hb\bar{b}}$. The Higgs-b-$\bar{b}$ coupling is increased through a small $\tan\beta$ (meaning that $\cos\beta$ is rather large), which then asks for a suppression of the neutralino-neutralino-Higgs coupling $C^{\tilde{\chi}\tilde{\chi}h}$ to keep the complete annihilation rate fixed at the value that produces the correct relic density. This is again achieved by increasing the μ-term [95]:

$$C^{\tilde{\chi}\tilde{\chi}h} = -g[(N_{12} - N_{11}\tan\theta_W)(-\sin\alpha N_{13} - \cos\alpha N_{14})] \ . \tag{5.13}$$

For small values of $\tan\beta$, a correct relic abundance is therefore only produced when μ is large, which explains the fine-tuned models in figure 5.7. We still need to explain why these almost purely bino-like neutralino scenarios do not map to the lowest possible spin-independent cross-sections.

As noted in section 5.3, only a negative wino component of the neutralino allows for cancellations in σ^{SI}. The just discussed scenarios, however, show a very small[2] μ plus a small $\tan\beta$. In this case $M_1 + \mu\tan 2\beta$ takes its smallest possible values, such that the wino component is positive and these scenarios are situated at the very left end of figure 5.6 and map accordingly to rather large values of σ^{SI}.

Whereas for positive μ it is in general true, that a large m_A and a large μ decrease σ^{SI} through a suppression of both contributions to σ^{SI}, the smallest possible values of σ^{SI} for negative μ occur when the cancellations between the light and heavy Higgs contribution are almost exact. Hence, the parameters need to be tuned against each other and it is not enough to just suppress both contributions. To clarify this statement, we plot in figure 5.8 the distribution of the CP-odd Higgs mass in the direct detection plane. We see that only at the exact Z-resonance m_A is large to get the smallest possible value for σ^{SI}, but away from the resonance models with heavier A map to larger σ^{SI}. Let us explain this in detail.

To get the smallest σ^{SI} both contributions should be preferably small and have opposite signs to cancel each other. As we explained previously, at the exact Z-resonance the higgsino component of the neutralino is decreased in order to compensate for the resonant enhancement of $\langle\sigma_{ann}v\rangle$ to respect the relic density condition. Thus, the μ-term is rather large and the neutralino-neutralino-light Higgs coupling rather small. To have exact cancellations also the heavy Higgs contribution must be small which is achieved by increasing m_A. At the exact resonance we hence find a picture similar to positive μ: both, μ and

[2]To avoid confusion: small here means a large $|\mu|$ and a negative sign.

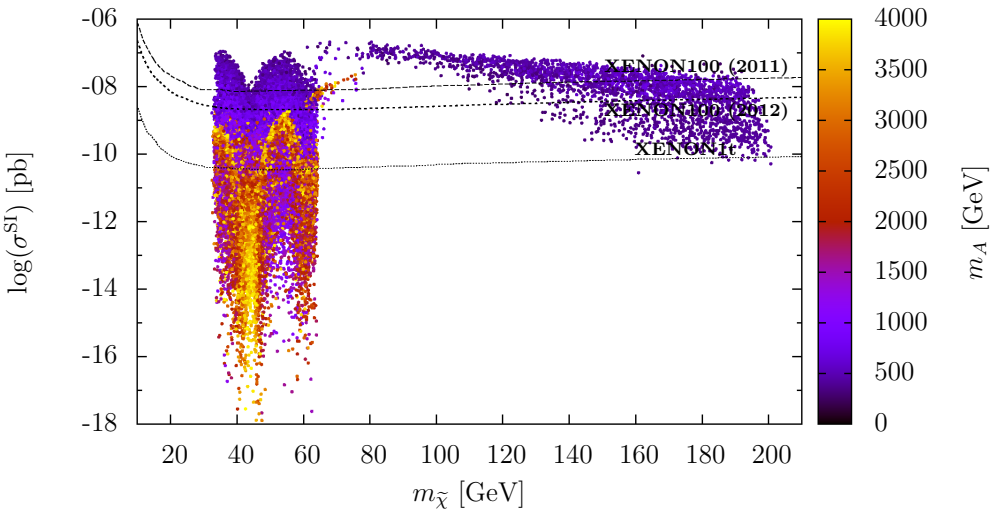

Figure 5.8.: The distribution of the CP-odd Higgs mass m_A of the scenarios with neutralino annihilation into light quarks in the direct detection plane. It is not true that the smallest possible σ^{SI} have the largest m_A as soon as the μ-term is negative. The branch at neutralino masses above 80 GeV consists of scenarios with very small m_A indicating that these are CP-odd and heavy Higgs mediated annihilations.

m_A, have to be large to get the smallest possible spin-independent cross-sections, which agrees perfectly with figure 5.8.

Further away from the resonance, however, the neutralino is more higgsino like and the contribution to σ^{SI} from the light Higgs is enhanced. To have cancellations away from the exact resonance, the heavy Higgs contribution must not be too small and hence m_A not too large. If it was, the heavy Higgs contribution would be too small to cancel out the light Higgs contribution. This explains figure 5.8. In section 5.6 we will quantify the possibility of fulfilling specific relations between parameters that result in an unnaturally small cross-section by introducing a measure of equation-tuning.

We still have to discuss the heavy and CP-odd Higgs resonances. These overlay each other and have a completely different shape compared to the Z- and h-resonances. Due to the lightness of the heavy Higgs, its contribution to σ^{SI} is always dominant and can never be canceled by the light Higgs. Hence, the spin-independent cross-section is always high. Only for neutralino masses above 120 GeV the annihilation in the early Universe may be on the exact resonance, when all constraints are taken into account (note again

that small m_A are strongly constrained), and we can again observe an increase of Δ_{tot} when $2m_{\widetilde{\chi}} \approx m_A$ is fulfilled, compare figure 5.7.

5.4.2. Lepton final states

In this section we discuss in detail the the mapping of the scenarios with lepton final states of neutralino annihilation into the direct detection plane and their tuning level. In figure 5.9 one can see that at the Z- and h-resonances again untuned models for every value of σ^{SI} are present. Other natural scenarios occur in the branch of the heavy Higgs and CP-odd Higgs resonance. Compared to the quark final states we see that the plane is more homogeneously filled and provides viable solutions at almost every point. A thick red stripe appears at direct detection cross-sections of about 10^{-11} pb. This overlays a whole region with medium-tuned models.

In principle neutralino annihilation into a pair of leptons is possible either via s-channel Higgs or t-channel light slepton exchanges (Since the majority of $\ell\bar{\ell}$ final states are $\tau\bar{\tau}$, we talk about light stau $\widetilde{\tau}_1$ exchange only). As a general rule we can say that whenever stau exchange is important the $\widetilde{\tau}_1$ will be light and whenever stau exchange does not contribute significantly to the annihilation cross-section, the stau mass is unrestricted and may be as large as our parameter space allows, *i.e.* roughly 4 TeV. For lepton final states we find in figure 5.10 that the $\widetilde{\tau}_1$ is always lighter than 450 GeV, such that they always influence $\langle\sigma_{ann}v\rangle$. Therefore, even on the exact Z-resonance, the contribution from stau exchanges to $\langle\sigma_{ann}v\rangle$ cannot be neglected and the interference between s-channel Higgs and t-channel stau exchanges always has to be considered. At the exact Z-resonance those two contributions need to be arranged precisely in a way that gives the correct relic abundance. This introduces relations among μ, that is important for the Z-exchange, and $\tan\beta$, which plays a role in the stau exchange. As a consequence cancellations in σ^{SI} are not possible and cross-sections below 10^{-13} pb do not occur.

Apart from the stripe from H and A mediated annihilations, the rest of the plane is mainly filled with slepton annihilation. Especially in the neutralino mass range between 65 and 80 GeV we find models for every possible σ^{SI}. This is completely different to the previously discussed quark final states and has been missed in past studies of the pMSSM [32, 56]. We want to stress that if a signal from direct detection experiments is reported in this mass region we can already say that slepton annihilation is the mechanism to get the correct relic abundance and we would have an idea for a promising production channel of neutralinos at the LHC.

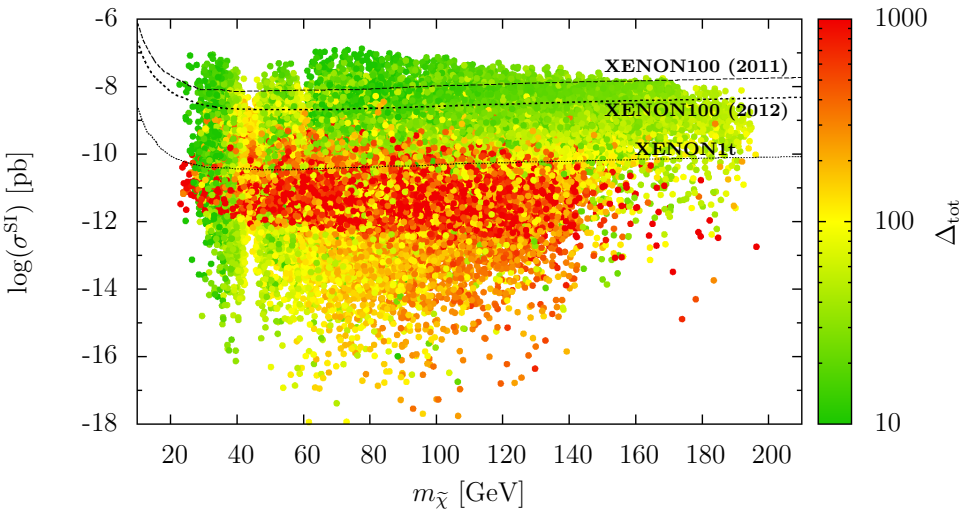

Figure 5.9.: All scenarios with dominant neutralino annihilation into a pair of leptons and their level of tuning in the direct detection plane.

The area filled with highly fine tuned models at mid range direct detection cross section corresponds to the models that feature the lightest possible staus. To explain how these come about, an investigation of the slepton mass matrix has to be done. For staus this is given by:

$$\boldsymbol{M}^2_{\tilde{l}} = \begin{pmatrix} m^2_{\tilde{l}_L} + (-\frac{1}{2} + \sin^2\theta_W) M_Z^2 \cos 2\beta + m_\tau^2 & m_\tau(A_\tau - \mu \tan\beta) \\ m_\tau(A_\tau - \mu\tan\beta) & m^2_{\tilde{l}_R} + \sin^2\theta_W M_Z^2 \cos 2\beta + m_\tau^2 \end{pmatrix} \tag{5.14}$$

To find the mass eigenstates we need to diagonalize the matrix by finding its eigenvalues. These are:

$$\begin{aligned} m^2_{\tilde{\ell}_{1,2}} =& \frac{1}{2}\Big[m^2_{\tilde{l}_L} + m^2_{\tilde{l}_R} - \frac{1}{2} M_Z^2 \cos 2\beta + 2m_\tau^2 \\ & \pm \sqrt{(m^2_{\tilde{l}_L} - m^2_{\tilde{l}_R} + (-\frac{1}{2} + 2\sin^2\theta_W) M_Z^2 \cos 2\beta)^2 + 4m_\tau^2 (A_\tau - \mu\tan\beta)^2}\Big] \,. \end{aligned} \tag{5.15}$$

Approximating $\cos 2\beta$ with -1, neglecting the factor of m_τ^2 and using $-0.5 + 2\sin\theta_W^2 \approx 0.04 = 1/25 = 1/5^2$, equation(5.15) simplifies into:

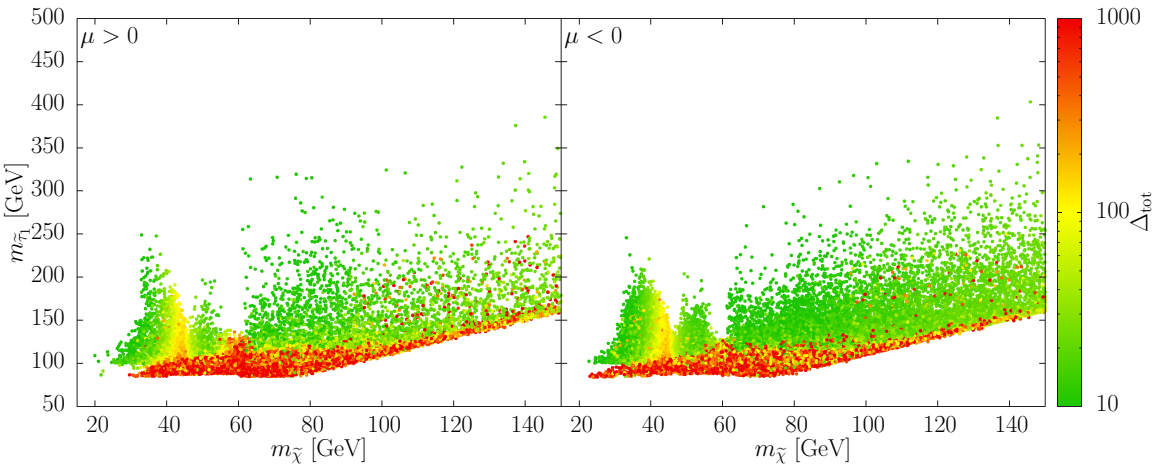

Figure 5.10.: The stau mass of scenarios with neutralino annihilation into leptons and their level of fine-tuning. We show the cases for a positive (left) and negative (right) μ-term separately and see that there is no difference. Stau interference is important in all regions.

$$m^2_{\tilde{l}_{1,2}} = \frac{1}{2}\left[m^2_{\tilde{l}_L} + m^2_{\tilde{l}_R} + M_Z^2\left(\frac{1}{2} \pm \sqrt{\left(\frac{m^2_{\tilde{l}_L}}{M_Z^2} - \frac{m^2_{\tilde{l}_R}}{M_Z^2} + \frac{1}{5^2}\right)^2 + 4\frac{m_\tau^2}{M_Z^4}(A_\tau - \mu\tan\beta)^2}\right)\right] . \tag{5.16}$$

The second term in the square root is heavily suppressed by a factor of $m_\tau^2/M_Z^4 \approx 10^{-8}$ GeV^{-2}. Since the A-terms are roughly of the order of the soft-masses of the sleptons, *i.e.* 10^3 GeV, this term is only important, when the product of μ and $\tan\beta$ is large. To see how the slepton masses behave for the smallest possible soft terms, we further assume $m^2_{\tilde{l}_L} \approx m^2_{\tilde{l}_R} \approx M_Z^2$:

$$m^2_{\tilde{\tau}_{1,2}} \simeq \frac{1}{2}\left[2M_Z^2 + M_Z^2\left(\frac{1}{2} \pm \left|\frac{m_\tau}{M_Z^2}(A_\tau - \mu\tan\beta)\right|\right)\right] . \tag{5.17}$$

For a small $A_\tau - \mu\tan\beta$ the slepton masses are always greater than the Z-mass, namely $\sqrt{5}/2 M_Z \approx 100$ GeV. To end up with smaller stau masses, we therefore need a high μ-term.

A second possibility to obtain light staus is when $m_{\tilde{l}_L} \gg m_{\tilde{l}_R}$ is fulfilled. As an approximation for the stau masses we find here:

$$m^2_{\tilde{\tau}_1} \approx m^2_{\tilde{l}_R} + \frac{M_Z^2}{4} - \frac{m_\tau^2 (A_\tau - \mu \tan\beta)^2}{16 m^2_{\tilde{l}_L}} \ . \tag{5.18}$$

One can see that $m_{\tilde{\tau}_1}$ is primarily determined by $m_{\tilde{l}_R}$ and for $\frac{m_\tau^2 (A_\tau - \mu \tan\beta)^2}{16 m^2_{\tilde{l}_L}} \sim 100^2$ GeV^2 the mass is suppressed by the off-diagonal elements. These two approximations show why scenarios with the lightest possible staus are severely fine-tuned.

Below neutralino masses of around 35 GeV we find for both signs of μ a separation of high and low fine-tuned models. For the scenarios with $m_{\tilde{\tau}_1} < 100$ GeV only stau mediated neutralino annihilation can be important and we find that $m_{\tilde{l}_L} \sim m_{\tilde{l}_R}$. A detailed study on light staus may be found in reference [62].

The scenarios with sleptons whose stau mass is strongly influenced by the off-diagonal elements posses, as we argued above, a very large μ-term, so that their wino component is positive and no cancellations in σ^{SI} appear, compare figure 5.6. Therefore they do not map to very small σ^{SI}.

5.4.3. W-boson final states

Here, we shortly discuss the annihilation of neutralinos into a pair of W-bosons. In figure 5.11 it is visible that all of these scenarios show a small level of fine-tuning and cancellations for σ^{SI} are possible, such that future direct search limits can be avoided. The annihilation is mediated via light charginos whose masses depend strongly on the μ-term, as we can see when looking at the chargino mass matrices. For the basis $\psi^\pm = (\widetilde{W}^+, \widetilde{H}_u^+, \widetilde{W}^-, \widetilde{H}_d^-)$ this matrix is given by:

$$\mathcal{L}_{\text{chargino mass}} = -\frac{1}{2} (\psi^\pm)^T \mathbf{M}_{\widetilde{C}} \psi^\pm + \text{c.c.} \tag{5.19}$$

$$\mathbf{M}_{\widetilde{C}} = \begin{pmatrix} 0 & X^T \\ X & 0 \end{pmatrix} \text{ with } X = \begin{pmatrix} M_2 & g v_u \\ g v_d & \mu \end{pmatrix} = \begin{pmatrix} M_2 & \sqrt{2} \sin\beta m_W \\ \sqrt{2} \cos\beta m_W & \mu \end{pmatrix} \ . \tag{5.20}$$

One then finds as a good approximation for the eigenmasses in the case of $\mu < M_2$ (which is mostly the case for these scenarios) through diagonalizing [50]:

$$m_{\widetilde{C}_1} \approx \mu - \frac{m_W^2 (\mu + M_2 \sin 2\beta)}{M_2^2 - \mu^2} \ . \tag{5.21}$$

Therefore the lightest chargino mass is primarily determined by the μ-term. Hence, the situation is clear: To have efficient chargino mediated annihilation, light charginos and

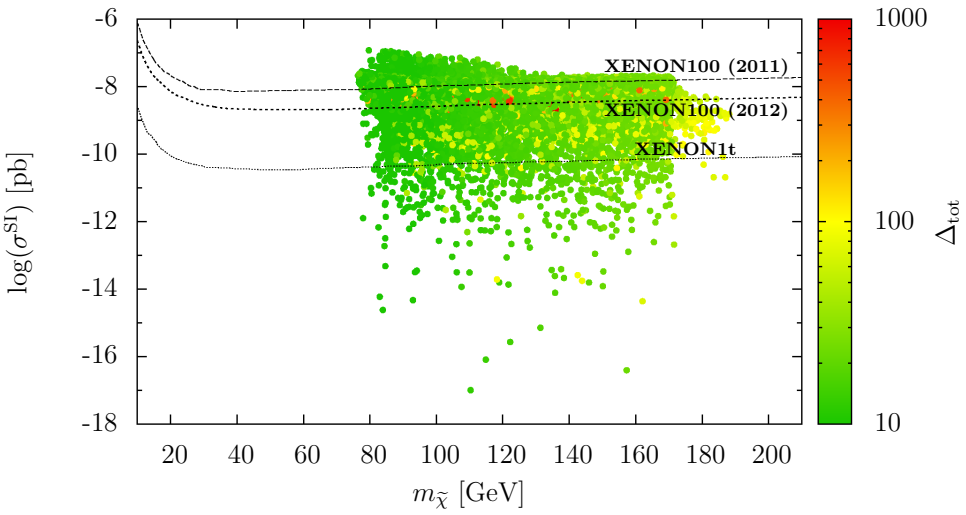

Figure 5.11.: All scenarios with W-boson final states as the dominant neutralino annihilation mechanism. A large number of untuned scenarios will survive future direct searches.

therefore a small μ-term are necessary, which results in low fine-tuning. Most of the scenarios are situated at values of σ^{SI} that will be tested by future direct searches, but cancellations between the heavy and light Higgs contributions allow some scenarios to avoid those.

5.4.4. Slepton coannihilations

A coannihilation describes a process in that the neutralino annihilates with a different supersymmetric particle into Standard Model particles. These processes are also important when the relic density is calculated. Neutralino coannihilations with sleptons include both, sneutrinos and staus. We find them to be of equally importance in our parameter space. For coannihilations to take place the participating slepton has to be almost mass degenerate with the neutralino. In figure 5.12 we plot their level of tuning in the direct detection plane.

Concentrating first on the stau coannihilation we observe here that for the interacting $\widetilde{\tau}_1$ a light mass is obtained through $m_{\tilde{l}_L} \gg m_{\tilde{l}_R}$, whereas models with $m_{\tilde{\ell}_L} \simeq m_{\tilde{l}_R}$ are very rare. This is simply a matter of probability: If we want the latter condition to be

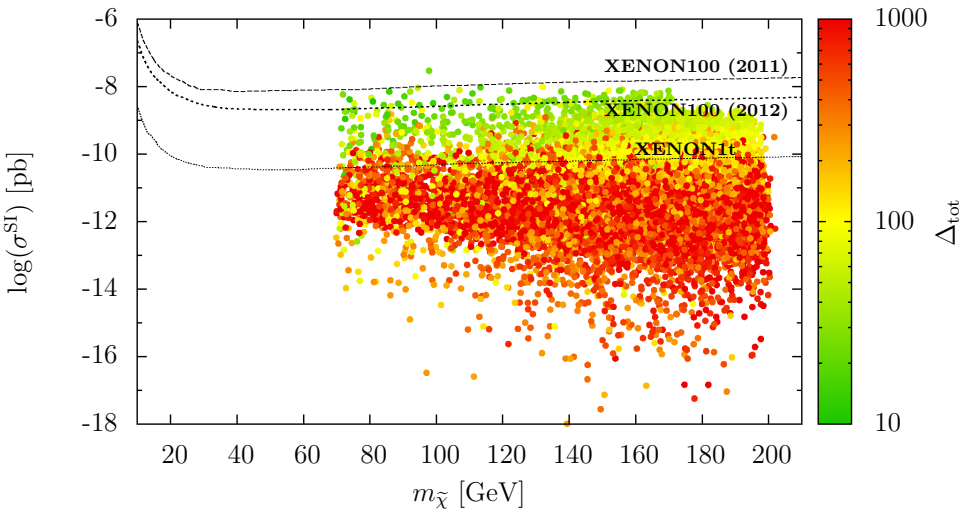

Figure 5.12.: All scenarios with dominant slepton coannihilation as the annihilation mechanism. XENON1t may probe all untuned scenarios.

responsible for creating light staus, both slepton soft mass parameters have to be small, *i.e.* of the order of 100 GeV. This is just a very small fraction of the parameter space, such that these models are rare due to the linear scanning method[3]. Stau coannihilations only appear for neutralino masses above approximately 80 GeV, since staus cannot be lighter than that.

For the sneutrino coannihilations we observe that $m_{\tilde{\ell}_R} \gg m_{\tilde{\ell}_L}$ must be given to have light sneutrinos. The mass of the sneutrino is given by [96]:

$$m_{\tilde{\nu}} = m_{\tilde{e}_L} + M_Z^2 \cos 2\beta \cos^2 \theta_W \ , \tag{5.22}$$

such that it is mainly given by $m_{\tilde{\ell}_L}$ (since this determines $\tilde{e}_L$). As $\cos 2\beta$ is negative, the sneutrino is always lighter than the selectron. It is even possible that the sneutrino becomes the LSP, but we did not consider this possibility in our study. The μ-term is virtually unimportant and can take all possible values. Cancellations in σ^{SI} are possible for both, sneutrino and stau coannihilations, but the complete untuned parameter space may be probed by the predicted XENON1t exclusion limit.

[3]Note that we did not perform a focused scan with these boundaries at this neutralino mass region.

5.5. The muon anomalous magnetic moment and the μ-term

In this section we discuss the influence of the muon anomalous magnetic moment condition on our scenarios. We explain how it is possible to correctly achieve the positive pull of a_μ compared to the Standard Model prediction for both, a positive and a negative sign of the μ-term. In reference [97] we find the MSSM loop contributions to a_μ:

$$a_\mu(\widetilde{W}-\widetilde{H},\widetilde{\nu}_\mu) = \frac{g^2}{8\pi^2}\frac{m_\mu^2 M_2 \mu\tan\beta}{m_{\widetilde{\nu}}^4}F_a\left(\frac{M_2^2}{m_{\widetilde{\nu}}^2},\frac{\mu^2}{m_{\widetilde{\nu}}^2}\right), \tag{5.23}$$

$$a_\mu(\widetilde{B},\widetilde{\mu}_L-\widetilde{\mu}_R) = \frac{g'^2}{8\pi^2}\frac{m_\mu^2 \mu\tan\beta}{M_1^3}F_b\left(\frac{m_{\widetilde{\mu}_L}^2}{M_1^2},\frac{m_{\widetilde{\mu}_R}^2}{M_1^2}\right), \tag{5.24}$$

$$a_\mu(\widetilde{B}-\widetilde{H},\widetilde{\mu}_L) = \frac{g'^2}{16\pi^2}\frac{m_\mu^2 M_1 \mu\tan\beta}{m_{\widetilde{\mu}_L}^4}F_b\left(\frac{M_1^2}{m_{\widetilde{\mu}_L}^2},\frac{\mu^2}{m_{\widetilde{\mu}_L}^2}\right), \tag{5.25}$$

$$a_\mu(\widetilde{W}-\widetilde{H},\widetilde{\mu}_L) = -\frac{g'^2}{16\pi^2}\frac{m_\mu^2 M_2 \mu\tan\beta}{m_{\widetilde{\mu}_L}^4}F_b\left(\frac{M_2^2}{m_{\widetilde{\mu}_L}^2},\frac{\mu^2}{m_{\widetilde{\mu}_L}^2}\right), \tag{5.26}$$

$$a_\mu(\widetilde{B}-\widetilde{H},\widetilde{\mu}_R) = -\frac{g'^2}{8\pi^2}\frac{m_\mu^2 M_1 \mu\tan\beta}{m_{\widetilde{\mu}_R}^4}F_b\left(\frac{M_1^2}{m_{\widetilde{\mu}_R}^2},\frac{\mu^2}{m_{\widetilde{\mu}_R}^2}\right). \tag{5.27}$$

Here, the positive defined functions F_a and F_b are given by:

$$\begin{aligned}
F_a(x,y) &= -\frac{G_3(x)-G_3(y)}{x-y}, \\
F_b(x,y) &= -\frac{G_4(x)-G_4(y)}{x-y}, \\
G_3(x) &= \frac{1}{2(x-1)^3}\left[(x-1)(x-3)+2\ln x\right], \\
G_4(x) &= \frac{1}{2(x-1)^3}\left[(x-1)(x+1)-2x\ln x\right].
\end{aligned}$$

For a positive μ the contributions from equations (5.26), the wino–higgsino–left-handed smuon loop, and (5.27), the bino–higgsino–right-handed smuon loop, give a negative pull to a_μ and hence must be dominated by the sum of equations (5.23), the wino–higgsino–muon sneutrino loop, (5.24), the bino–left-handed smuon–right-handed smuon loop, and (5.25), the bino–higgsino–left-handed smuon loop. As is well known, there is in general no difficulty to achieve this and to get the correct predictions for a_μ. In figure 5.13

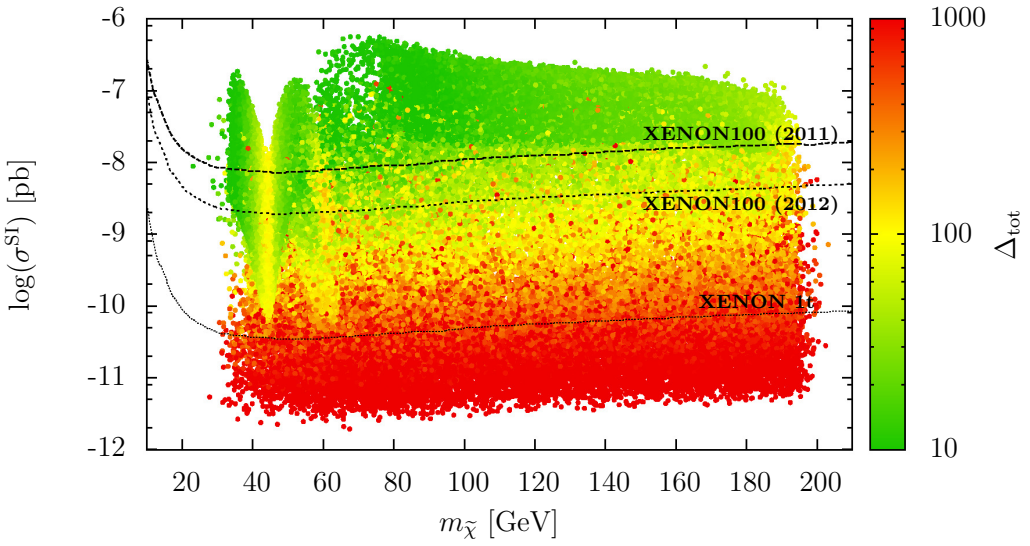

Figure 5.13.: Presenting the fine-tuning of our models in the direct detection plane after applying the a_μ condition for positive values of the μ-term.

we plot the models for positive μ that survive the a_μ condition and find, comparing to figure 5.3, that the results essentially do not change.

It is believed that a_μ cannot be fulfilled for a negative μ-term if M_1 and M_2 are positive [98]. However, the total amount of the achieved positive pull of a_μ can be sufficient to correctly deviate from the Standard Model prediction, when equations (5.26) and (5.27) dominate. This situation occurs in the limit of $m_{\widetilde{l}_L}/m_{\widetilde{l}_R} \gg 1$, see left panel of figure 5.14. In this case the $\widetilde{\tau}_1$'s are always light ($\lesssim 400$ GeV) due to equation (5.18) and, compare to section 5.4.2, scenarios with dominant neutralino annihilation into lepton final states via light stau exchange are therefore the models left-over after applying the a_μ condition. In figure 5.15 we show the level of tuning of the models that pass all experimental limits for a negative μ-term.

It is very important to note that a_μ is strongly depends on the smuon parameters. Satisfying a_μ becomes easier once one abandons the slepton mass generation universality since the relic density condition, which restricts the stau mass, would then become independent of a_μ.

In our set-up we found that for large negative values of μ the contributions of equations

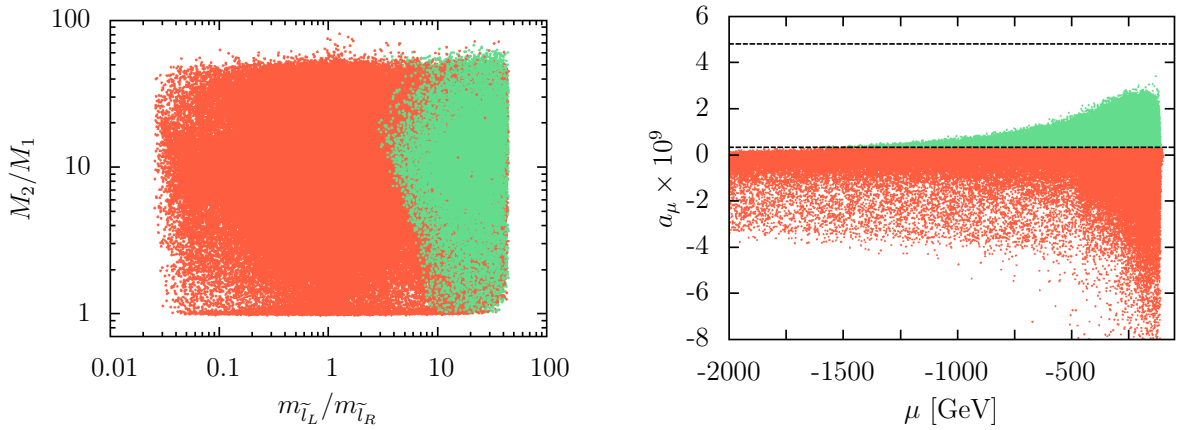

Figure 5.14.: The green scenarios satisfy the a_μ condition. The left plot shows that $m_{\tilde{l}_L}/m_{\tilde{l}_R}$ must be much greater than one in order to respect a_μ for a negative μ-term; the right panel shows how a lower limit of μ arises through the a_μ condition.

(5.23) and (5.24) become important again due to the loop functions F_a and F_b. Then the negative sign of μ pulls of a_μ to negative values again, such that the experimental limits cannot be respected anymore. Hence, a lower limit on μ of about -1500 GeV emerges, see the right panel of figure 5.14. Low fine-tuned scenarios are then favored when the a_μ condition is applied and models with large negative values of μ are automatically removed. These include the scenarios whose stau mass is strongly influenced by $(A_\tau - \mu \tan\beta)$, highly fine-tuned scenarios from Higgs-resonant neutralino annihilation and many models with slepton coannihilations. This shows that a negative sign of μ is not at all in contradiction to the muon anomalous magnetic moment condition even though we did not distinguish between slepton generations. In figure 5.15 we especially see that models at the Z- and h-resonances can avoid direct detection by XENON1t.

5.6. Sensitivity of the direct detection cross-section

We have seen in section 5.3 that a cancellation between the two most important contributions to the direct detection cross-section is possible when $M_1 + \mu \tan\beta$ is positive and that in this way a suppression of σ^{SI} for a negative μ-term may occur. Scenarios might show up where these cancellations are almost exact and values of σ^{SI} as low as 10^{-22} pb may appear. While these models are, of course, not excluded from the theory, we are faced with another instance of a highly sensitive quantity. If σ^{SI} is very small the cancellations

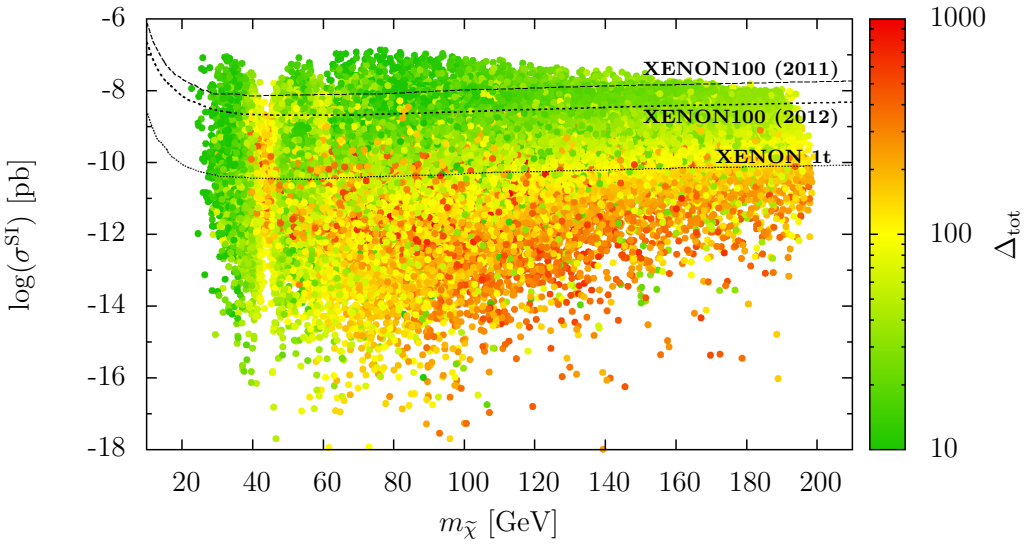

Figure 5.15.: Showing the level of fine-tuning in the direct detection plane for negative μ after the a_μ condition has been applied

are extremely well tuned against each other, which only happens in a tiny fraction of the complete parameter space. We therefore define another measure tuning in analogy to the sensitivity of the Z-mass:

$$\Delta \mathrm{f_i} \equiv \left| \frac{\partial \ln \sigma^{\mathrm{SI}}}{\partial \ln p_i} \right| \quad , \qquad \Delta_\mathrm{f} \equiv \sqrt{\sum\nolimits_{p_i=\mu,\tan\beta,M_1,M_2,m_A} \{\Delta \mathrm{f_i}\}^2} \quad . \tag{5.28}$$

This sensitivity is different in its interpretation to the Z-mass tuning. The latter one measures how well the value of the Z-mass is reproduced, so that there is a direct connection to the physical process of electroweak symmetry breaking. This electroweak fine-tuning connects the "old" theory, the Standard Model, with the theory in which one wants to embed it, here the MSSM. When we introduce the MSSM as an extension of the SM we must be able to reduce the extended theory to the well established one and the electroweak fine-tuning is an indicator how well this can be done. It indicates an unnaturally large separation of the electroweak and the SUSY breaking scale and how well the hierarchy problem of the SM may still be solved.

The tuning of σ^{SI} instead measures how close the specific parameter choice is at the

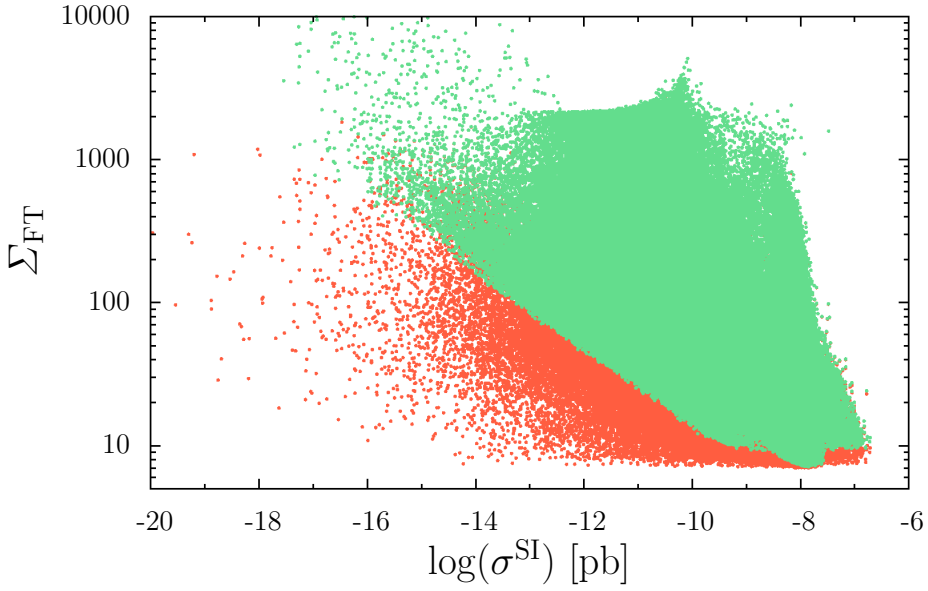

Figure 5.16.: The effect of adding the functional tuning (green models) to the electroweak fine-tuning (ref models). A minimal amount of fine-tuning can be found for a given value of $\sigma^{\rm SI}$ that increases when $\sigma^{\rm SI}$ decreases.

hypersurface where the cancellations are exact. Without a symmetry asking our parameters to be close to this surface, it appears rather unlikely and unnatural that the relation is almost fulfill exactly which leads us to the introduction of the tuning measure $\Delta \mathrm{f_i}$ as an indicator for this improbability.

To evaluate the sensitivity of $\sigma^{\rm SI}$ we chose a variation of its determining parameters by 0.01 % of their total range[4] and approximated expression (5.28) by:

$$\Delta \mathrm{f_i} \simeq \frac{p_i}{\sigma^{\rm SI}} \frac{\sigma^{\rm SI}(p_i + \delta) - \sigma^{\rm SI}}{\delta} \ . \tag{5.29}$$

We then calculated with `micrOMEGAs` the relative variation for $\mathrm{p_i} = \{M_1, M_2, \mu, \tan\beta, m_A\}$. The overall fine-tuning measure that includes both, the electroweak and the functional tuning, is then defined as:

$$\Sigma_{\rm FT} \equiv \sqrt{\Delta^2_{\rm tot} + \Delta^2_{\rm f}} \ . \tag{5.30}$$

In this way we deal with both tunings on equal footing.

[4]This choice is to some extend arbitrary, but as we found the maximal tuning $\Delta_{\rm tot}$ to be of order 10^4, we chose the relative variation to be $1/\Delta_{\rm tot}(\mathrm{p_{max}} - \mathrm{p_{min}})$.

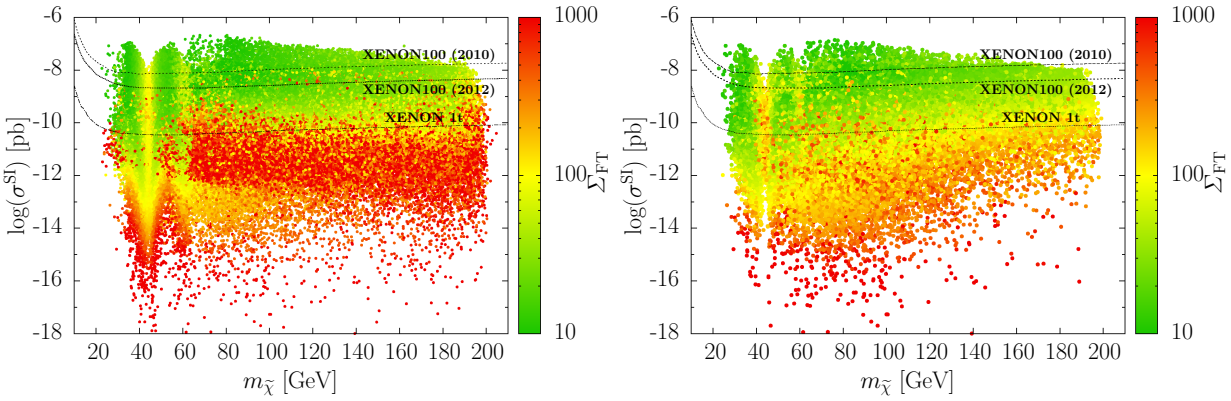

Figure 5.17.: The distribution of the fine-tuning measure Σ_{FT}, that additionally includes the functional tuning of σ^{SI}, in the direct detection plane. This only applies to scenarios with negative μ since no cancellations are possible for the positive sign case. The a_μ condition has been applied in the right panel.

We present our results in the $\Sigma_{\mathrm{FT}} - \sigma^{\mathrm{SI}}$-plane and find a minimal amount of tuning corresponding to each given value of the direct detection cross section. In general, scenarios with a small σ^{SI} that initially had a small tuning level Δ_{tot} are mapped to higher values of the new tuning measure Σ_{FT}. The smallest direct detection cross section for $\Sigma_{\mathrm{FT}} \leq 100$ is approximately 6×10^{-14} pb.

In figure 5.17 we additionally show how the overall fine-tuning measure, Σ_{FT}, maps into the direct detection plane. It is visible, compare to figures 5.4 and 5.15, that for those scenarios in which the cancellations suppress σ^{SI} below approximately 10^{-14} pb the functional tuning measure becomes dominant and brings the overall tuning into an unacceptable range. For larger cross-sections the fine-tuning is still dominated by the sensitivity of the Z-mass and no change to the previously discussed results is observed. Comparing the left- and right-panel of figure 5.17 one can again observe the removal of the highly fine-tuned band containing models with light staus whose mass is strongly influenced by the off-diagonal stau mass matrix elements, when the a_μ constraint is applied. We see that even when the functional tuning measure is taken into account scenarios that possess a fine-tuning Σ_{FT} lower than 100 are possible in the pMSSM avoiding all of our applied constraints and direct searches.

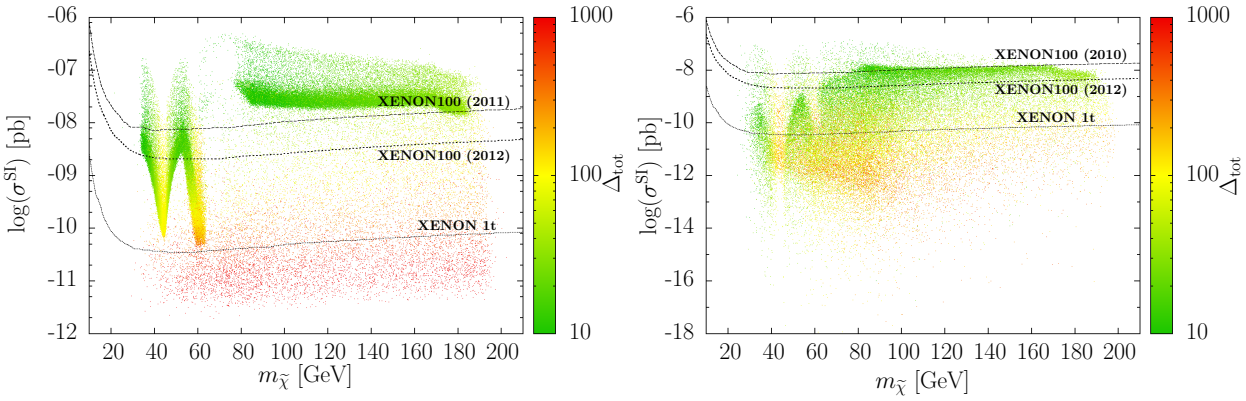

Figure 5.18.: The level of fine-tuning and additionally the density of our scenarios arising from a homogeneously scan of the parameter space. This may be interpreted as a probability measure for a given area. We show the cases for positive (left panel) and negative μ (right panel) separately and have applied the a_μ condition in both cases.

5.7. Probability distribution

So far we have neglected completely the probability distribution of our simulated models in the direct detection plane. We have shown several plots from scans that covered the complete parameter ranges as explained in section 4.2. To calculate the fine-tuning for every accessible part of the pMSSM, we also scanned some smaller regions of the parameter space separately, *i.e.* we also performed focused scans. This implies, of course, that the parameter space is not covered homogeneously and hence a possible statistical interpretation of the collected simulated data is destroyed. Only the envelope has a meaning since points lying outside can never be reached. To recover a probabilistic interpretation, we show in figure 5.18 only those scenarios, that were obtained by the global (randomized) scans of the parameter space and a subsequent removal of the points that do not respect the experimental bounds. It is immediately apparent that some regions are statistically more important. We distinguish again between positive (left panel) and negative μ (right panel), because the results are qualitatively different. For a positive μ-term, we see that the regions from Z, h, H and A resonant annihilations and the light chargino mediated annihilation into W-bosons have a stronger weight than light stau annihilations. For negative μ, however, these do play an important role, especially in the neutralino mass region between 65 and 80 GeV.

Adding this measure of probability to the previously discussed level of tuning, we should now expect signals in the untuned, densely populated parameter regions.

6. Conclusions

In this thesis we performed a scan over an eleven-dimensional parameter space of the low-energy phenomenological minimal supersymmetric standard model and analyzed how much tuning is necessary to reach a certain point in the plane spanned by the neutralino mass and the spin-independent direct detection cross-section σ^{SI} (direct detection plane) in order to find out to which extent direct detection experiments can test the natural supersymmetric parameter space. As input parameters we chose the bino (M_1), wino (M_2) and gluino (M_3) soft-masses, the ratio of the vacuum expectation values of the two Higgs doublets ($\tan\beta$), the supersymmetric Higgs mass parameter (μ), the pseudo-Higgs mass (m_A), a universal trilinear coupling constant (a_0), soft-mass parameters for the first and second ($m_{\tilde{q}_{1,2}}$) and third ($m_{\tilde{q}_3}$) generation of scalar quarks as well as mass parameters for the superpartners of the left-handed ($m_{\tilde{\ell}_L}$) and right-handed ($m_{\tilde{\ell}_R}$) leptons. These have been randomly scanned to cover the neutralino mass range below 200 GeV and we particularly allowed for a negative μ-term.

In the scan we applied all current experimental data that probes the supersymmetric parameter space. From the cosmological side we used the strongest bounds possible by taking into account the upper and lower limit of the relic density. The simulated scenarios respect accurate measurements on the electroweak sector of the Standard Model by the LEP collider and also very recent measurements of the LHC on supersymmetric particle searches, branching ratios and especially the recent strong evidence for a Higgs boson at a mass of about 125 GeV. Another constraint arises from the new exclusion limits published by the XENON100 collaboration. Additionally, the measured deviation of the muon anomalous magnetic moment from the Standard Model prediction has been included and, to stress its impact, discussed separately for both signs of the μ-term.

We first discussed the most important contribution to the thermally averaged neutralino annihilation cross-section that is crucial to produce the correct relic abundance. We showed in figure 5.2 how the mechanisms arrange in the direct detection plane and found that each mechanism has a preferred region. If direct dark matter experiments report a positive signal in future experiments, a connection could in this way be drawn to find

promising production channels of neutralinos at the LHC. In this context we excluded neutralino annihilation to be responsible for the claimed excess of photon signals in the Fermi LAT data at a neutralino mass of about 130 GeV.

We plotted the distribution of the fine-tuning measure in the direct detection plane for positive (figure 5.3) and negative (5.4) μ finding distinctions between both cases. For positive μ a great part of the untuned parameter space has already been tested and mostly excluded by direct detection experiments. Scenarios with little fine-tuning especially survive in regions where the neutralino annihilates through resonant Z- or light Higgs boson exchanges. Away from these regions a clear tendency for higher fine-tuning for smaller cross-sections is visible, which is due to a necessary increase of μ to decrease the higgsino components of the neutralino. For negative μ cancellations in the direct detection cross-section shift many untuned solutions below the current direct search limits and a great part of the natural parameter space has not yet been tested. At the Z- and h-resonances we can again observe a vertical stripe in which the fine tuning stays low for every possible value of the direct detection cross-section σ^{SI}. In general, for a given point in the direct detection plane negative values of μ are favored from the fine-tuning perspective due to the shift of σ^{SI}. In the following we presented why these cancellations in the direct detection cross-section only occur for negative μ and showed in figure 5.6 the necessity for the wino component of the neutralino to be negative.

We continued explaining in detail the mapping of the scenarios with a negative μ-term into the direct detection plane for all possible annihilation mechanisms separately. In figure 5.7 we found that quark final states can still explain the dark matter riddle at the Z- and h-resonance even if XENON1t does not observe a signal. Neutralino annihilation into a pair of leptons offers valid solutions in the complete neutralino mass range through light stau-exchange, see figure 5.9. Most of the scenarios with chargino mediated annihilation into W-bosons will be tested by XENON1t, however, cancellations in σ^{SI} allow some untuned models to avoid possible detection, compare figure 5.11. Slepton coannihilations are mainly situated below the predicted XENON1t exclusion limit, however these scenarios have large tunings as was presented in figure 5.12.

Next we investigated the effect of the muon anomalous magnetic moment on our models and saw that for both signs of μ many models survive. As was known before, there is no great difficulty in respecting a_μ for positive μ and we did not find any impact of the condition on our models, see figure 5.13. For negative μ we showed that it is, in contrast to earlier works in the literature, possible to fulfill the condition as long as $m_{\tilde{\ell}_L} \gg m_{\tilde{\ell}_R}$ (see figure 5.14). In this case we know from approximating the slepton

masses by equation (5.18) that staus are always light and help to produce the correct relic abundance. Hence, most of the scenarios that survive show dominant annihilation into a pair of leptons. We pointed out that further distinction between slepton generations will make it simpler to respect a_μ since the relic density condition, which constraints the stau mass, will then become independent of a_μ, which mainly depends on the smuon parameters. We also found a lower bound on μ of about -1.5 TeV, which automatically eliminates the most tuned models.

To quantify the cancellations in σ^{SI} we introduced a measure of "equation-tuning" analogously to the definition of electroweak fine-tuning in section 5.6 and found that scenarios that have a direct detection cross-section smaller than $\approx 10^{-15}$ pb are always unacceptably tuned. Finally, we showed the probability to reach a certain point in the direct detection plane when performing a homogeneous, randomized scan in figure 5.18. We concluded that for positive μ the Z- and h-resonance area is the statistically preferred region when direct searches are included. For negative μ light stau annihilation also forms a statistically important mechanism.

Acknowledgements

I owe the biggest thanks to my parents: I lack adequate words for the support you gave me during my studies and for all the possibilities you opened up for my future.
I want to thank Manfred and Yasutaka for their help to find a PhD position and for the ideas and the work they put into our paper. I did not expect to be part of a publication during my diploma and will always remember the photo session when finally submitting.
To Manfred I owe special thanks for the possibility to visit the winter school in Schladming and to Thomas for the opportunity to attend the Invisibles pre-meeting in Madrid and to give my first talk at a conference.
I enjoyed my time at the institute, especially all the dinners and drinks I shared and parties I celebrated with everyone. Leaving is not easy for me and I will keep this year in very good memory.
Stefan has earned a special place here, as it is almost impossible to arrive at work before him. If someone wants to take my desk, he first has to translate all the following words into German: Mehlspeisen, Standseilbahn, Jause, Beistrich, Tischverteiler und Schrieb. Not even all Austrians know these.
At the end, I want to express again how thankful I am for all the questions answered, mistakes found and, in general, for the great supervision by Yasutaka!

A. Notations and conventions

As we stated in the thesis, we use the notation of reference [50]. Hence, see this review for more details. This appendix gives details about our notation and conventions regarding the Weyl representation of spinors. The position and momentum four-vectors are:

$$x^\mu = (t,\, \vec{x}), \qquad\qquad p^\mu = (E,\, \vec{p}) \ , \tag{A.1}$$

and the spacetime-derivative:

$$\partial_\mu = (\partial/\partial t,\, \vec{\nabla}) \ . \tag{A.2}$$

The sign convention for our metric is:

$$\eta_{\mu\nu} = \mathrm{diag}(+1, -1, -1, -1) \ . \tag{A.3}$$

The Dirac equation for four-component spinors is given by:

$$\mathcal{L}_{\mathrm{Dirac}} \ = \ i\overline{\Psi}_{D}\gamma^\mu\partial_\mu\Psi_{D} - M\overline{\Psi}_{D}\Psi_{D} \ \ , \tag{A.4}$$

where we use the following γ and σ matrices:

$$\gamma^\mu = \begin{pmatrix} 0 & \sigma^\mu \\ \overline{\sigma}^\mu & 0 \end{pmatrix}, \qquad\qquad \gamma_5 = \begin{pmatrix} -1 & 0 \\ 0 & 1 \end{pmatrix}, \tag{A.5}$$

$$\begin{aligned} \sigma^0 = \overline{\sigma}^0 &= \begin{pmatrix} 1 & 0 \\ 0 & 1 \end{pmatrix}, \qquad & \sigma^1 = -\overline{\sigma}^1 &= \begin{pmatrix} 0 & 1 \\ 1 & 0 \end{pmatrix}, \\ \sigma^2 = -\overline{\sigma}^2 &= \begin{pmatrix} 0 & -i \\ i & 0 \end{pmatrix}, \qquad & \sigma^3 = -\overline{\sigma}^3 &= \begin{pmatrix} 1 & 0 \\ 0 & -1 \end{pmatrix} \ . \end{aligned} \tag{A.6}$$

The four-component Dirac spinor is given by two two-component Weyl spinors where the different indices α, $\dot{\beta}$ denote the different behavior under Lorentz transformations:

$$\Psi_{D} = \begin{pmatrix} \xi_{\alpha} \\ \chi^{\dagger\dot{\alpha}} \end{pmatrix} \tag{A.7}$$

$$\overline{\Psi}_{D} = \Psi_{D}^{\dagger} \begin{pmatrix} 0 & 1 \\ 1 & 0 \end{pmatrix} = \begin{pmatrix} \chi^{\alpha} & \xi_{\dot{\alpha}}^{\dagger} \end{pmatrix} \quad , \tag{A.8}$$

When we apply the projection operators

$$P_L = (1 - \gamma_5)/2, \qquad P_R = (1 + \gamma_5)/2 \tag{A.9}$$

to this Dirac spinor, we find:

$$P_L \Psi_{D} = \begin{pmatrix} \xi_{\alpha} \\ 0 \end{pmatrix}, \qquad P_R \Psi_{D} = \begin{pmatrix} 0 \\ \chi^{\dagger\dot{\alpha}} \end{pmatrix} . \tag{A.10}$$

Hence, the dotted and undotted indices correspond to left- and right handed two-component spinors, respectively. It then follows that the Hermitian conjugate of a left-handed Weyl spinor is right-handed, and vice versa:

$$\psi_{\dot{\alpha}}^{\dagger} \equiv (\psi_{\alpha})^{\dagger} = (\psi^{\dagger})_{\dot{\alpha}} \, , \tag{A.11}$$

$$(\psi^{\dagger\dot{\alpha}})^{\dagger} = \psi^{\alpha}. \tag{A.12}$$

Spinor indices are contracted by the antisymmetric ϵ-symbol:

$$\epsilon^{12} = -\epsilon^{21} = \epsilon_{21} = -\epsilon_{12} = 1, \qquad \epsilon_{11} = \epsilon_{22} = \epsilon^{11} = \epsilon^{22} = 0, \tag{A.13}$$

in the following way:

$$\xi_{\alpha} = \epsilon_{\alpha\beta}\xi^{\beta}, \qquad \xi^{\alpha} = \epsilon^{\alpha\beta}\xi_{\beta}, \qquad \chi_{\dot{\alpha}}^{\dagger} = \epsilon_{\dot{\alpha}\dot{\beta}}\chi^{\dagger\dot{\beta}}, \qquad \chi^{\dagger\dot{\alpha}} = \epsilon^{\dot{\alpha}\dot{\beta}}\chi_{\dot{\beta}}^{\dagger} \, . \tag{A.14}$$

Our notation for contracted indices is:

$$\psi^{\alpha}{}_{\alpha} \qquad \text{or} \qquad \bar{\psi}_{\dot{\alpha}}{}^{\dot{\alpha}} \tag{A.15}$$

.

This then yields that contracted spinors do not get a minus sign when they are interchanged:

$$\xi\chi \equiv \xi^{\alpha}\chi_{\alpha} = \xi^{\alpha}\epsilon_{\alpha\beta}\chi^{\beta} = -\chi^{\beta}\epsilon_{\alpha\beta}\xi^{\alpha} = \chi^{\beta}\epsilon_{\beta\alpha}\xi^{\alpha} = \chi^{\beta}\xi_{\beta} \equiv \chi\xi \tag{A.16}$$

One may use all the above to show some useful relations:

$$\xi^{\dagger}\chi^{\dagger} = \chi^{\dagger}\xi^{\dagger} = (\xi\chi)^{*}. \tag{A.17}$$

$$\xi^{\dagger}\bar{\sigma}^{\mu}\chi = -\chi\sigma^{\mu}\xi^{\dagger} = (\chi^{\dagger}\bar{\sigma}^{\mu}\xi)^{*} = -(\xi\sigma^{\mu}\chi^{\dagger})^{*} \tag{A.18}$$

$$\xi\sigma^{\mu}\bar{\sigma}^{\nu}\chi \;=\; \chi\sigma^{\nu}\bar{\sigma}^{\mu}\xi \;=\; (\chi^{\dagger}\bar{\sigma}^{\nu}\sigma^{\mu}\xi^{\dagger})^{*} = (\xi^{\dagger}\bar{\sigma}^{\mu}\sigma^{\nu}\chi^{\dagger})^{*}, \tag{A.19}$$

B. Anticommuting variables

We again refer to [50] as a reference. As we saw in the thesis, given an anticommuting variable η an expression η^2 is zero. We will use this to define derivatives and integration with anticommuting variables. Consider a function of η and expand:

$$f(\eta) = f_0 + \eta f_1. \tag{B.1}$$

Then, we simply define:

$$\frac{df}{d\eta} = f_1. \tag{B.2}$$

and therefore the product rule for two distinct anticommuting variables η, η'

$$\frac{d(\eta'\eta)}{d\eta} = -\frac{d(\eta\eta')}{d\eta} = -\eta'. \tag{B.3}$$

For integration we define

$$\int d\eta = 0, \qquad \int d\eta\, \eta = 1, \tag{B.4}$$

and find again by expanding:

$$\int d\eta\, f(\eta) \;=\; f_1. \tag{B.5}$$

Then it follows:

$$\int d\eta\, f(\eta + \eta') = \int d\eta\, f(\eta), \tag{B.6}$$

and for integration by parts:

$$\int d\eta\, \frac{df}{d\eta} = 0, \tag{B.7}$$

The delta-function is defined by:

$$\int d\eta\, \delta(\eta - \eta')\, f(\eta) \;\; = \;\; f(\eta'), \tag{B.8}$$

which gives:

$$\delta(\eta - \eta') \;\; = \;\; \eta - \eta'. \tag{B.9}$$

Bibliography

[1] F. Gianotti, "Status of Standard Model Higgs searches in ATLAS," *Talk at CERN seminar "Latest update in the search for the Higgs boson"*, CERN, Geneva, Switzerland, 4 July 2012.

[2] J. Incandela, "Status of Standard Model Higgs searches in CMS," *Talk at CERN seminar "Latest update in the search for the Higgs boson"*, CERN, Geneva, Switzerland, 4 July 2012.

[3] K. Begeman, A. Broeils, and R. Sanders, "Extended rotation curves of spiral galaxies: Dark haloes and modified dynamics," *Mon.Not.Roy.Astron.Soc.*, vol. 249, p. 523, 1991.

[4] D. Clowe, M. Bradac, A. H. Gonzalez, M. Markevitch, S. W. Randall, *et al.*, "A direct empirical proof of the existence of dark matter," *Astrophys.J.*, vol. 648, pp. L109–L113, 2006.

[5] E. Komatsu *et al.*, "Seven-Year Wilkinson Microwave Anisotropy Probe (WMAP) Observations: Cosmological Interpretation," *Astrophys.J.Suppl.*, vol. 192, p. 18, 2011.

[6] E. Aprile, "Latest xenon100 results," *Talk given at Dark Attack 2012*, 18.07.2012.

[7] XENON100 collaboration, "Dark Matter Results from 225 Live Days of XENON100 Data," 2012.

[8] R. Bernabei *et al.*, "New results from DAMA/LIBRA," *Eur.Phys.J.*, vol. C67, pp. 39–49, 2010.

[9] G. Angloher, M. Bauer, I. Bavykina, A. Bento, C. Bucci, *et al.*, "Results from 730 kg days of the CRESST-II Dark Matter Search," *Eur.Phys.J.*, vol. C72, p. 1971, 2012.

[10] C. Aalseth *et al.*, "Results from a Search for Light-Mass Dark Matter with a P-type Point Contact Germanium Detector," *Phys.Rev.Lett.*, vol. 106, p. 131301, 2011.

[11] J. Kopp, T. Schwetz, and J. Zupan, "Light Dark Matter in the light of CRESST-II," *JCAP*, vol. 1203, p. 001, 2012.

[12] E. Aprile *et al.*, "Dark Matter Results from 100 Live Days of XENON100 Data," *Phys.Rev.Lett.*, vol. 107, p. 131302, 2011.

[13] E. Aprile *et al.*, "First Dark Matter Results from the XENON100 Experiment," *Phys.Rev.Lett.*, vol. 105, p. 131302, 2010.

[14] Z. Ahmed *et al.*, "Results from a Low-Energy Analysis of the CDMS II Germanium Data," *Phys.Rev.Lett.*, vol. 106, p. 131302, 2011.

[15] H. Goldberg, "Constraint on the Photino Mass from Cosmology," *Phys.Rev.Lett.*, vol. 50, p. 1419, 1983.

[16] J. R. Ellis, J. Hagelin, D. V. Nanopoulos, K. A. Olive, and M. Srednicki, "Supersymmetric Relics from the Big Bang," *Nucl.Phys.*, vol. B238, pp. 453–476, 1984.

[17] G. Jungman, M. Kamionkowski, and K. Griest, "Supersymmetric dark matter," *Phys.Rept.*, vol. 267, pp. 195–373, 1996.

[18] L. Bergstrom, "Nonbaryonic dark matter: Observational evidence and detection methods," *Rept.Prog.Phys.*, vol. 63, p. 793, 2000.

[19] J. R. Ellis, G. Ridolfi, and F. Zwirner, "Radiative corrections to the masses of supersymmetric Higgs bosons," *Phys.Lett.*, vol. B257, pp. 83–91, 1991.

[20] J. R. Ellis, G. Ridolfi, and F. Zwirner, "On radiative corrections to supersymmetric Higgs boson masses and their implications for LEP searches," *Phys.Lett.*, vol. B262, pp. 477–484, 1991.

[21] Y. Okada, M. Yamaguchi, and T. Yanagida, "Upper bound of the lightest Higgs boson mass in the minimal supersymmetric standard model," *Prog.Theor.Phys.*, vol. 85, pp. 1–6, 1991.

[22] H. E. Haber and R. Hempfling, "Can the mass of the lightest Higgs boson of the minimal supersymmetric model be larger than m(Z)?," *Phys.Rev.Lett.*, vol. 66, pp. 1815–1818, 1991.

[23] M. Drees and M. M. Nojiri, "One loop corrections to the Higgs sector in minimal supergravity models," *Phys.Rev.*, vol. D45, pp. 2482–2492, 1992.

[24] G. Degrassi, S. Heinemeyer, W. Hollik, P. Slavich, and G. Weiglein, "Towards high precision predictions for the MSSM Higgs sector," *Eur.Phys.J.*, vol. C28, pp. 133–143, 2003.

[25] O. Buchmueller, R. Cavanaugh, A. De Roeck, J. Ellis, H. Flacher, *et al.*, "Likelihood Functions for Supersymmetric Observables in Frequentist Analyses of the CMSSM and NUHM1," *Eur.Phys.J.*, vol. C64, pp. 391–415, 2009.

[26] J. R. Ellis, K. Enqvist, D. V. Nanopoulos, and F. Zwirner, "Observables in Low-Energy Superstring Models," *Mod.Phys.Lett.*, vol. A1, p. 57, 1986.

[27] R. Barbieri and G. Giudice, "Upper Bounds on Supersymmetric Particle Masses," *Nucl.Phys.*, vol. B306, p. 63, 1988.

[28] S. S. AbdusSalam, B. C. Allanach, F. Quevedo, F. Feroz, and M. Hobson, "Fitting the Phenomenological MSSM," *Phys.Rev.*, vol. D81, p. 095012, 2010.

[29] S. Sekmen, S. Kraml, J. Lykken, F. Moortgat, S. Padhi, *et al.*, "Interpreting LHC SUSY searches in the phenomenological MSSM," *JHEP*, vol. 1202, p. 075, 2012.

[30] A. Arbey, M. Battaglia, and F. Mahmoudi, "Implications of LHC Searches on SUSY Particle Spectra: The pMSSM Parameter Space with Neutralino Dark Matter," *Eur.Phys.J.*, vol. C72, p. 1847, 2012.

[31] D. Albornoz Vasquez, G. Belanger, J. Billard, and F. Mayet, "Probing neutralino dark matter in the MSSM & the NMSSM with directional detection," *Phys.Rev.*, vol. D85, p. 055023, 2012.

[32] M. W. Cahill-Rowley, J. L. Hewett, A. Ismail, and T. G. Rizzo, "The Higgs Sector and Fine-Tuning in the pMSSM," 2012.

[33] S. Weinberg, "Cosmology," *Cambridge University Press*, 2008.

[34] various authors edited by: Gianfranco Bertone, "Particle dark matter," *Cambridge University Press*, 2010.

[35] A. Bottino, F. Donato, N. Fornengo, and S. Scopel, "Lower bound on the neutralino mass from new data on CMB and implications for relic neutralinos," *Phys.Rev.*, vol. D68, p. 043506, 2003.

[36] P. J. E. Peebles, "The origin of galaxies and clusters of galaxies," *Science*, vol. 224, pp. 1285–1391, 1984.

[37] S. Dodelson and L. M. Widrow, "Sterile-neutrinos as dark matter," *Phys.Rev.Lett.*, vol. 72, pp. 17–20, 1994.

[38] T. Asaka, S. Blanchet, and M. Shaposhnikov, "The nuMSM, dark matter and neutrino masses," *Phys.Lett.*, vol. B631, pp. 151–156, 2005.

[39] R. Peccei and H. R. Quinn, "CP Conservation in the Presence of Instantons," *Phys.Rev.Lett.*, vol. 38, pp. 1440–1443, 1977.

[40] R. Peccei and H. R. Quinn, "Constraints Imposed by CP Conservation in the Presence of Instantons," *Phys.Rev.*, vol. D16, pp. 1791–1797, 1977.

[41] M. S. Turner, "Windows on the Axion," *Phys.Rept.*, vol. 197, pp. 67–97, 1990.

[42] Z. Berezhiani, "Mirror world and its cosmological consequences," *Int.J.Mod.Phys.*, vol. A19, pp. 3775–3806, 2004.

[43] J. Espinosa, T. Konstandin, J. No, and M. Quiros, "Some Cosmological Implications of Hidden Sectors," *Phys.Rev.*, vol. D78, p. 123528, 2008.

[44] E. W. Kolb, D. J. Chung, and A. Riotto, "WIMPzillas!," pp. 91–105, 1998.

[45] G. Servant and T. M. Tait, "Is the lightest Kaluza-Klein particle a viable dark matter candidate?," *Nucl.Phys.*, vol. B650, pp. 391–419, 2003.

[46] S. B. Gudnason, C. Kouvaris, and F. Sannino, "Dark Matter from new Technicolor Theories," *Phys.Rev.*, vol. D74, p. 095008, 2006.

[47] J. L. Feng, A. Rajaraman, and F. Takayama, "SuperWIMP dark matter signals from the early universe," *Phys.Rev.*, vol. D68, p. 063504, 2003.

[48] J. R. Ellis, K. A. Olive, Y. Santoso, and V. C. Spanos, "Gravitino dark matter in the CMSSM," *Phys.Lett.*, vol. B588, pp. 7–16, 2004.

[49] L. Covi, H.-B. Kim, J. E. Kim, and L. Roszkowski, "Axinos as dark matter," *JHEP*, vol. 0105, p. 033, 2001.

[50] S. P. Martin, "A Supersymmetry primer," 1997.

[51] H. Kalka/G.Soff, "Supersymmetry," *Teubner Studienbcher*, 1997.

[52] L. J. Hall, D. Pinner, and J. T. Ruderman, "A Natural SUSY Higgs Near 126 GeV," *JHEP*, vol. 1204, p. 131, 2012.

[53] M. Perelstein and C. Spethmann, "A Collider signature of the supersymmetric golden region," *JHEP*, vol. 0704, p. 070, 2007.

[54] R. Kitano and Y. Nomura, "Supersymmetry with Small mu: Connections between Naturalness, Dark Matter, and (Possibly) Flavor," 2006.

[55] M. Perelstein and B. Shakya, "Fine-Tuning Implications of Direct Dark Matter Searches in the MSSM," *JHEP*, vol. 1110, p. 142, 2011.

[56] M. Farina, M. Kadastik, D. Pappadopulo, J. Pata, M. Raidal, *et al.*, "Implications of XENON100 and LHC results for Dark Matter models," *Nucl.Phys.*, vol. B853, pp. 607–624, 2011.

[57] O. Buchmueller, R. Cavanaugh, A. De Roeck, M. Dolan, J. Ellis, *et al.*, "Supersymmetry in Light of 1/fb of LHC Data," *Eur.Phys.J.*, vol. C72, p. 1878, 2012.

[58] O. Buchmueller, R. Cavanaugh, A. De Roeck, M. Dolan, J. Ellis, *et al.*, "Higgs and Supersymmetry," 2011.

[59] G. Belanger, F. Boudjema, P. Brun, A. Pukhov, S. Rosier-Lees, *et al.*, "Indirect search for dark matter with micrOMEGAs2.4," *Comput.Phys.Commun.*, vol. 182, pp. 842–856, 2011.

[60] A. Djouadi, J.-L. Kneur, and G. Moultaka, "SuSpect: A Fortran code for the supersymmetric and Higgs particle spectrum in the MSSM," *Comput.Phys.Commun.*, vol. 176, pp. 426–455, 2007.

[61] F. Mahmoudi, "SuperIso v2.3: A Program for calculating flavor physics observables in Supersymmetry," *Comput.Phys.Commun.*, vol. 180, pp. 1579–1613, 2009.

[62] D. Albornoz Vasquez, G. Belanger, and C. Boehm, "Revisiting light neutralino scenarios in the MSSM," *Phys.Rev.*, vol. D84, p. 095015, 2011.

[63] B. Dumont, G. Belanger, S. Fichet, S. Kraml, and T. Schwetz, "Mixed sneutrino dark matter in light of the 2011 XENON and LHC results," 2012.

[64] K. Nakamura *et al.*, "Review of particle physics," *J.Phys.G*, vol. G37, p. 075021, 2010.

[65] G. Aad *et al.*, "Search for squarks and gluinos using final states with jets and missing transverse momentum with the ATLAS detector in $\sqrt{s} = 7$ TeV proton-proton collisions," *Phys.Lett.*, vol. B710, pp. 67–85, 2012.

[66] S. Chatrchyan *et al.*, "Search for Supersymmetry at the LHC in Events with Jets and Missing Transverse Energy," *Phys.Rev.Lett.*, vol. 107, p. 221804, 2011.

[67] G. A. *et al.* [ATLAS Collaboration], "Search for squarks and gluinos with the ATLAS detector using final states with jets and missing transverse momentum and 4.7 fb^{-1} of $\sqrt{s} = 7$ TeV proton-proton collision data," *ATLAS-CONF-2012-033*, 2012.

[68] A. Parker, "SUSY Searches (ATLAS/CMS): the Lady Vanishes," *ICHEP 2012*, 4-11 July 2012, Melbourne, Australia.

[69] "Precision electroweak measurements on the Z resonance," *Phys.Rept.*, vol. 427, pp. 257–454, 2006.

[70] G. Aad *et al.*, "Search for neutral MSSM Higgs bosons decaying to tau+ tau- pairs in proton-proton collisions at $\sqrt{s} = 7$ TeV with the ATLAS detector," *Phys.Lett.*, vol. B705, pp. 174–192, 2011.

[71] S. Chatrchyan *et al.*, "Search for neutral Higgs bosons decaying to tau pairs in pp collisions at $\sqrt{s}$=7 TeV," *Phys.Lett.*, vol. B713, pp. 68–90, 2012.

[72] G. Abbiendi *et al.*, "Search for chargino and neutralino production at s**(1/2) = 192-GeV to 209 GeV at LEP," *Eur.Phys.J.*, vol. C35, pp. 1–20, 2004.

[73] L. Calibbi, T. Ota, and Y. Takanishi, "Light Neutralino in the MSSM: a playground for dark matter, flavor physics and collider experiments," *JHEP*, vol. 1107, p. 013, 2011.

[74] R. Aaij *et al.*, "Strong constraints on the rare decays $B_s \to \mu^+\mu^-$ and $B^0 \to \mu^+\mu^-$," *Phys. Rev. Lett. 108,*, vol. 231801, 2012.

[75] G. Bennett *et al.*, "Final Report of the Muon E821 Anomalous Magnetic Moment Measurement at BNL," *Phys.Rev.*, vol. D73, p. 072003, 2006.

[76] G. Aad *et al.*, "Combined search for the Standard Model Higgs boson using up to 4.9 fb-1 of pp collision data at $\sqrt{s}$= 7 TeV with the ATLAS detector at the LHC," *Phys.Lett.*, vol. B710, pp. 49–66, 2012.

[77] S. Chatrchyan *et al.*, "Combined results of searches for the standard model Higgs boson in pp collisions at $\sqrt{s}$ = 7 TeV," *Phys.Lett.*, vol. B710, pp. 26–48, 2012.

[78] G. Aad *et al.*, "Search for the Standard Model Higgs boson in the diphoton decay channel with 4.9 fb-1 of pp collisions at $\sqrt{s}$=7 TeV with ATLAS," *Phys.Rev.Lett.*, vol. 108, p. 111803, 2012.

[79] S. Chatrchyan *et al.*, "Search for the standard model Higgs boson decaying into two photons in pp collisions at $\sqrt{s}$=7 TeV," *Phys.Lett.*, vol. B710, pp. 403–425, 2012.

[80] ATLAS Collaboration, "An update to the combined search for the Standard Model Higgs boson with the ATLAS detector at the LHC using up to 4.9 fb^{-1} of *pp* collision data at $\sqrt{s}$=7 TeV," *ATLAS-CONF-2012-019*, 2012.

[81] CMS Collaboration, "Combined results of searches for a Higgs boson in the context of the standard model and beyond-standard models," *CMS-PAS-HIG-12-008*, 2012.

[82] E. Barberio *et al.*, "Averages of $b-$hadron and $c-$hadron Properties at the End of 2007," 2008.

[83] D. Asner *et al.*, "Averages of b-hadron, c-hadron, and tau-lepton Properties," 2010.

[84] M. Antonelli *et al.*, "Precision tests of the Standard Model with leptonic and semileptonic kaon decays," 2008.

[85] H. K. Dreiner, J. S. Kim, and O. Lebedev, "First LHC Constraints on Neutralinos," 2012.

[86] P. P. Giardino, K. Kannike, M. Raidal, and A. Strumia, "Reconstructing Higgs boson properties from the LHC and Tevatron data," *JHEP*, vol. 1206, p. 117, 2012.

[87] J. R. Espinosa, M. Muhlleitner, C. Grojean, and M. Trott, "Probing for Invisible Higgs Decays with Global Fits," 2012.

[88] E. Aprile *et al.*, "The XENON100 Dark Matter Experiment," *Astropart.Phys.*, vol. 35, pp. 573–590, 2012.

[89] E. Aprile, "The XENON1T Dark Matter Search Experiment," 2012.

[90] P. Grothaus, M. Lindner, and Y. Takanishi, "Naturalness of Neutralino Dark Matter," 2012.

[91] C. Weniger, "A Tentative Gamma-Ray Line from Dark Matter Annihilation at the Fermi Large Area Telescope," 2012.

[92] S. Choi, J. Kalinowski, G. A. Moortgat-Pick, and P. Zerwas, "Analysis of the neutralino system in supersymmetric theories," *Eur.Phys.J.*, vol. C22, pp. 563–579, 2001.

[93] T. Falk, A. Ferstl, and K. A. Olive, "New contributions to neutralino elastic cross-sections from CP violating phases in the MSSM," *Phys.Rev.*, vol. D59, p. 055009, 1999.

[94] A. Bottino, F. Donato, N. Fornengo, and S. Scopel, "Neutralino properties in the light of a further indication of an annual modulation effect in WIMP direct search," *Phys.Rev.*, vol. D59, p. 095003, 1999.

[95] T. Nihei, L. Roszkowski, and R. Ruiz de Austri, "Exact cross-sections for the neutralino WIMP pair annihilation," *JHEP*, vol. 0203, p. 031, 2002.

[96] T. Falk, K. A. Olive, and M. Srednicki, "Heavy sneutrinos as dark matter," *Phys.Lett.*, vol. B339, pp. 248–251, 1994.

[97] G.-C. Cho, K. Hagiwara, Y. Matsumoto, and D. Nomura, "The MSSM confronts the precision electroweak data and the muon g-2," *JHEP*, vol. 1111, p. 068, 2011.

[98] Y. G. Kim, T. Nihei, L. Roszkowski, and R. Ruiz de Austri, "Upper and lower limits on neutralino WIMP mass and spin independent scattering cross-section, and impact of new (g-2)(mu) measurement," *JHEP*, vol. 0212, p. 034, 2002.

Erklärung:

Ich versichere, dass ich diese Arbeit selbstständig verfasst habe und keine anderen als die angegebenen Quellen und Hilfsmittel benutzt habe.

Heidelberg, den 27.07.2012 .....